Strål
säkerhets
myndigheten
Swedish Radiation Safety Authority

Author: Ali R. Massih

Research

2014:21

Effects of additives on uranium dioxide fuel behavior

Report number: 2014:21 ISSN: 2000-0456
Available at www.stralsakerhetsmyndigheten.se

SSM perspective

Background

There is a large interest the nuclear fuel field, both in Sweden and internationally, for doping nuclear fuel pellets with non-absorber additives in order to improve the light water reactor (LWR) fuel performance. The suppliers that manufacture fuel for Swedish power plants each have developed their own product line and their own type of doped fuel pellets. In the last few years, the fuel products have reached a level of maturity sufficient for the usage of nuclear fuel with additives in large scale in commercial reactors.

Objectives

Nuclear fuel that is used in Swedish commercial reactors shall be thoroughly tested according to systematic test plans and proven to be of high quality and performance before it can be introduced. It is also important that the behavior of the fuel can be described well with analytical tools. To meet these requirements, proven operation and ability to model, testing and research are necessary. Based upon the results of the research conclusions about the fuel behavior can be drawn and databases for model development can be built. From a regulator point of view it is important to monitor that the research is properly performed and that models are well substantiated.

Nuclear fuel pellets with additives have somewhat different properties compared to standard LWR nuclear fuel. For example, an additive fuel has a higher density and larger mean grain size, which leads to a lower fuel densification and a higher degree of fission products trapping, respectively, during reactor operation. Tests of the behavior of nuclear fuel pellets have been performed by different fuel suppliers in different test reactors. SSM have commissioned Ali Massih at Quantum Technologies AB to gather the publically available information to make a comparison between different types of additives and tests and also to contribute to the development of models to be used in analytical tools.

Results

Ali Massih has a long experience of design of nuclear fuel and the models that are necessary to analyze fuel behavior. Ali has collected the publically available information, sorted out the parameters that are important to the models, and presents their mathematical descriptions. Quantum Technologies AB develops and uses the codes and competence that SSM requires for supervision of fuel performance analysis.

This report will form a basis for the reviews that SSM does when the license holders applies for use of nuclear fuel with additives. The report is also intended as a reference to the models that Quantum Technologies AB has developed. The report and the models will be a valuable source of information for SSM and other parties when discussing the performance of doped fuel.

Need for further research

Research in the field of nuclear fuel with additives is continuing. Some of the current questions regard the way fission products are trapped within the pellets; which kinds of compositions do they form, in which material microstructure does the compounds reside. From the answers to these questions a better understanding of the behavior of fuel pellets with high burnup and the fuel rod behavior during power transients will be gained.

Project information

Contact person SSM: Jan in de Betou
Reference: SSM2012-2653

Strål
säkerhets
myndigheten
Swedish Radiation Safety Authority

Author: Ali R. Massih
Quantum Technologies AB, Uppsala, Sweden

2014:21

Effects of additives on uranium dioxide fuel behavior

Date: January 2014
Report number: 2014:21 ISSN: 2000-0456
Available at www.stralsakerhetsmyndigheten.se

This report concerns a study which has been conducted for the Swedish Radiation Safety Authority, SSM. The conclusions and viewpoints presented in the report are those of the author/authors and do not necessarily coincide with those of the SSM.

Contents

Abstract

The main incentive to dope UO_2 fuel with a small amount of metal oxides, such as Cr_2O_3 is to enlarge fuel grain size, increase fuel density and possibly make softer fuel pellets. Enlarging fuel grain size ($> 30\ \mu$m) will extend the diffusion path for fission product gases to grain boundaries, through which most of the gas is released from fuel pellet. Hence, the outcome would be a delay in thermal-activated gas release at a given fuel temperature. Increasing fuel density puts more ^{235}U mass per fuel assembly, while leading to less fuel densification during irradiation. Softer pellets, i.e. fuel with a higher creep rate and/or lower yield strength can reduce the intensity of pellet-cladding mechanical interaction during reactor power ramps, alleviating the risk of cladding failure. Additives may also affect the thermophysical properties of UO_2 fuel, such as heat capacity, thermal expansion and thermal conductivity. However, experimental data and theoretical analysis indicate that if the concentration of the additive is low (e.g. for Cr_2O_3 dopant < 0.2 wt%), these properties are hardly affected.

The aim of this report is to assess data and models for some important properties of UO_2-base fuel containing additives. The additives considered are those investigated and reported in the literature. The main additive discussed here is Cr_2O_3, but also we include Al_2O_3, MgO and Nb_2O_5. Appropriate models for thermophysical properties are assessed and recommended for M_2O_3-type (M: metal) additives and even for MgO-doped UO_2. Fission gas diffusivity data and correlations are assessed and used in a standard model for fission gas release and gaseous swelling to evaluate these quantities. Moreover, the effects of grain size on gas release and swelling are assessed. Available data and correlations for thermal creep of Nb_2O_5- and Cr_2O_3-doped fuels are evaluated critically, and possible creep mechanisms are delineated. The results of some in-reactor irradiation programs, ramp tests and transients on additive fuel are briefly reviewed. The report also intends to provide a foundation for model implementation in a fuel rod performance code.

Sammanfattning

De främsta skälen till att tillföra små mängder av metalloxider, som exempelvis Cr_2O_3, till kärnbränsle av UO_2 är att öka materialets kornstorlek och densitet, samt om möjligt göra bränslekutsarna mjukare. En ökning av bränslets kornstorlek (> 30 μm) ökar diffusionslängden för gasformiga fissionsprodukter till materialets korngränser, genom vilka den största delen gas avges från bränslekutsen. Resultatet torde vara en fördröjning av termiskt aktiverad gasavgivning från bränslet vid en given temperatur. En ökning av bränslets densitet ger större mängd ^{235}U per bränsleknippe och leder till mindre bränsleförtätning under bestrålning. Mjukare kutsar, det vill säga bränsle med en högre kryptöjningshastighet och/eller lägre sträckgräns, kan mildra mekanisk växelverkan mellan kuts och kapsling under effekthöjningar (ramper) vid reaktordrift, vilket skulle minska risken för kapslingsbrott. Tillsatser kan också påverka UO_2-bränslets termofysikaliska egenskaper, såsom värmekapacitet, termisk längdutvidgning och värmeledningsförmåga. Experimentella data och teoretisk analys antyder emellertid att om koncentrationen av tillsatserna är låg (t.ex. < 0.2 viktprocent av tillsatsämnet Cr_2O_3), så påverkas dessa egenskaper endast marginellt.
Målet med denna rapport är att utvärdera data och modeller för viktiga egenskaper hos UO_2-baserat bränsle innehållande tillsatser. Tillsatserna som beaktas är de för vilka studier finns rapporterade i öppen litteratur. Huvudakligen diskuteras Cr_2O_3, men vi inkluderar även Al_2O_3, MgO och Nb_2O_5. Lämpliga modeller för termofysikaliska egenskaper utvärderas och rekommenderas för UO_2-bränsle med tillsatser av typen M_2O_3 (M: metall), men även för MgO-dopad UO_2. Data och korrelationer för diffusivitet hos fissionsgas i UO_2 med nämnda tillsatsämnen analyseras och används i en standardmodell för fissionsgasavgivning och gassvällning, i syfte att utvärdera dessa egenskaper och hur de påverkas av tillsatsämnena. Även inverkan av bränslets kornstorlek på gasavgivning och svällning utvärderas. Tillgängliga data och korrelationer för termiskt kryp i Nb_2O_5- och Cr_2O_3-dopat bränsle utvärderas kritiskt, och möjliga krypmekanismer beskrivs. Resultat från utvalda reaktorbestrålningsprogram, rampprov och transienter på bränsle med tillsatser granskas översiktligt. Rapporten avses tjäna som underlag för implementering av modeller i beräkningsprogram för bränsle-stavanalys.

1 Introduction

Addition of small amounts of certain metal oxides, such as Cr_2O_3 and or Al_2O_3, to UO_2 fuel enlarges the fuel grain size, increases fuel density and possibly makes the fuel pellets softer. Enlarging fuel grain size (> 30 μm) will extend the length of the diffusion path for fission product gases to grain boundaries, through which most of the gas is released from the fuel pellet. Hence, the outcome would be a delay in thermal-activated fission gas release at a given fuel temperature. In like manner, the main gaseous swelling contribution in UO_2 emanates from grain boundary gas bubbles, which would reduce as a results of larger grain size [1]. Increasing fuel density puts more ^{235}U mass per fuel assembly while generating more fission products per fuel volume and also leading to less fuel densification during irradiation. Softer pellets, i.e. fuel with a higher creep rate and/or lower yield strength can reduce the intensity of pellet-cladding mechanical interaction during reactor power ramps, thus lessening the risk of cladding failure. Additives may also affect the thermophysical properties of UO_2 fuel. These comprise enthalpy, heat capacity, thermal expansion and thermal conductivity, if the dopant level is sufficiently high, say ≥ 0.5 wt%.

The additive oxides experimented with since 1960s, both in laboratory and in-reactor, include TiO_2 [2–5], Nb_2O_5 [5–9], Cr_2O_3 [10, 11], V_2O_5 [3], La_2O_3 [2, 6], MgO [12, 13], Al-Si-O [14–16]. Cr_2O_3-doped UO_2 fuels have also been irradiated in commercial boiling water and pressurized water reactors (BWR and PWR), while MgO doped UO_2 fuels have been irradiated in an advanced gas cooled reactor (AGR) as reported in the literature [17–19] and [20, 21]. There are other additives such as Gd_2O_3 [22] and Er_2O_3 [23, 24] used as burnable absorbers (BAs) in UO_2. These additives are utilized for in-core fuel management schemes and can be subjects of separate studies with emphasis on the neutronic aspects and, hence, are not discussed here. However, for Gd_2O_3, extensive thermophysical data and models are available in the literature and we may take advantage of those studies to use them as analogy to assess the properties of Cr_2O_3, if applicable.

The specific dopants influence the trapping and diffusion of fission product gases xenon and krypton, and also the self diffusion of U^{4+} ions in UO_2. The prevailing defects in UO_2 are oxygen vacancies and interstitials. Additions of, e.g., trivalent chromium, aluminium, or gadolinium as Cr_2O_3, Al_2O_3 and Gd_2O_3 should, in general, increase the concentration of vacancies in UO_2, thereby decreasing the concentration of uranium vacancies via the equilibrium between cation and anion vacancies [25]. Hence, the rate of uranium diffusion is expected to be reduced by introduction of trivalent atoms in UO_2. On the other hand, an addition of pentavalent niobium ions, e.g., Nb_2O_5, should enhance cation diffusion. These effects, in turn, affect the diffusion and release of fission product gases produced during reactor operation in and from fuel pellets. An important factor is the state of oxygen in the fuel, namely the chemical potential of oxygen, which itself is controlled by the oxygen-to-uranium ratio of the compound and the temperature.

Nevertheless, there are also appreciable differences between the various trivalent compounds or so-called sesquioxides. For example, the ionic radii for Al^{+3}, Cr^{3+}, and Gd^{3+} are 0.5, 0.64 and 0.94 Å, respectively [26]. The corresponding solid solubility limits for Al_2O_3 and Cr_2O_3 in UO_2 at 1700°C are 70 and 700 weight part per million (wppm), respectively [27], while for Gd_2O_3 it is substantially higher than that for Cr_2O_3 [28]. The former two dopants are grain enlarger while Gd_2O_3 is not. Recent atomic scale computations suggest that the trivalent oxides comprising Cr_2O_3 and Gd_2O_3 preferentially enter UO_2 by associating the substitutional ion with an oxygen vacancy [29]. The larger cation ions, e.g., Gd^{3+}, tend to form oxygen vacancy clusters, whereas the smaller ones, e.g., Cr^{3+} generate prefer-

entially isolated defects. Middleburgh et al.'s results [29] indicate that the solubility limit of the smaller cation containing trivalent oxides, such as Cr_2O_3, is controlled by the oxidation state of the uranium dioxide, that is, the amount of Cr^{3+} that can enter solution is highly dependent on the degree of hyperstoichiometry. On the other hand, larger cations, such as Gd^{3+}, which already are highly soluble in UO_2, would not be much more stable in UO_{2+x} and hence their solubility is not greatly affected by the degree of hyperstoichiometry.

The objective of this report is to assess data and models for some important properties of UO_2-base fuel containing additives. The additives considered are those investigated and reported in the literature. The main additive discussed here is Cr_2O_3, but we also consider the attributes of Al_2O_3, MgO and Nb_2O_5 in uranium dioxide. The report also intends to provide a foundation for model implementation in a fuel rod performance computer code.

The plan of this report is as follows. Section 2 reviews briefly some physical and material characteristics of the dopants. Appropriate models for thermophysical properties, comprising enthalpy, heat capacity, thermal expansion and thermal conductivity, are assessed and recommended for M_2O_3-type (M: metal) additives, and even for MgO-doped UO_2 fuel, in section 3. In section 4, fission gas diffusivity data and correlations are assessed and used in a standard model for fission gas release and gaseous swelling, to evaluate these quantities as a function of temperature and irradiation time. Moreover, the effects of grain size on gas release and swelling are evaluated in this section. Section 5 reviews briefly available data and correlations for thermal creep of Nb_2O_5- and Cr_2O_3-doped fuels. These are evaluated critically, and possible creep mechanisms are delineated. In addition, data on the effects of additives Cr_2O_3 and Al-Si-O on the yield stress of UO_2 at high temperatures are briefed. The results of some in-reactor irradiation programs, ramp tests and transients on additive fuels are briefly reviewed in section 6. Section 7 concludes the report with a summary and some remarks. The mathematical formulae for the thermophysical properties and the fission gas release model are placed in the appendices.

2 UO_2 plus additives

As noted in the preceding section, the main impetus for introducing additives in UO_2 fuel is to improve fuel performance by increasing fuel grain size, minimizing fuel densification during irradiation and possibly making a softer fuel. Of course, large grain size (> 30 μm) may also be achieved in undoped UO_2 but that would require higher sintering temperatures and longer sintering times than vendors usually apply to fabricate standard light water reactor (LWR) fuel pellets (1600-1750°C/5-10 h [30]). Minimizing the sintering conditions could result in appreciable economic benefits both by reducing fabrication costs and increased production rates [31].

One way of achieving the same results is by addition of small amounts of appropriate metal oxides to UO_2 powder during manufacturing. For example, Arborelius et al. [17] report that in order to produce high density, large grain size LWR fuel, AUC (ammonium uranyl carbonate) converted UO_2 powder is mixed with small quantities of additives in the form of oxides for about one hour to obtain full homogeneity. In case of a Cr_2O_3-dopant, e.g. 1000 wppm (weight part per million) of Cr_2O_3-dopant was mixed with UO_2 powder, then the powder was pressed to green pellets with a force of about 50 kN. The green pellets were sintered in a H_2/CO_2 atmosphere at a maximum temperature of 1800°C for 14 h to a solid UO_2 pellet. The mean fuel grain size and density obtained for the doped UO_2 were 44 μm and 10.62 g/cm^3, respectively, as compared to 11 μm and 10.52 g/cm^3 of the standard Westinghouse Sweden undoped UO_2 fuel [17].

Industrial groups in France led by AREVA NP have utilized and doped UO_2 fuels for LWRs over the years [18, 19, 32, 33]. In particular, chromium oxide with a concentration of 0.16 wt% is used as an additive with grain size varying in the range of 50 to 70 μm, figure 1. These materials have densities in a range of 96 to 97 %TD (theoretical density) and have exhibited less in-reactor densification than standard UO_2 fuel. Increasing the fuel density also gives an increase in the ^{235}U mass per fuel assembly for employing fuel utilization schemes with longer reactor cycles, considering that Cr_2O_3 has a very small impact on thermal neutron absorption. Factors governing microstructure development of Cr_2O_3-doped UO_2 during sintering are investigated by Bourgeois et al. [34] and Leenaers et al. [35], whereas the lattice parameter and theoretical density of this fuel have been determined by Cardinaels et al. [36]. Solid solubility of Cr_2O_3 in UO_2 is discussed in [27, 34, 36].

In table 1, we have listed some metal oxides used or experimented with as fuel additives in thermal reactors. A combination of these oxides, e.g. Al_2O_3-Cr_2O_3 also have been used in UO_2. Included in the table are the values for the thermal neutron capture cross-section ($\sigma_{\rm ab}^{\rm th}$) for the additive elements. It is seen that Al and Mg will have the best neutronic performance (i.e. lowest $\sigma_{\rm ab}^{\rm th}$), whereas La, Ti and V are the poorest in this respect. Table 2 gives typical fuel elemental composition for a 0.16 wt% Cr_2O_3-doped UO_2 and that of two variants of "pure" or standard UO_2 fuel.

Table 1: Oxides and their base metals used as additives in UO_2 fuel [26].

Base element	Al	Ca	Cr	La	Mg	Nb	Si	Ti	V
Atomic mass	26.98	40.08	51.996	138.91	24.31	92.91	28.09	47.88	50.94
$\sigma_{\rm ab}^{\rm th}$(barns)	0.23	0.43	3.1	8.9	0.064	1.15	0.16	6.1	5.06
Major oxide	Al_2O_3	CaO	Cr_2O_3	La_2O_3	MgO	Nb_2O_5	SiO_2	TiO_2	V_2O_5

$\sigma_{\rm ab}^{\rm th}$: Thermal neutron capture cross-section.

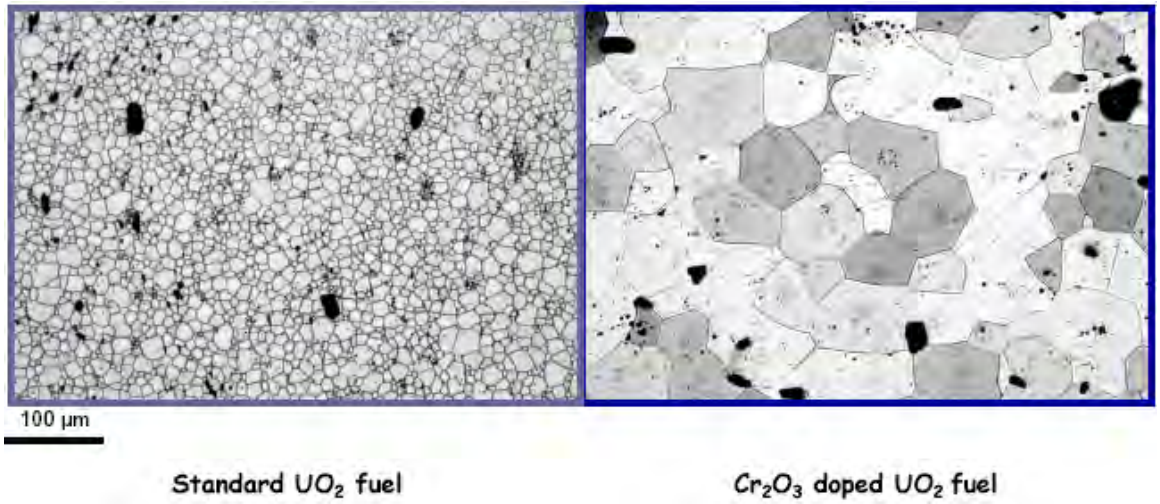

Figure 1: Micrographs of AREVA NP Cr_2O_3-doped (grain size 60 μm) and standard UO_2 (grain size 8 μm) fuels; from Delafoy et al. [18, 33].

Table 2: Typical UO_2-base fuel elemental composition (wppm).

Dopant [Ref.]	Cr_2O_3 [37]	Undoped [37]	Undoped [31]
Grain size (μm)	70	11	8
Fuel density (%TD)	95.97	96.26	97.83
Al	6	8	<10
B	0.1	0.1	0.15
C	5	5	200
Ca	5	5	<5
Cd	0.2	0.2	<0.2
Cr	**1079**	5	<5
Cl	3	3	...
F	3	3	<5
Fe	10	10	40
Mg	0.5	0.5	<1
N	10	10	...
Ni	2	2	10
Si	4	4	<10
W	0.5	0.5	...

TD: Theoretical density of UO_2 = 10.97 g/cm^3 [26].

Radford and Pope [31] compared the effect of addition of oxides of titanium, niobium, vanadium, barium and Ti-Ba at different levels, ranging from 0.05 to 1.66 mol% metal, to the UO_2 powder characterized in the far right column of table 2. These elements all suppressed the density during the initial sintering below about 1200°C followed by enhancing the density at intermediate temperatures (1200-1400°C). At higher levels of concentrations, especially for Ti and Ca-Ti, a pronounced sweeping of the fine pores ($< 2\mu$m) was observed [31]. The grain size was increased with the level of the additives, figure 2.
So, additives affect physical properties of UO_2. They influence fuel thermodynamics and the kinetic processes involved during fabrication and reactor operation. This is due to restructuring of point defects and defect processes in UO_2. Uranium dioxide has a face-

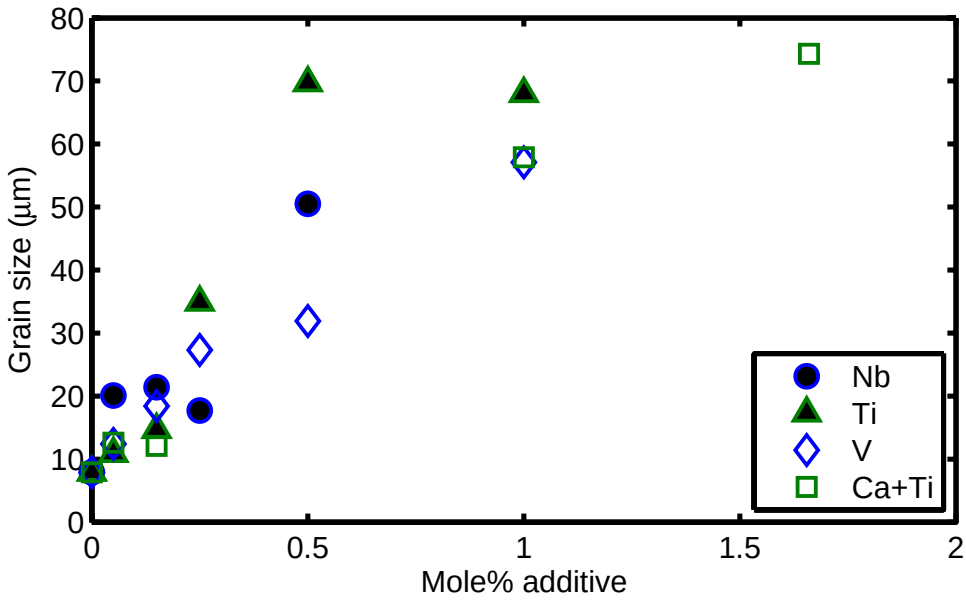

Figure 2: Grain size versus concentration level of additive metal after Radford and Pope [31]; Nb and Ti more strongly affect grain size than V or Ca+Ti.

centered cubic (fcc) crystal with fluorite structure named after the compound CaF_2. The unit cell contains four molecules of UO_2. It is face-centered with respect to the uranium ions, which occupy the octahedral positions (0,0,0), (1/2,1/2,0), (1/2,0,1/2) and (0,1/2,1/2), whereas the oxygen ions occupy the (1/4,1/4,1/4) and its equivalent positions (tetrahedrally coordinated by uranium). Interstitial ions may be accommodated at octahedral vacant sites [38].

The UO_2 fuel can also readily take up oxygen interstitially to form hyperstoichiometric UO_{2+x}, where x can range as high as 0.25 at high temperatures; U_4O_9 will precipitate out as the temperature is lowered. Hypostoichiometric uranium dioxide UO_{2-x} form under low partial pressures of oxygen at high temperatures. They revert to stoichiometric UO_2 and precipitate metallic U upon cooling [30]. The properties of the uranium dioxide phase strongly vary as a function of the the oxygen to metal uranium atom ratio (O/U). The variation of the chemical potential of oxygen μ_{O} with the O/U ratio is very distinct. It reflects the equilibrium between oxygen in the crystal lattice and the gas phase. In the hypostoichiometric domain, μ_{O} is relatively low, that is, the oxygen is strongly bonded in the lattice. Whereas in the hyperstoichiometric domain μ_{O} is much higher, since the bonding of the O^{2-} ions in the interstitial sites is relatively weak. The variation of μ_{O} data as a function of O/U ratio and temperature is related to the evolution of the defect concentration in the crystal. Various suggestions for the defect chemistry in $UO_{2\pm x}$ have been presented but are still subject of dispute [38].

In addition to point defects such as cation and anion vacancies and interstitials, the combination of these point defects is also of importance, especially under irradiation. Such defects include the oxygen Frenkel pair, uranium Frenkel pair, the uranium-oxygen divacancy pair, Schottky defect (one U and two O vacancies separated), and the bound-Schottky trivacancy; see Liu et al. for illustrations [39].[1]

Regarding the effect of additive Nb_2O_5 on the point defect structure of UO_2, Matsui and Naito's experimental results [40] indicate that for the same μ_{O}, the O/M ratio for Nb_2O_5-

doped UO_2, is larger than that for undoped, implying that the concentrations of oxygen interstitials and cation (U) vacancies are increased by Nb_2O_5 addition. This nonstoichiometric effect on defect structure may be responsible for the augmentations of the diffusion coefficients of cations and fission gas (see section 4) due to Nb_2O_5 doping. The enhancement of the cation diffusion by addition of Nb_2O_5 is generally explained by the following defect structure [41]: Higher valent Nb^{5+} ions, substituting for the U^{4+} ions in the UO_2 lattice, impart an effective positive charge to the lattice. This should increase the concentration of oxygen interstitials and decrease that of oxygen vacancies, thereby increasing the concentration of cation vacancies through the Schottky defects in equilibrium. The increase in the concentrations of cation vacancies and oxygen interstitials is expected to increase the diffusivities of cation and fission gas. Moreover, the enhanced cation diffusion would increase the creep and grain growth rates.

As regards the effect of Cr_2O_3 dopant on the point defect structure of UO_2, Kashibe and Une [11] assumed that Cr atoms enter interstitial sites in the UO_2 lattice and are ionized to a trivalency of +3. Their thermodynamic analysis [11] shows that for slightly hyperstoichiometric $(U,Cr)O_{1+x}$, in equilibrium, the uranium vacancy concentration is proportional to the square of Cr^{3+} concentration. Thus, by dissolving Cr^{3+} ions into the UO_2 lattice, it is expected that the concentrations of cation vacancies and oxygen interstitials increase, thereby both cation and fission gas diffusivity would increase. However, author's generic thermodynamic calculations for trivalent dopants (M_2O_3) show that for hypostoichiometric $(U,M)O_{1-x}$, when M^{3+} ions substitute for U^{4+} ions in UO_2, this has the opposite effect. That is, oxygen vacancies increase while oxygen interstitials decrease with M_2O_3 concentration [42]; see section 4.3 for concrete examples.

Before closing this section, we should note that for a dopant to be an effective grain growth promoter, i.e. to enhance self diffusion, it should be in solid solution at the applicable sintering condition. For example, for the dopant Nb_2O_5 in UO_2 at the sintering temperature of 1700°C and μ_{O_2} between -420 and -470 kJ/molO_2, the solubility limit is estimated to be about 0.4 wt% [43]. Beyond that limit, the second phase with composition close to Nb_2UO_6 has been observed at grain boundaries of the fuel [43]. For Cr_2O_3 in UO_2, Leenaers et al. [35] using electron probe microanalysis (EPMA) have found that for specimens sintered at 1600°C ($\mu_{O_2} = -370$ kJ/molO_2), 1660°C ($\mu_{O_2} = -370$ kJ/molO_2), 1760°C ($\mu_{O_2} = -360$, $\mu_{O_2} = -390$ kJ/molO_2), the solubility limits for Cr_2O_3 are 0.095, 0.126 and 0.149 wt%, respectively.

3 Thermophysical properties

In this section some important solid-state physical properties of doped UO_2, affecting nuclear reactor fuel behavior, are appraised. The properties comprise enthalpy, heat capacity, thermal expansion, and thermal conductivity. We assess the influence of trivalent ions, e.g. Cr^{3+} added as Cr_2O_3 or generically M_2O_3 to UO_2, on these properties. We also review the thermal conductivity of magnesium doped UO_2 fuel which is available in the literature.
We are interested in relationships or data that describe the temperature and doping concentration dependance of the aforementioned quantities. However, we could not find such relationships or data systematically, except for MgO additive, in the literature. It is usually stated that the thermophysical behavior for doped and pure UO_2 are the same or similar and hence the same model correlations can be used for both fuel types irrespective of the dopant concentration [17, 33, 44]. The doping concentrations utilized by the fabricators in the form of M_2O_3 usually vary between 500 and 2000 wppm. Because, strictly speaking, such dopants, even in small amount, affect the properties of interest, we have used generic relationships for trivalent oxides added to uranium oxide to calculate its effect as a function of temperature. In particular, relationships that describe UO_2 alloyed with Gd_2O_3 are selected as our platform for M_2O_3 additives, since they are well established with ample experimental basis; however, we account and/or point out the differences between Gd_2O_3 and Cr_2O_3 or any other trivalent oxide additive compounds.

3.1 Enthalpy and heat capacity

Fuel enthalpy H_p and its derivative with respect to temperature, the heat capacity or specific heat, are key fuel behavior parameters for reactor safety analysis. For example, the heat capacity of fuel affects the Doppler feedback during a reactor excursion, since it is the heat capacity that determines fuel temperature during an excursion: the higher is the temperature, the larger is the Doppler feedback and the larger reduction in the associated fuel reactivity. In fact, regarding the sensitivity of excursion yields on fuel parameters, the heat capacity, C_p, is considered to be the most important through its effect on the value of the Doppler constant [45].
From room temperature to 1000 K, the increase in heat capacity is governed by the harmonic lattice vibrations or phonons, which may be described by a Debye model [46, 47]. The Debye temperature Θ_D of UO_2 in the temperature range 300-1000 K is less than 600 K, hence the Debye function is almost unity by $T > 1000$ K, where harmonic C_p reaches an asymptotic limit. Also, a minor contribution to heat capacity is provided by thermal excitation of localized electrons of U^{4+}, i.e. $(5f)^2$ electrons in the crystal field (CF) levels. At low temperatures, this contribution is $\propto T$, while, at high temperatures, where the concentration of U^{4+} decreases via $U^{4+} \rightarrow U^{3+} + U^{5+}$, C_p becomes virtually independent of temperature [46].
Between 1000 and 1500 K, the heat capacity increase arises from the anharmonicity of the lattice vibrations as reflected in thermal expansion. From 1500 to 2670 K ($= T_c$: the critical temperature[2]), an anomalous exponential rise in enthalpy H_p and the associated C_p is observed; see, e.g. the forthcoming figure 7. This is attributed to the formation of lattice and electronic defects. The C_p peak measured at $T_c \approx 0.8T_{\mathrm{melt}}$ is similar to that observed in ionic fluorides, which exhibit a superionic second-order (or λ) phase transition to a disordered state prior to melting [48, 49]. The main contributor to this thermodynamic anomaly seems to be the buildup of Frenkel defects in the crystalline structure [50, 51]. For

$T_c < T < T_{\mathrm{melt}}$, the Frenkel defect concentration becomes saturated and Schottky defects become important. From T_c to T_{melt}, C_p is characterized by a steep descending wing of the transition peak, due to the rapid saturation of the defect concentration, anion disordered phase, followed by a weakly increasing stage caused by the creation of more energetic atomic defects (UO_2 Schottky trios) [46].

The question is how and to what degree the introduction of trivalent oxides in UO_2 would affect the different stages of C_p versus T curve? As noted in the foregoing section, introducing a trivalent doping element such as Cr, Gd, La, Al, etc. in UO_2 leads to formation of Frenkel pairs of oxygen. The concentration of these Frenkel pairs (x) can be estimated from a generic formula derived years ago by Szwarc [52] by thermodynamic analysis, namely

$$x = \sqrt{2}\exp\Big(\frac{\Delta S_f}{2R}\Big)\exp\Big(-\frac{\Delta H_f}{2RT}\Big), \tag{1}$$

where ΔS_f and ΔH_f are the entropy and enthalpy of formation per Frenkel pair and other symbols have their usual meanings. Now the anomalous increase in the heat capacity can be quantified by an excess (extra) heat capacity term accounting for the formation of the Frenkel pairs of oxygen

$$\begin{aligned}\Delta C_p &= \frac{d(x\Delta H_f)}{dT}\\ &= \frac{(\Delta H_f)^2}{\sqrt{2}RT^2}\exp\Big(\frac{\Delta S_f T - \Delta H_f}{2RT}\Big).\end{aligned} \tag{2}$$

The total heat capacity is then written

$$C_p = C_{p0} + \Delta C_p, \tag{3}$$

where C_{p0} is the heat capacity resulting from contributions of phonons (lattice vibrations), electrons and the Schottky defects.

Both ΔS_f and ΔH_f are decreasing functions of the additive concentration, as can be seen from figures 3-4. These figures are based on various experimental data put together by Matsui et al. [53], here averaged, to show the trend of the enthalpy and entropy of the Frenkel oxygen pair formation with the content of different dopants (M = Y, Gd, La, Sc, Eu) in UO_2.

From second-degree polynomial curve fits to these data (Appendix A), we have used equation (2) to calculate the excess heat capacity as a function of the cation content at several temperatures, figure 5. It is seen that the excess heat capacity is an increasing function of temperature and the cation content in UO_2, however, at high contents it levels off.

Matsui and colleagues also found that the onset temperature of the heat capacity anomaly decreases with the dopant content. This was especially distinct for Gd dopant as indicated in an earlier paper by Naito [54], figure 6.

Let's next calculate the total heat capacity C_p according to equation (3) using for C_{p0} relationships based on the data by Inaba et al. [55] on $U_{1-y}Gd_yO_2$; also appraised in [56] and listed in Appendix A. The results of calculations as a function of temperature for several (low) concentrations of dopant, related to the weights of Cr_2O_3 in UO_2, are plotted in figure 7. It is seen that for temperatures less than 1600 K, the results are almost identical. For $T \geq 1600$ there is an increase in heat capacity with an increase in dopant concentration, but the deviations are insignificant in the range of concentrations considered. For example, the maximum deviation in heat capacity from "pure" UO_2 to UO_2 + 0.24 wt% additive is

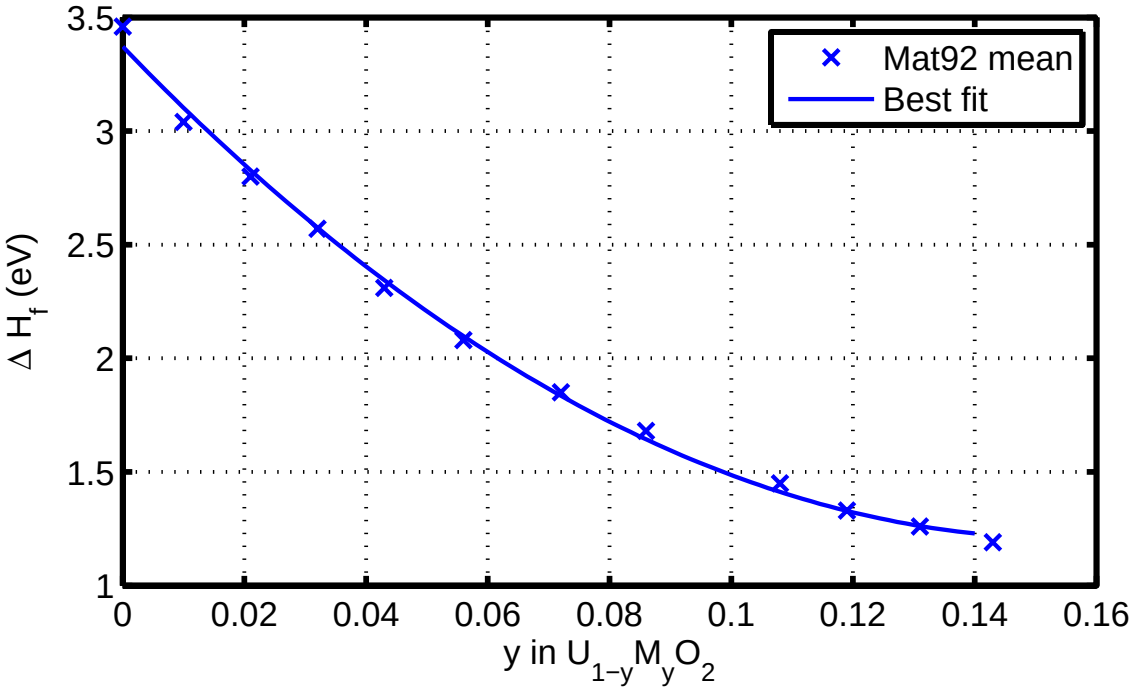

Figure 3: Enthalpy of Frenkel pair formation as a function of the dopant (M) content y in UO_2 based on data presented in Mat92 [53].

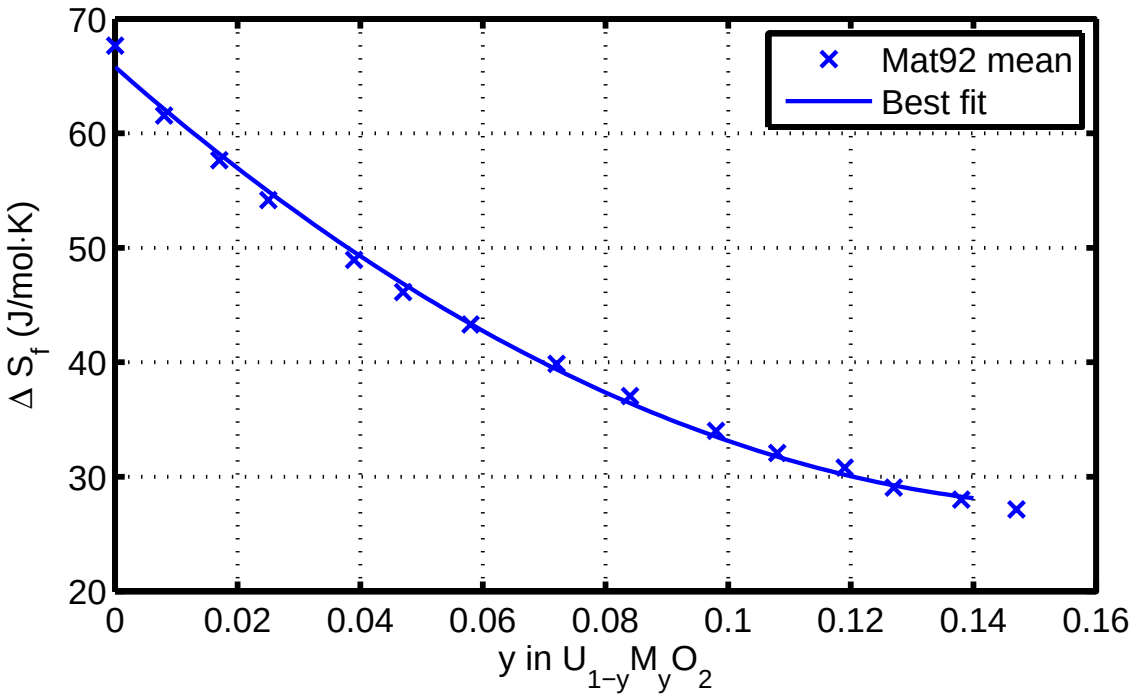

Figure 4: Entropy of Frenkel pair formation as a function of the dopant (M) content y in UO_2 based on data presented in Mat92 [53].

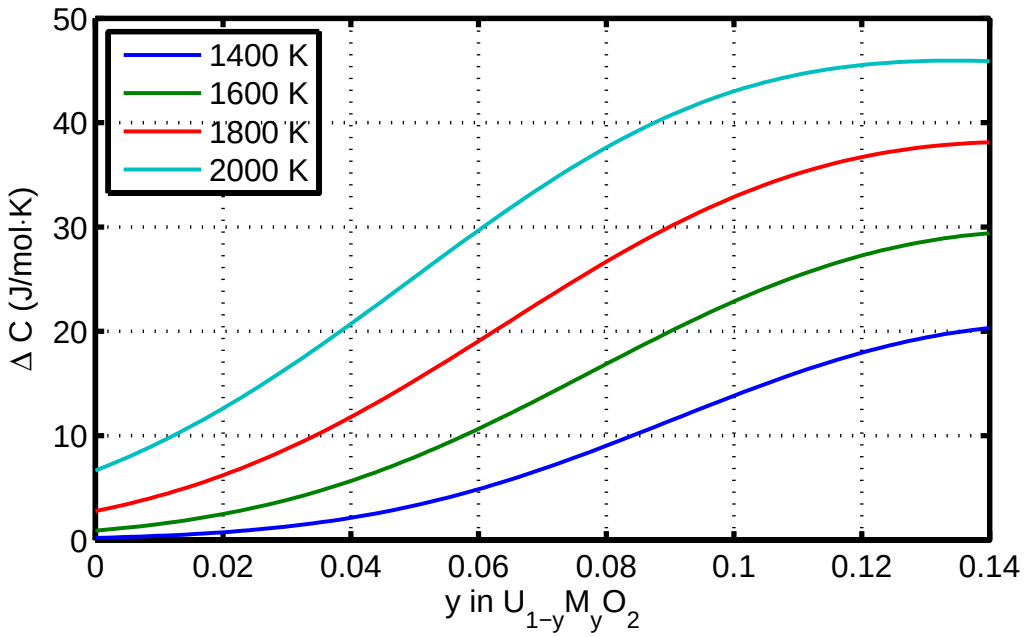

Figure 5: Excess heat capacity due to the Frenkel pair formation as a function of the dopant (M) content y in UO_2 based on data presented in figures 3-4 and equation (2).

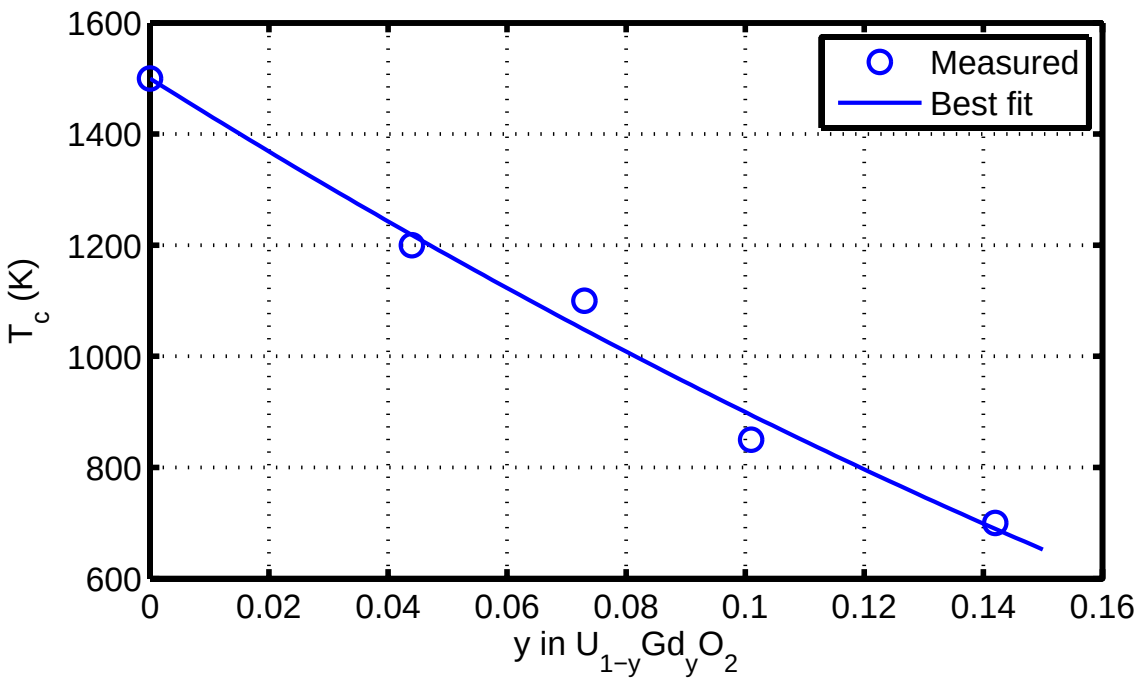

Figure 6: Temperature onset for heat capacity anomaly T_c as a function of the dopant (Gd) content y in UO_2 based on the data presented by Naito [54].

about 1.5% at 2200 K. Regarding fuel enthalpy, relative to the enthalpy at room temperature, for the considered dopant concentrations and temperature range, the calculated values are indistinguishable from that of pure UO_2.

3.2 Thermal expansion

The coefficient of thermal expansion (α) for an isotropic solid such as UO_2 is defined as

$$\alpha = \frac{1}{L}\Big(\frac{\partial L}{\partial T}\Big)_P = \frac{1}{3V}\Big(\frac{\partial V}{\partial T}\Big)_P = \frac{1}{3B}\Big(\frac{\partial P}{\partial T}\Big)_V, \tag{4}$$

where L is the linear dimension of the crystal, V its volume, and P the applied pressure. Here, $B = -V(\partial P/\partial V)_T$ is the bulk modulus.
Thermal expansion data on doped UO_2 (except mixed with Gd_2O_3) are virtually non-existent. Arborelius et al. [17] mention that UO_2 mixed with 0.1 wt% Cr_2O_3 exhibits the same behavior as UO_2 in the temperature range 293 to 1773 K. Here, we apply the empirical correlation for (U,Gd)O_2 [56] based on the data of Une [57] to the dopant contents of interest, see Appendix A. The results in the temperature range of 300 to 2400 K indicate that up to the dopant concentration of 0.5 wt%, the deviations in thermal expansion of doped UO_2 from that of pure UO_2 is insignificant. Figure 8 shows this deviation as a function of temperature relative to 0.5 wt% dopant.
We should mention that there is a thermodynamic relationship between the specific heat and the thermal expansion coefficient [58], namely

$$\alpha = \frac{\gamma C_p}{3BV_m}, \tag{5}$$

where γ is the Grüneisen parameter (dimensionless) and V_m the molar volume. For UO_2, $\gamma = 2.17$, $B = 208$ GPa and $V_m = 24.62$ cm^2/mol [59]. This relationship indicates that temperature and dopant concentration dependence of the coefficient of thermal expansion follows that of the heat capacity, since B is weakly dependent on these quantities.

3.3 Thermal conductivity

The accommodation of trivalent oxides (M_2O_3) in UO_2 matrix distorts the lattice of the matrix locally. For example, for M = Cr, the chromium oxide, Cr_2O_3 consists of the rhombohedral primitive cell, where Cr atoms are eight-coordinated with two oxygen layers. The lattice constants at room temperature for Cr_2O_3 are $a = 4.937$ Å and $c = 3.627$ Å [60]. Conversely, UO_2 has a face-centered cubic lattice with $a = 5.458$ Å with 4 molecules per unit cell. The presence of chromium implies a strong distortion of the UO_2 lattice in its surrounding and results in an increase in the population of defects. It is expected that the number of defects increases with the chromium content, so the thermal conductivity decreases with the increase in chromium content. But the rate of decrease gets smaller at higher temperatures. All this is expected to have an impact on the phonon-lattice and phonon-phonon interactions, leading to a decrease of the thermal conductivity of (U, M)O_{2-x}.
Klemens's thermal conductivity model [61], which is based on the relaxation-time theory when phonon-phonon scattering and phonon-point defect scattering occur simultaneously, is suitable for the aforementioned description. According to this model, the lattice or

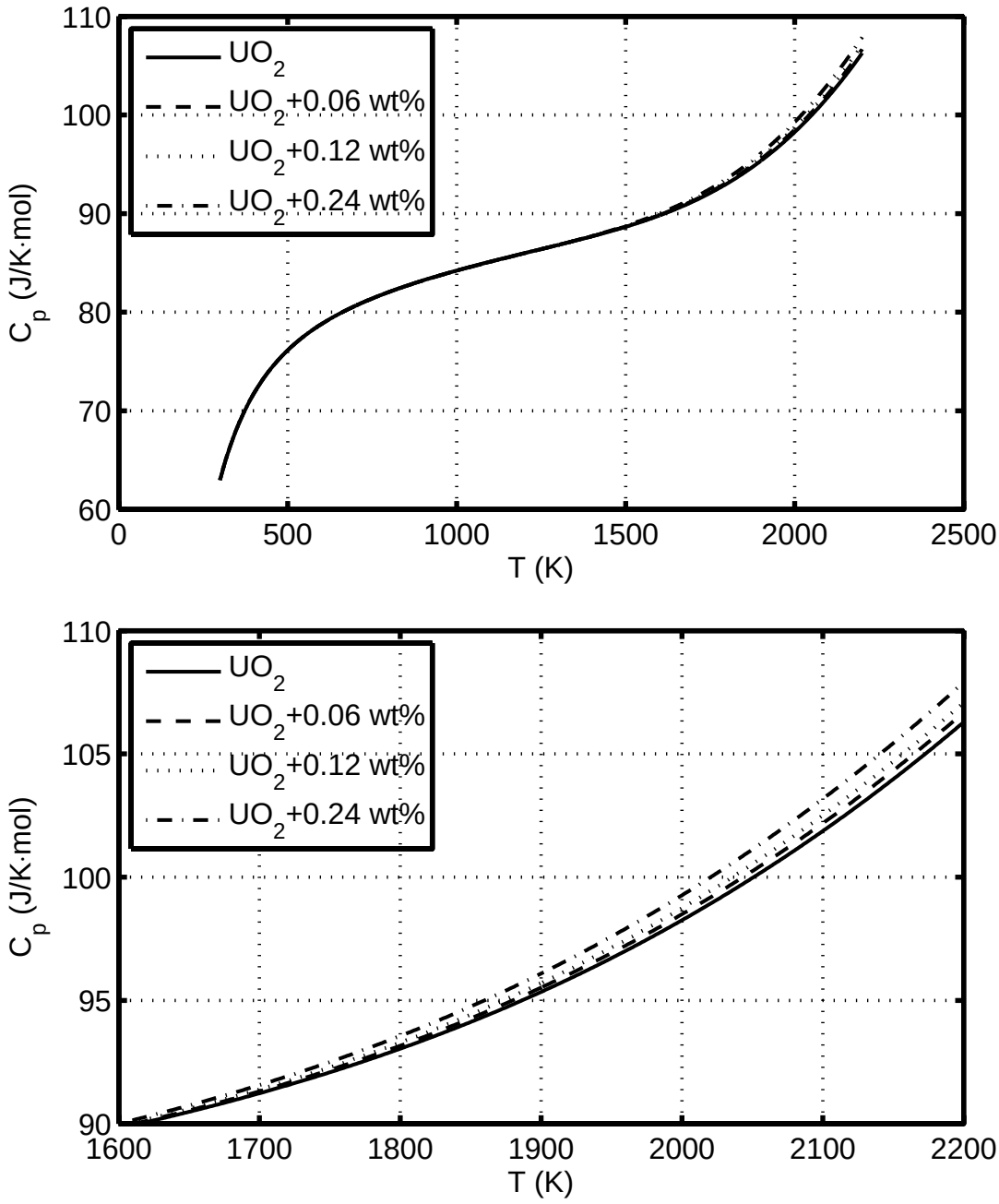

Figure 7: Heat capacity of UO_2 versus temperature as a function of the dopant (M_2O_3) mass content.

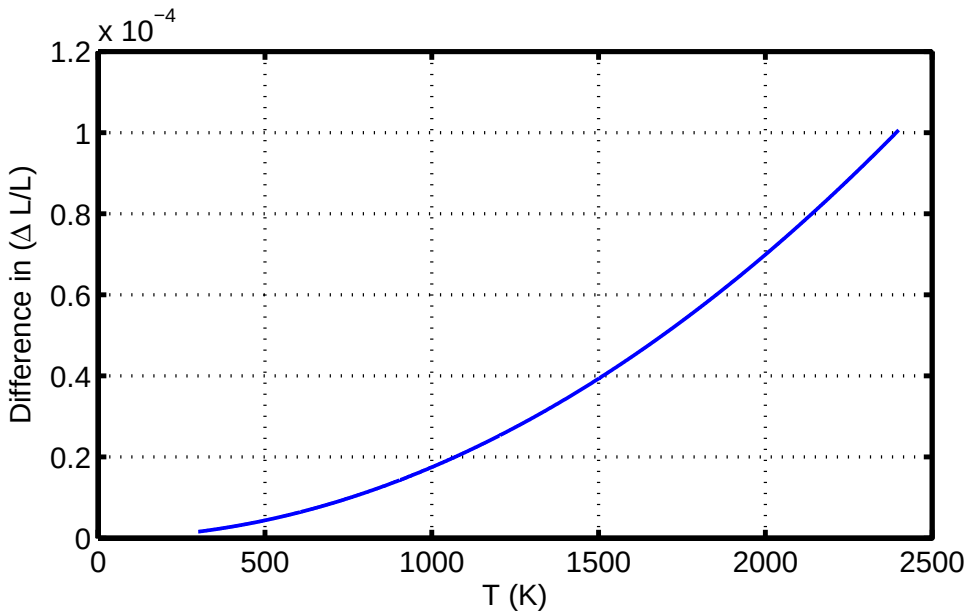

Figure 8: Calculated difference between the relative thermal expansion, $\Delta L/L \equiv [L(T) - L(273)]/L(273)$, of pure UO_2 and 0.5 wt% doped UO_2 with M_2O_3.

phonon thermal conductivity λ_p can be expressed by

$$\lambda_p = \frac{\lambda_0}{w}\arctan(w), \tag{6}$$

$$w = \sigma(\Gamma\lambda_0)^{1/2}, \tag{7}$$

where λ_0 is the thermal conductivity for point defect free UO_2, σ is a physical constant[3] and Γ characterizes the sum of the phonon scattering cross sections of the impurity atoms [62]; it is expressed as

$$\Gamma = \sum_i x_i\Big[\Big(\frac{\Delta M_i}{M}\Big)^2 + \xi\Big(\frac{\Delta r_i}{r}\Big)^2\Big], \tag{8}$$

where x_i is the atomic fraction of point defect i, r the average ionic radius, M the average mass, Δr_i and ΔM_i are the difference in ionic radius and mass between an impurity i and a matrix, respectively, and $\xi = 39$ according to Abeles [62], but can be taken as an adjustable parameter.

In case of mixture of two kinds of compounds A (e.g. UO_2) and B (e.g. Cr_2O_3), equation (8) becomes

$$\Gamma = x(1-x)\Big[\Big(\frac{\Delta M}{M}\Big)^2 + \xi\Big(\frac{\Delta r}{r}\Big)^2\Big], \tag{9}$$

$$\Delta M = M_A - M_B, \tag{10}$$

$$\Delta r = r_A - r_B, \tag{11}$$

$$M = xM_A + (1-x)M_B. \tag{12}$$

From these relations we see that the larger is the mass (or the ionic radius) difference between the UO_2 and the dopant, the larger would be Γ. Comparison between the values for

dopants Cr_2O_3 and Gd_2O_3 are listed in table 3. Hence, adding Cr_2O_3 has a closer λ_p to UO_2 than adding Gd_2O_3. A usable correlation based on equation (7) is given in Appendix A for UO_2 with the additive Gd_2O_3. In addition to the phonon contribution to the thermal conductivity, there is an additive electronic term λ_e from the transport of heat by electrons, which is considered to be impurity (dopant) independent and it becomes effective at temperatures beyond 1800 K. Uranium dioxide, being classified as a Mott-Hubbard insulator, its λ_e temperature dependence is rather subtle [63, 64]. Despite this, Ronchi et al. [65] based on the theoretical analysis of Casado et al. [63] and the experimental work of Killeen [10] have obtained a usable formula for λ_e in the form

$$\lambda_e = \frac{A_0}{T^{3/2}} \exp(-\epsilon/k_B T) \tag{13}$$

where A_0 and ϵ are constants given in Appendix A for UO_2.
At high temperatures ($T \geq 2000$ K), there is also radiative heat transfer due to diffusion of photons, which may contribute to the thermal conductivity of fuel. This term varies with temperature as $\lambda_r \propto T^3$. However, analysis by Young [66] indicates that for UO_2 $\lambda_r << \lambda_e$, and hence we ignore it here.
In figure 9, the thermal conductivity is plotted as a function of temperature for UO_2 and doped UO_2 for several concentrations of dopants. The correlation, based on the aforementioned theory, for $(U_{1-y},Gd_y)O_2$ is used with adjusted weights for Gd_2O_3. It is seen that as the concentration of dopant is increased, the thermal conductivity is decreased for temperatures below 800 K. Nevertheless, this decrease in thermal conductivity is insignificant for dopant concentrations up to 2000 wppm. We should nmention that fuel porosity (or density) also will affect the thermal conductivity. A denser, less porous fuel gives a higher thermal conductivity than a lighter one. The applied thermal conductivity correlation is listed in Appendix A.

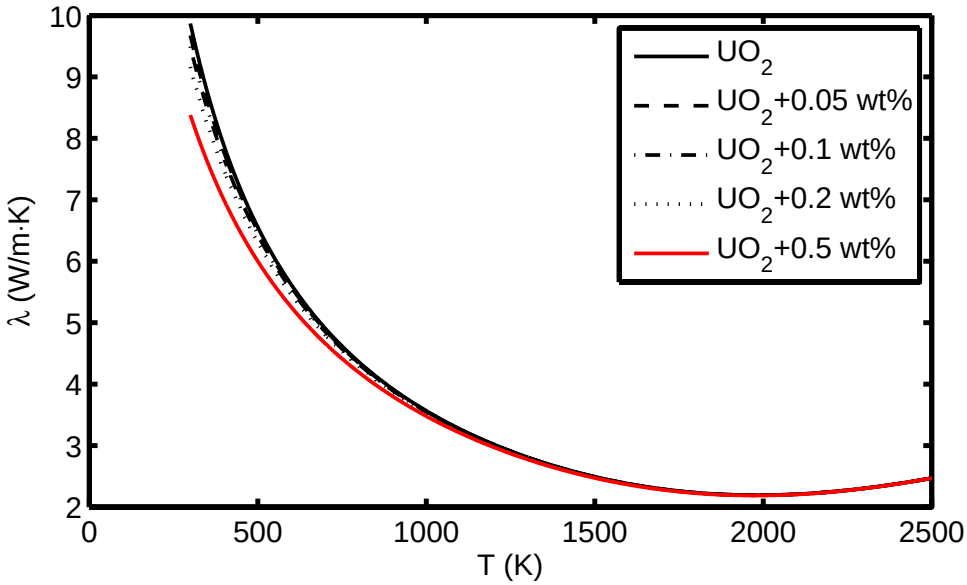

Figure 9: Calculated thermal conductivity λ of UO_2 versus temperature as a function of dopant (M_2O_3) mass content, see Appendix A.

Table 3: Mass and ionic radius difference between UO_2 and dopants calculated according to eqs.(10)-(12) for $x = 0.998$, see e.g. [26].

Formula	M_i	$\Delta M/M$	Ion	r_i (Å)	$\Delta r/r$
UO_2	270.07	...	U^{4+}	0.93	...
Cr_2O_3	152.02	0.437	Cr^{3+}	0.64	0.312
Gd_2O_3	362.50	-0.342	Gd^{3+}	0.94	-0.011

We mention next the thermal conductivity of magnesium doped UO_2 determined by Fujino et al. [67] as a function of temperature for Mg concentrations of 0, 5, and 15 at.%. Fujino et al. [67], within a large program on irradiation behavior of Mg doped (and also Mg-Nb doped and Ti doped) UO_2, made thermal diffusivity measurements of the unirradiated and irradiated fuel pellets. They used laser-flash method for that purpose. The temperature was measured by In-Sb infrared detector. Measurements were made at every 200 K from 473 to 1673 K.

The thermal conductivity is the product of thermal diffusivity and heat capacity. In more detail, $\lambda = \nu\rho C_p$, where ν is thermal diffusivity, ρ the bulk density and C_p the heat capacity of the specimen. The heat capacity was not measured by Fujino and colleagues but calculated (approximately) by combining that of MgO and UO_2 using a mixing rule

$$C_p(\mathrm{Mg}_y\mathrm{U}_{1-y}\mathrm{O}_{2-y}) = yC_p(\mathrm{MgO}) + (1-y)C_p(\mathrm{UO}_2), \tag{14}$$

where separate heat capacity data for MgO and UO_2 were used from the literature [67]. Based on these measurements and calculations, a relationship for thermal conductivity (phonon contribution) as a function of temperature and Mg concentration in UO_2 was established (Appendix A). Figure 10 depicts this correlation for unirradiated samples (UO_2 with 96%TD) for several Mg concentrations. It is seen that the conductivity first decreases with Mg concentrations up to 5 at% Mg-UO_2, then raises again and exceeds that of UO_2 at 15 at% Mg-UO_2. The irradiation (burnup) reduces the thermal conductivity in a usual way, e.g. see [68]. It can be argued that at low Mg concentrations, the thermal conductivity is reduced by phonon-impurity scattering, while at higher Mg concentrations, samples are largely composed of MgO and UO_2, and the former compound has a higher thermal conductivity than the latter.

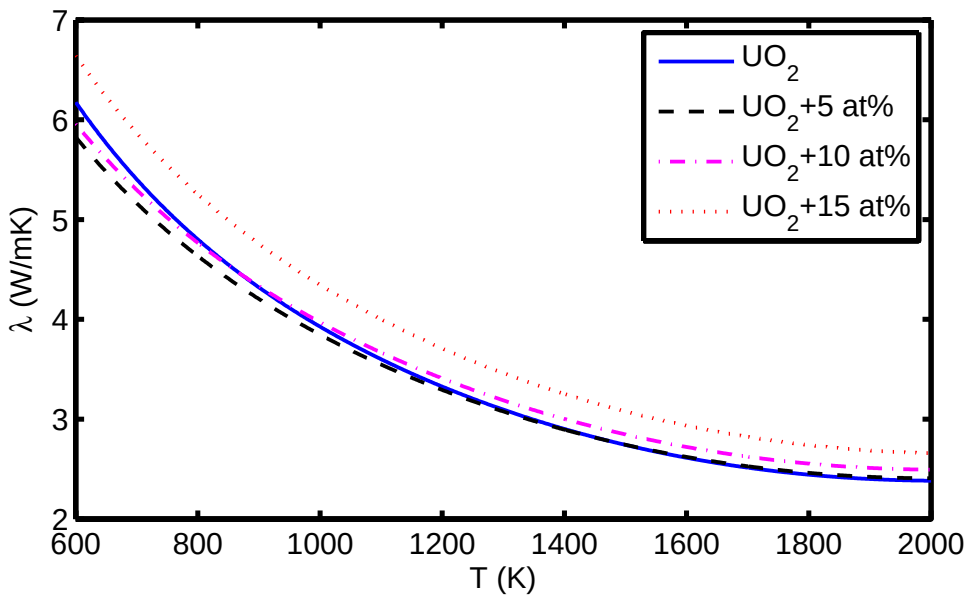

Figure 10: Calculated thermal conductivity λ versus temperature of UO_2 as a function of dopant (Mg) content, see Appendix A.

4 Fission gas behavior

Fission product gases Xe and Kr comprise roughly 13% of the fission products, and are insoluble in UO_2 fuel [30, 69]. At reactor operating temperatures, the gases migrate to fuel grain boundaries, dislocation loops or preexisting pores where they aggregate into bubbles. A portion of these gases, primarily through the grain boundary gas bubble interlinkage, escape to free surfaces of the fuel [70]. The amount of fission gas released depends crucially on the operating conditions (linear power density and fuel burnup) and is a subtle and important part of the fuel rod design. Nevertheless, due to modest power ratings and restriction on linear heat generation rate (LHGR) versus fuel burnup (thermal-mechanical operating limit), most UO_2 fuel in LWR core retain 95% and more of its gas. As pointed out by Lassmann and Benk [71] the fission gas behavior needs to be embraced in fuel rod analysis because:

- The fission gases xenon and krypton degrade the thermal conductivity of the backed-filled helium gas inside the fuel rod, decreasing the gap conductance and thereby elevating fuel temperatures. Enhanced fuel temperatures may further increase fission gas release and may even initiate an unstable process called "thermal feedback."
- The release of fission gases increases the rod internal pressure. This pressure increase may limit the design life of a fuel rod since the inner pressure should not exceed a prescribed pressure.
- The swelling due to gaseous fission products may lead to enhanced pellet-cladding mechanical interaction, especially during anticipated or postulated reactor transients, which may cause fuel cladding failure.
- The release of radioactive gases from UO_2 to the free volume of fuel rod would decrease the safety margin of a nuclear plant. In this regard, the nuclear fuel matrix is considered as the first barrier to the release of radioactive fission products [72].

Hence, an assessment of fission gas behavior in various UO_2 doped fuels is prudent and indispensable. Since the concentrations of dopants are usually quite low in UO_2, the main effect of additives is on the fission gas diffusivity and the fuel grain size, which in turn affect gas release [6].
In this section, we first assess fission gas diffusivity data reported in the literature for some UO_2 doped fuels, where appropriate correlations are compared against those for undoped UO_2 as a function of temperature. Next, these correlations are used in a fission gas release and a gaseous swelling model to evaluate gas release and fuel swelling as a function of irradiation time at different constant fuel temperatures. Moreover, the effect of grain size is studied. The considered additives include Cr_2O_3, Al_2O_3, and Nb_2O_5.

4.1 Fission gas diffusivity in UO_2-base fuels

As noted in section 3, additives alter the stoichiometry or the oxygen to uranium ratio of UO_2 fuel. The effect of the O/U ratio on the fission gas diffusion has been studied and assessed by a number of investigators in the past, see e.g. [25, 73–75] and references therein. They indicated that the fission gas release rate from hyperstoichiometric UO_{2+x} is higher than that from stoichiometric UO_2. On the other hand, the gas diffusion coefficient is lowered in hypostoichiometric UO_{2-x} relative to UO_2.

The effect of additives on diffusion coefficient of xenon has been investigated by Matzke [2, 25, 76] and Long et al. [77]. Matzke obtained gas release curves of radioactive xenon from UO_2, doped with 0.1 mole% Nb_2O_5, Y_2O_3, La_2O_3 or TiO_2. The xenon was introduced by ion bombardment technique and reactor irradiation. Also, he obtained the uranium self-diffusion coefficients in the same specimens. The fission gas release data were obtained following a short reactor irradiation at elevated temperatures after a fast release (burst) within the first few minutes. The cumulative gas release fraction increased linearly with the square-root of time or $t^{1/2}$. This part of the release was used to evaluate the diffusion coefficients (see below). Matzke's results are summarized in table 4. From the fact that the doping did not affect appreciably the xenon release in the specimens at low doses, 5×10^{20} fissions/m^3, whereas it greatly enhanced the uranium diffusion, Matzke concluded that xenon does not diffuse in uranium or oxygen vacancies.

Table 4: Ratio of Xe diffusivity in fuel containing 0.1 mol% additives to that for pure UO_2 determined upon irradiation to low dose; from Matzke [76].

Fuel Oxide	Fission density fissions/m^3	Temperature 1400°C	1550°C
UO_2+Nb_2O_5	5×10^{20}	0.32	1.29
UO_2+Y_2O_3	5×10^{20}	0.79	1.00
UO_2+La_2O_3	5×10^{20}	0.37	0.93

Experiments by Long et al. [77] indicated that the diffusion coefficient of xenon from UO_2 doped with 10-30 mol% Y_2O_3 appeared to be about 20-50 times larger than that from undoped UO_2. MacDonald [78] and Killeen [6, 79] indicated no reduction in the fission gas release rate for the large grain UO_2 fuels (grain size: 50-100 μm) doped with 0.1 wt% TiO_2, 0.4 wt% Nb_2O_5, or 0.5 wt% Cr_2O_3, when compared to undoped fuels (grain size: $< 10\,\mu$m). To clarify these results, these workers suggest enhanced fission gas diffusions in the doped fuels. Nevertheless, it is believed that at higher fuel burnups, the diffusion coefficient of the fission gases in additive fuel may become similar to that in undoped UO_2, since solid fission products soluble in the UO_2 lattice such as rare earth elements and zirconium are accumulated in higher concentrations than in initial additive concentrations.
Nonetheless, since none of these past experiments were conducted at controlled oxygen potentials, no definite conclusions on the effect of additives on fission gas behavior could be drawn. For this reason, a new set of more careful experiments were conducted in Japan by Une and his coworkers to quantify the effect of additives and the oxygen potential on fission gas diffusion and release in and from UO_2 fuel [5, 11, 41].

4.1.1 Specimens

In the first series of ^{133}Xe diffusivity measurements (1987), Une and company [41] prepared specimens by mixing 0.5 wt% Nb_2O_5 and 0.20 wt% TiO_2 with UO_2 powder, followed by pressing and sintering in hydrogen gas at 1750°C for 8 h for the Nb_2O_5 mixture and at 1700°C for 2 h for the TiO_2 mixture. Undoped UO_2 pellets were sintered in H_2 at 1700°C for 2 h. In the subsequent 1998 tests, Kashibe and Une [11] studied the effect of additives, Cr_2O_3, Al_2O_3, SiO_2 and MgO, on diffusive release of ^{133}Xe from UO_2 fuel. In the 1998 measurements, Kashibe and Une sintered the undoped and (Cr_2O_3, Al_2O_3 or SiO_2)-mixed UO_2 compacts in hydrogen at 1750°C for 2 h. Whereas, they sintered the MgO-mixed

UO_2 compact in argon at 1660°C for 2 h to form a $(U,Mg)O_2$ solid solution with good homogeneity. Then they annealed it in a slightly oxidizing atmosphere of wet N_2+8%H_2 at 1660°C for 2 h and finally, in a reducing atmosphere of dry N_2+8%H_2 at 1660°C for 2 h to precipitate MgO particles of nanometer size in the UO_2 matrix. In table 5, we summerize the basic material characteristics of these specimens including their Booth equivalent sphere radius a_e; cf. Sec. 4.1.3. More details can be found in the original papers [11, 41].

Table 5: Nominal values of the specimens basic characteristics used by Une et al. for fission gas diffusivity and release measurements, where a_e is the Booth equivalent sphere radius.

Fuel pellet	Content	Grain size	Density	O/M ratio	a_e	Ref.
-	wt%	μm	g/cm^3	-	μm	-
UO_2	...	15	10.71	2.001,2.004	1.88	[11]
+ Nb_2O_5	0.5	NA^a	10.41	NA	2.03	[41]
+ TiO_2	0.2	NA^b	10.68	NA	2.62	[41]
+ Cr_2O_3	0.065	15	10.73	2.002	1.63	[11]
+ Al_2O_3	0.076	30	10.75	2.002	1.73	[11]
+ SiO_2	0.085	17	10.75	2.002	1.28	[11]
+ MgO	0.50	26	10.46	1.999	3.75	[11]

^{a} 110 μm with density 10.8 g/cm^3 in ref. [5]; ^{b} 85 μm with density 10.8 g/cm^3 [5].

4.1.2 Irradiation and annealing

Une and colleagues [11, 41] irradiated the specimens in evacuated quartz capsules for 6 h at a thermal neutron flux of 5.5×10^{13} neutrons/cm^{2}s in the Japan Atomic Energy Research Institute (JAERI) test reactor JRR-4, yielding a total dose of 1.2×10^{17} fissions/cm^3 (4 MWd/tU). After irradiation, the specimens were cooled for a period of 7-10 days to allow the short-lived nuclides to decay.
In the 1998 experiment, Kashibe and Une [11] used Mo capsule containing the irradiated specimen (Cr_2O_3, Al_2O_3 or SiO_2)-mixed UO_2, to heat by induction furnace in a stepwise manner from 1100-1600°C with a heating rate of 1.7°C/s, temperature step of 100°C and a holding time of 1 h. Sweep gas was a high purity He+2%H_2 mixture at a flow rate of 60 cm^3/min. The β-activity, with an energy of 346 keV and half-life of 5.27 d, of released ^{133}Xe during heating was continuously measured within an ionization chamber. After the annealing experiments, the residual ^{133}Xe in the specimen was determined upon dissolving the powder in hot nitric acid. The annealing procedure in Une et al.'s 1987 experiment (Nb_2O_5,TiO_2 with UO_2 specimens) was similar but details were different [41]. The method used by Une and company to determine the xenon diffusivity was that used by Davies and Long [80].

4.1.3 Fission gas diffusivity and release

For post-irradiation annealing experiments, the cumulative fractional release, F, may be related to the equivalent sphere radius, a_e, and the effective gas diffusivity D by the following short time approximation of Booth's equivalent sphere model [81]

$$F(t) \approx \frac{6}{a_e}\sqrt{Dt/\pi}, \tag{15}$$

where the approximation should be valid for $F \leq 0.3$.[4] The equivalent radius is expressed as $a_e = 3/S\rho$ where S is the specific surface area and ρ the bulk density of the specimen. The burst release is usually observed followed by a steady state release. Hence, D can be calculated from the steady state part of a plot of F versus the square-root of time t. The specific surface area S was determined by BET[5] measurements [11, 41].

Kashibe and Une [11] measured fractional release of ^{133}Xe gas during a ≈ 6 h stepwise heating ramp test from 1100 to 1600°C for undoped and (Cr_2O_3, Al_2O_3 or SiO_2)-doped UO_2. The total release obtained in this set of measurements were larger in the order: Cr_2O_3-UO_2 (16.5%), undoped and Al_2O_3-UO_2 (12%), and SiO_2-UO_2 (4.8%). The ^{133}Xe release of the Cr_2O_3-UO_2 at high temperatures of 1500-1600°C was clearly greater than that of undoped and Al_2O_3-UO_2 specimens. In another set of identical measurements the ^{133}Xe release of MgO-UO_2 and undoped-UO_2 were determined. The two specimens had comparable release values. Thus, Kashibe-Une's measurements indicate that the additive Cr_2O_3 enhances the diffusive release of ^{133}Xe and the additive SiO_2 suppresses it. On the other hand, the additives Al_2O_3 and MgO have no appreciable effect on gas release.

Kashibe and Une evaluated the diffusion coefficient of ^{133}Xe for specimens annealed according to the stepwise pattern from 1100 to 1600°C from the least squares fitted gradient of $36D/(a_e^2\pi)$ obtained by the $F^2 - t$ plot of equation (15). In this fitting, Kashibe and Une precluded the 1100°C data since they did not fit well due to a small amount of ^{133}Xe. The obtained results are in the form of Arrhenius relation with different or same coefficients listed in table 6, where we have also included Une et al.'s 1987 results [41] on UO_2-Nb_2O_5 and UO_2-TiO_2 samples.

Some remarks on the results presented in table 6 are merited. The experimentally determined diffusivity for the insoluble Al_2O_3-doped UO_2 and the soluble MgO-doped UO_2 (dissolved concentration: 0.08 wt%) are almost equivalent to that of the undoped UO_2. The diffusivities for these three specimens are approximated by the same Arrhenius relation, see table 6.

The scatter in Kashibe-Une's data from undoped UO_2 samples were within 30%, relative to the corresponding Arrhenius relation. Moreover, the values of diffusion coefficient for the undoped UO_2 obtained by Kashibe-Une's 1998 study [11] was about three times larger than the values reported by Une et al. in 1987 [41] in the temperature range of 1473-1873 K. Compared to the 1987 activation energy of 264 kJ/mol, the 1998 value is slightly smaller, by about 30 kJ/mol. Une and Kashibe attribute this difference in diffusion coefficient for undoped UO_2 to a difference in the annealing pattern. Namely, in the 1998 Kashibe-Une experiments, a stepwise annealing pattern (annealing time 1 h) was used, whereas in the Une et al. 1987 experiments a one-step annealing (12 h) was used. Moreover, Kashibe and Une note that slight differences during the specimen preparation and irradiation may affect the diffusion coefficients for undoped UO_2 in the two experiments. Regarding the doped UO_2 results, Une et al.'s 1987 paper [41] does not provide data on grain size and the O/M ratio of the samples.

In figure 11 Arrhenius plots of ^{133}Xe in undoped and doped UO_2 with various additives per table 6 are compared. Note that the xenon diffusivity in (Al_2O_3 or MgO)-doped UO_2 is the same as in undoped UO_2 according to [11]. Figure 12 compares the temperature dependence of ^{133}Xe in undoped UO_2 with that in UO_2+Cr_2O_3 and UO_2+Nb_2O_5. It is seen that for temperatures below 1500 K, xenon diffusivity in UO_2 is somewhat higher than that in UO_2+Cr_2O_3, while for $T > 1600$ K it is vice versa. However, xenon diffusivity in UO_2+Nb_2O_5 is resolutely higher than in UO_2. It is worthwhile to compare Une's diffusivity for undoped UO_2 (table 6) with the corresponding ones used in the literature, figure 13. In

this figure Dav63 is the Davies and Long xenon diffusivity in UO_2 [80], which is widely used in the literature and usually is attributed to Turnbull et al. [82].

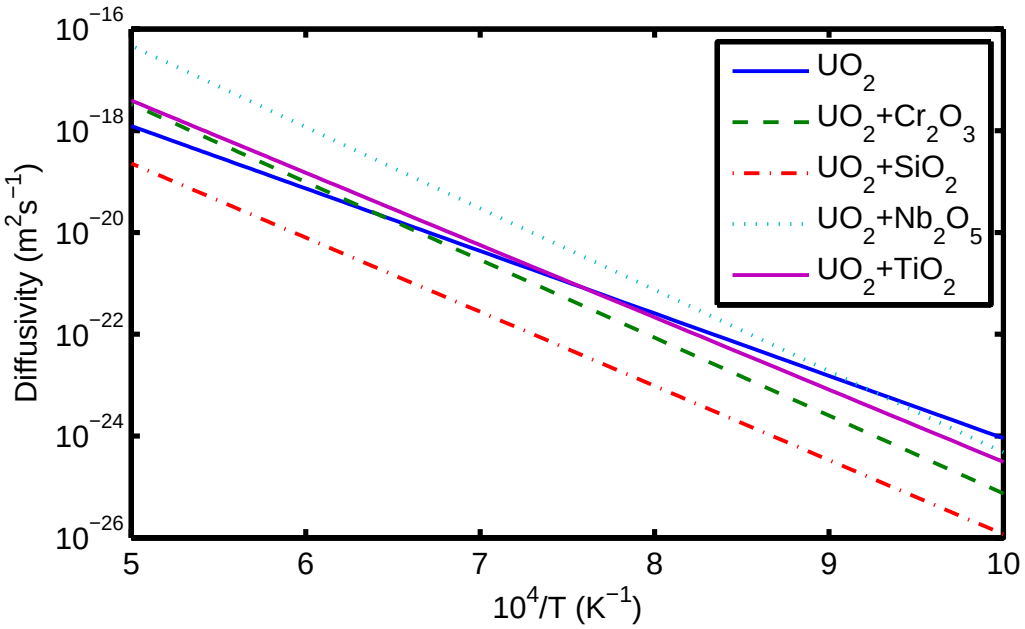

Figure 11: Effective diffusivity of ^{133}Xe versus inverse temperature in undoped and doped UO_2 with various additives in temperature range 1000 to 2000 K, see tables 5 and 6. ^{133}Xe diffusivity in (Al_2O_3 or MgO)-doped UO_2 is the same as in UO_2.

Table 6: Diffusivity of ^{133}Xe in UO_2 with and without additives evaluated from gas release measurements, with $D = D_0 \exp(-Q_D/RT)$.

Fuel	Temperature range	D_0	Q_D	Source
-	K	m^2/s	J/mol	-
UO_2	$1473 - 1873$	1.7×10^{-12}	235000	[11]
+ Nb_2O_5	$1273 - 1873$	4.6×10^{-9}	306000	[41]
+ TiO_2	$1273 - 1873$	5.0×10^{-11}	272000	[41]
+ Cr_2O_3	$1473 - 1873$	1.5×10^{-10}	293000	[11]
+ MgO	$1473 - 1873$	1.7×10^{-12}	235000	[11]
+ Al_2O_3	$1473 - 1873$	1.7×10^{-12}	235000	[11]
+ SiO_2	$1473 - 1873$	4.4×10^{-12}	279000	[11]

4.2 Model computations

In this subsection we present the results of model computations on fission gas release (FGR) and gaseous swelling for some of the fuel types discussed in the foregoing section, including UO_2+Cr_2O_3. The standard model [83–85] for fission gas release through grain-boundary saturation and re-solution is utilized. The grain size, fuel density and gas diffusivity data listed in tables 5 and 6 are used as input to the model. These computations are considered as generic and putative rather than *bona fide*, specific to given experiments or irradiation conditions.

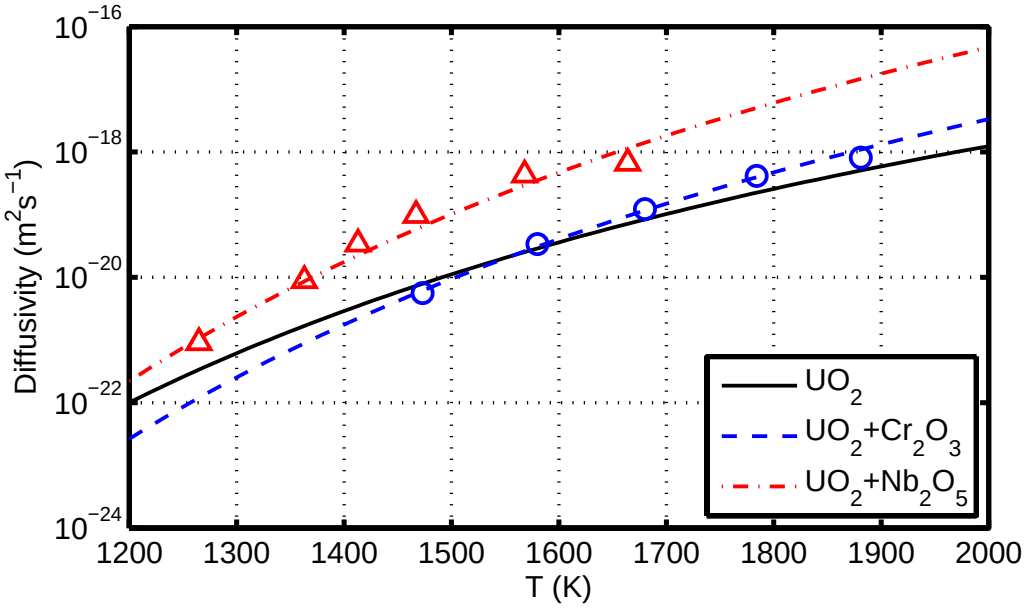

Figure 12: Effective diffusivity of ^{133}Xe as a function of temperature in UO_2, UO_2+0.5wt%Nb_2O_5 and UO_2+0.065wt%Cr_2O_3, see tables 5 and 6.

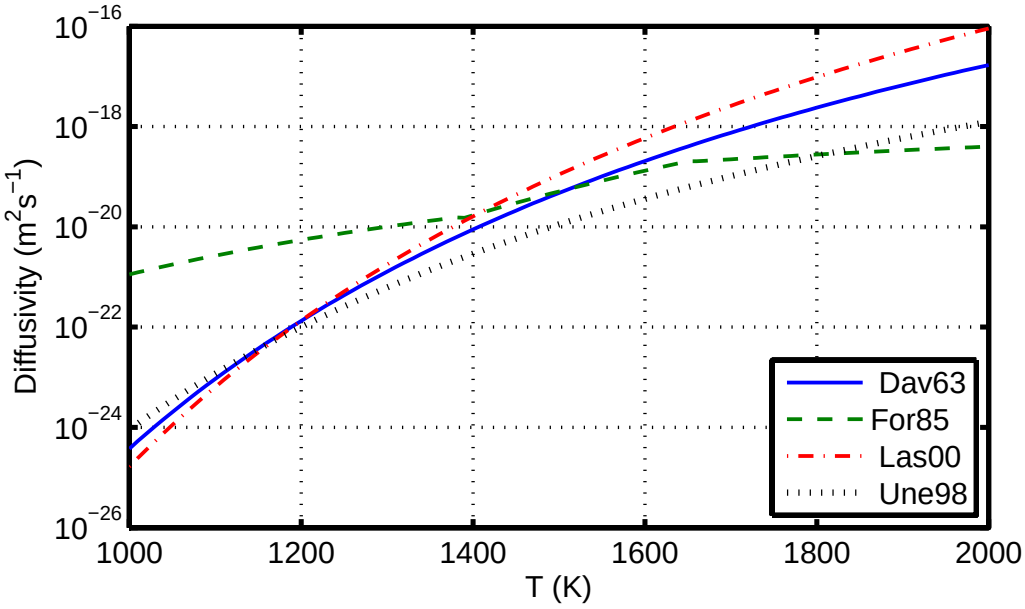

Figure 13: Comparison between various effective thermal diffusion coefficients used for fission gas in UO_2 from the literature, where Dav63 [80], For85 [83], Las00 [71], Une98 [11].

4.2.1 Fission gas release

The equations for the standard fission gas release model through grain boundary saturation and re-solution used in our computations are outlined in Appendix B. The input data to the model, except those for gas diffusivity, fuel density and grain size which are given in tables 5 and 6 or otherwise specified, are listed in table B1 of Appendix B.
Let us first calculate the threshold for the onset of thermal gas release using the aforementioned model, where threshold temperature vs. irradiation time (or fuel burnup) is evaluated. We compare the behavior of undoped UO_2 and UO_2+Cr_2O_3 in figure 14. It is seen that for irradiation times less than 5000 h, the threshold temperature for UO_2+Cr_2O_3 is below that of undoped UO_2, in conformity with the diffusivity results displayed in figure 12. Here, for fission gas production rate, a linear power density (or LHGR) of 27 kW/m was used, cf. table B1, Appendix B.

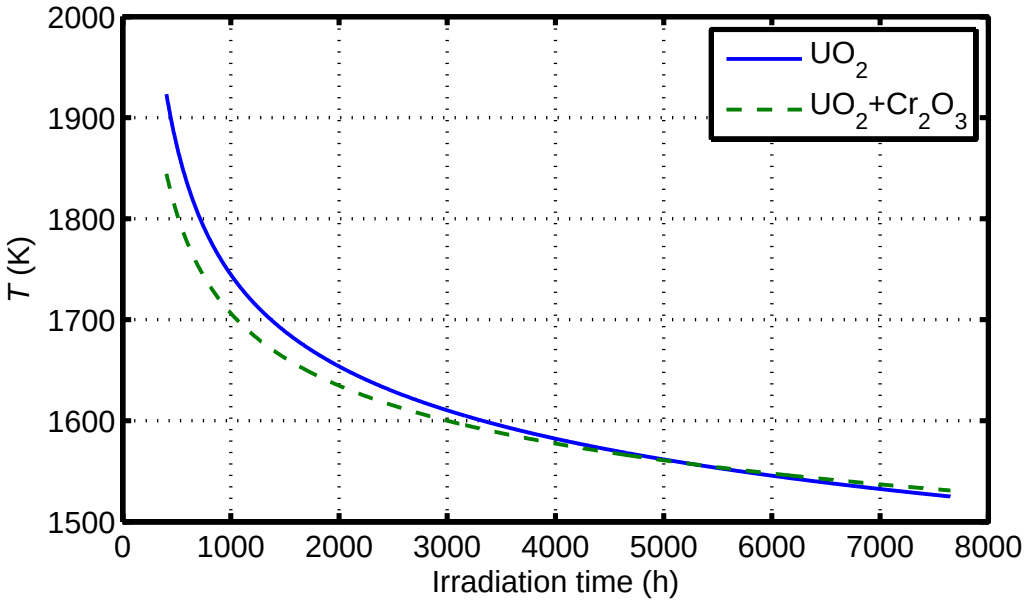

Figure 14: Calculated temperature versus irradiation time for the onset of thermal gas release (grain boundary saturation) for two types of fuel using the model outlined in Appendix B.

In a series of figures 15-17, we plot the results of our computations of thermal fission gas release versus irradiation time at several constant local fuel temperatures, 1600-2000 K, for (Cr_2O_3, Al_2O_3, Nb_2O_5)-doped and "pure" UO_2 fuels. It is seen that among these four samples, the Nb_2O_5-doped has the largest FGR while the Al_2O_3-doped the lowest. The relative gas release from the Cr_2O_3-doped sample depends on the temperature, i.e., at 1600 K its release is in the order of that from "pure" UO_2, while at 2000 K it is close to that from Nb_2O_5-doped sample.
We recall that the grain radius for pure UO_2 and Cr_2O_3-doped sample was the same, whereas for Nb_2O_5-doped sample we used a grain radius of 55 μm in our computations, see table 5. To illustrate the impact of grain size on FGR, we have done computations on release from the Cr_2O_3-doped sample for several grain sizes. The results at 1800 K are shown in figure 18. The release rate is predicted to be inversely dependent on the fuel grain size.

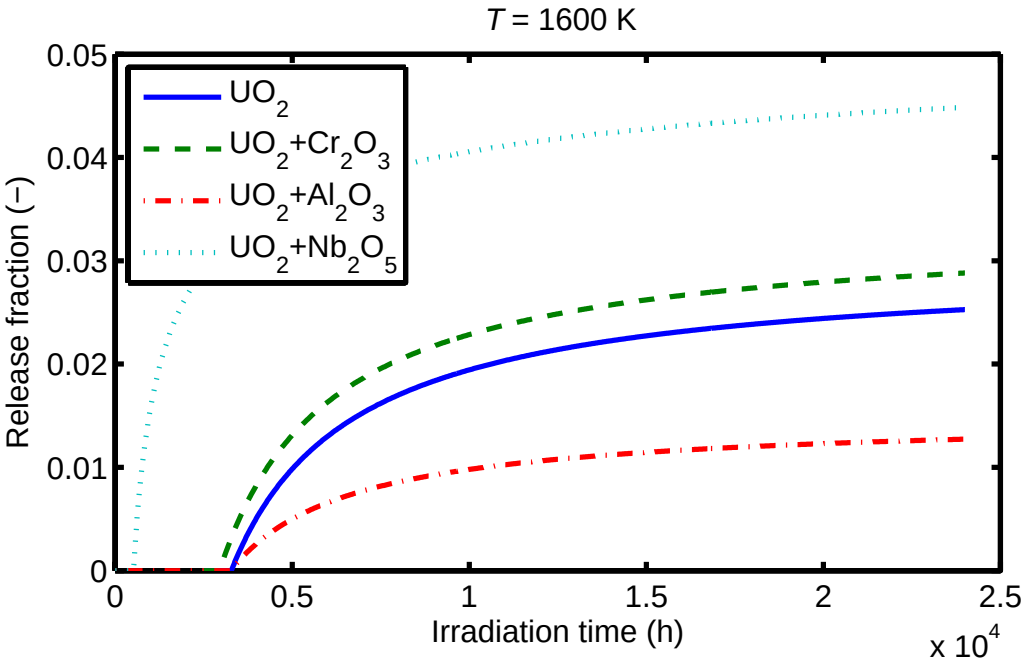

Figure 15: Calculated fractional fission gas release from different UO_2-base fuels at a constant temperature of 1600 K, using the model outlined in Appendix B.

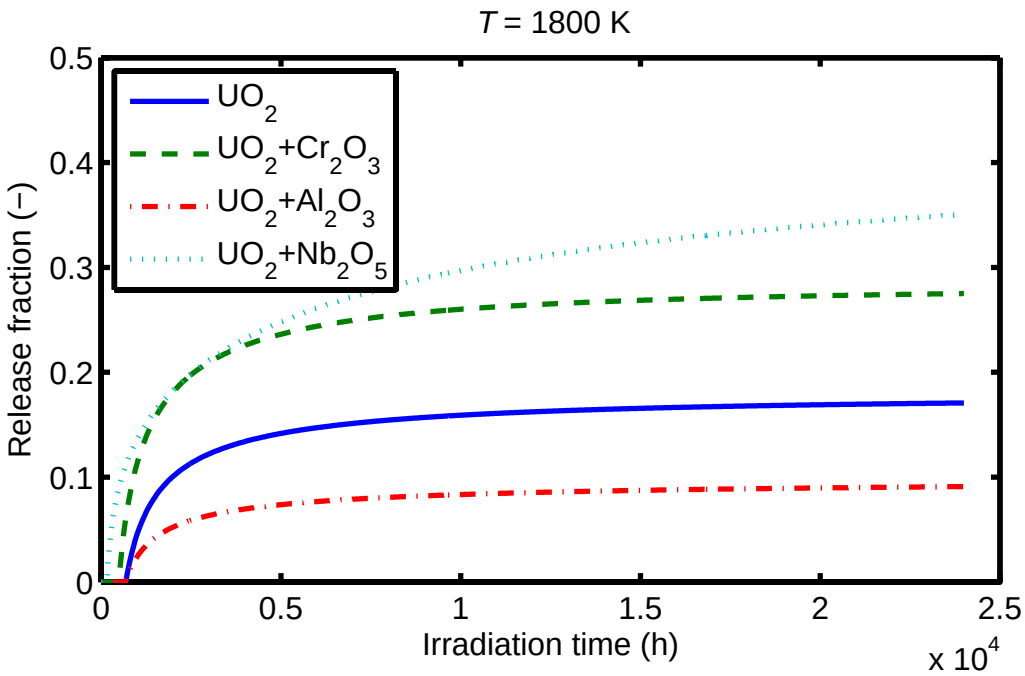

Figure 16: Calculated fractional fission gas release from different UO_2-base fuels at a constant temperature of 1800 K, using the model outlined in Appendix B.

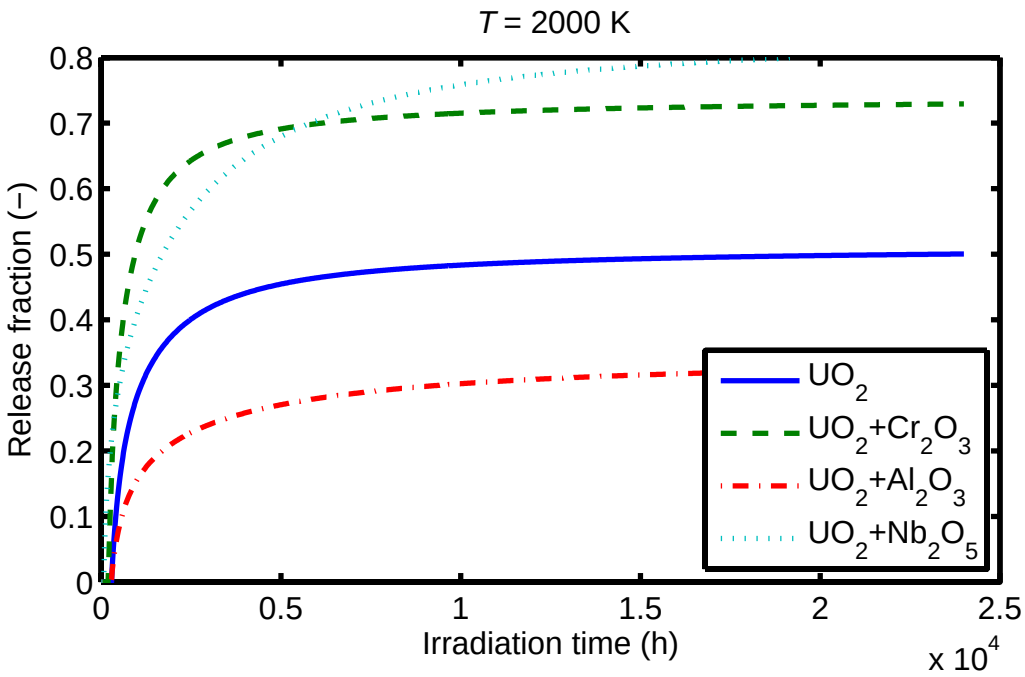

Figure 17: Calculated fractional fission gas release from different UO_2-base fuels at a constant temperature of 2000 K, using the model outlined in Appendix B.

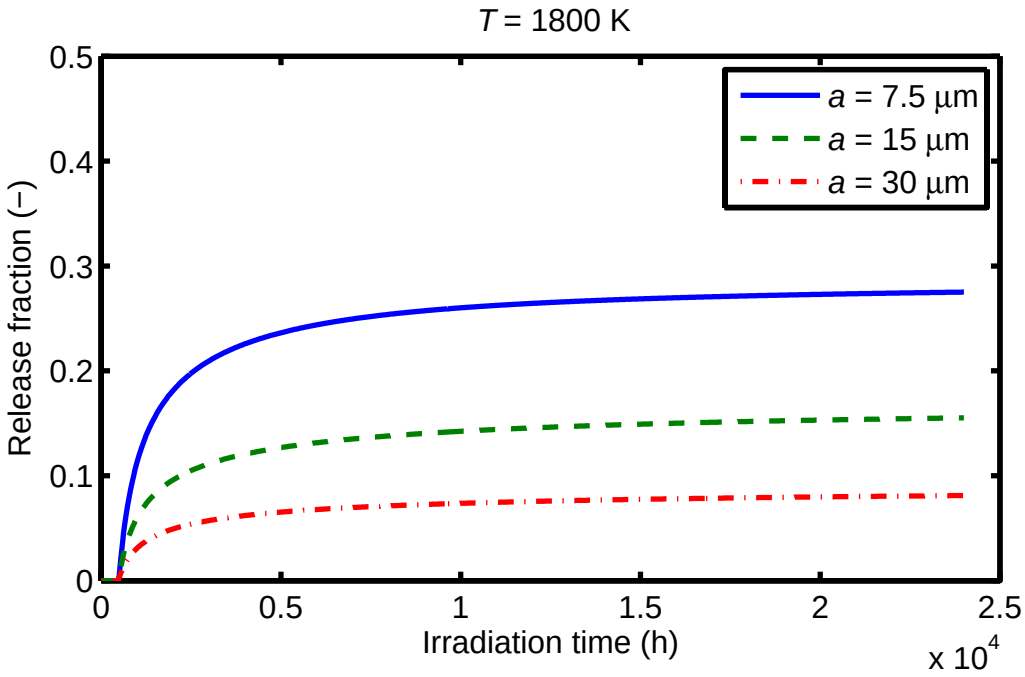

Figure 18: Calculated fractional fission gas release from a Cr_2O_3-doped UO_2 sample at a constant temperature of 1800 K for several grain radii, using the model outlined in Appendix B.

4.2.2 Fuel gaseous swelling

Fuel swelling is the increase in volume by the fission products located in the fuel. The solid fission products are theoretically predicted to contribute to fuel swelling on the average by 0.032% per MWd(kgU)$^{-1}$ [86]. The contribution of gaseous fission products to fuel swelling includes rare gases such as krypton and xenon in solid solution and the volume change arising from the formation of fission gas filled bubbles. For the gases in solid solution and the small intragranular gas bubbles, it is estimated that they contribute about 0.056% per MWd(kgU)$^{-1}$ to matrix swelling rate [87]. The intergranular gas bubbles can make the largest contribution to volume change depending on temperature and their amount. Large fission gas bubbles with diameters around a few microns on grain faces and also along grain edges have been observed [88]. At sufficiently high exposures and temperatures, the bubbles interlink, forming a tunnel network, which concomitantly leads to gaseous swelling and gas release [89, 90].

It is plausible that for the considered UO_2-base fuels, with low concentration of additives, the solid fission product swelling is the same as that for pure UO_2. So here we only evaluate fission gas swelling due to intergranular gas (grain face) bubbles. The model we use here rests on the fission gas release model employed in the foregoing subsection and outlined in Appendix B. The method for computation of swelling is fully described in [91] and hence is not repeated here.

We basically repeat our FGR computations presented in section 4.2.1 for fuel swelling. Figures 19-21 show the relative increase in fuel volume $\Delta V/V$ versus irradiation time at several constant local fuel temperatures, 1600-2000 K, for (Cr_2O_3, Al_2O_3, Nb_2O_5)-doped and "pure" UO_2 fuels. As can be seen, among these four specimens, Cr_2O_3-doped sample has the highest swelling rate, while Nb_2O_5-doped sample has the lowest. It is a combination of gas diffusion, grain boundary saturation and grain size, which yields the present behavior.[6] Note that gaseous swelling saturation is an inverse function of grain size [91]. Figure 22 illustrates this for the Cr_2O_3-doped UO_2 sample. It is also seen that the larger is the grain size, the smaller is the swelling rate and the saturation value.

4.3 Discussion

Let us briefly draw attention to some experimental results regarding the effects of additives and grain size on UO_2 fuel FGR and swelling behavior. In a 1980 paper, Sawbridge et al. [92] report the performance of fuel from an experiment, which was loaded into the Windscale experimental AGR (advanced gas-cooled reactor) in the UK in February 1970, aimed to assess the effects of magnesia (MgO) additions to UO_2 and grain size on fission product release. The fuel elements (assemblies) were discharged unfailed after 1840 effective full power days or EFPD, where the doped fuel pellets had attained burnups between 24.5 and 28.5 MWd/kgU. The details of the fuel rod design, material characteristics and irradiation history are described in [92]. Two fuel elements contained standard UO_2 fuel and two others contained three pins (rods) of experimental fuel doped with 5 mol% MgO, sintered to a density of 10.25 g/cm^3 with a mean linear intercept grain size of about 35 μm. Pre-irradiation measurements suggested that ≈ 0.8 mol% of the MgO was in solid solution in UO_2 with the remainder present as intra- and inter-granular precipitates. The remaining pins contained 97% dense UO_2 with a grain size of about 4 μm (reference design). A number of conclusions could be drawn from this study:

(i) Post-irradiation examination of fuel pins containing large grain sized UO_2 pellets doped

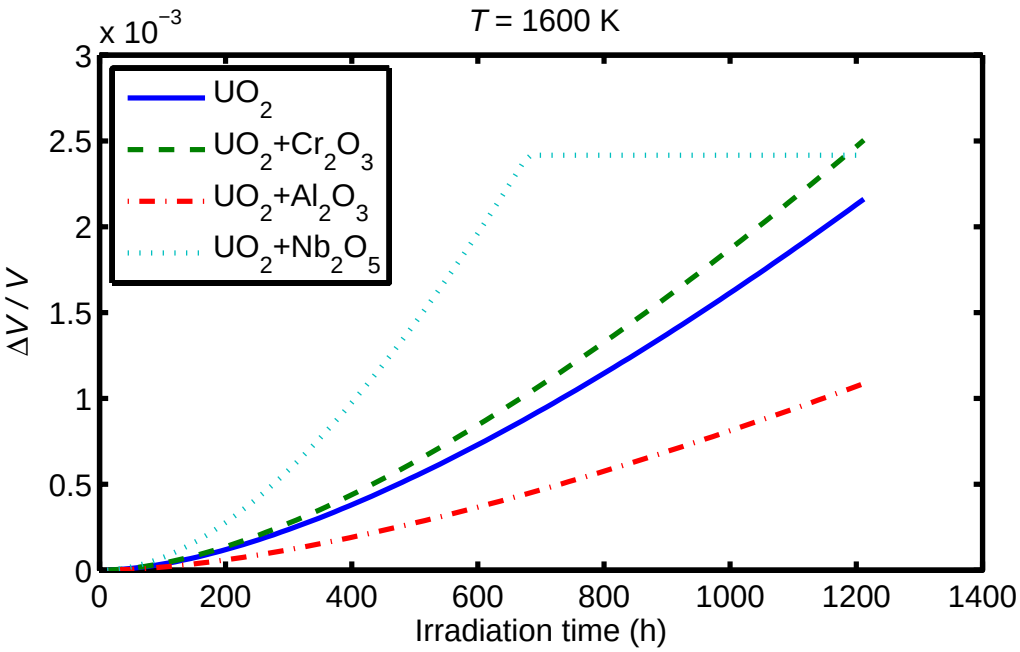

Figure 19: Calculated relative increase in fuel volume versus time for different UO_2-base fuels at a constant temperature of 1600 K, using the gaseous swelling model in [91].

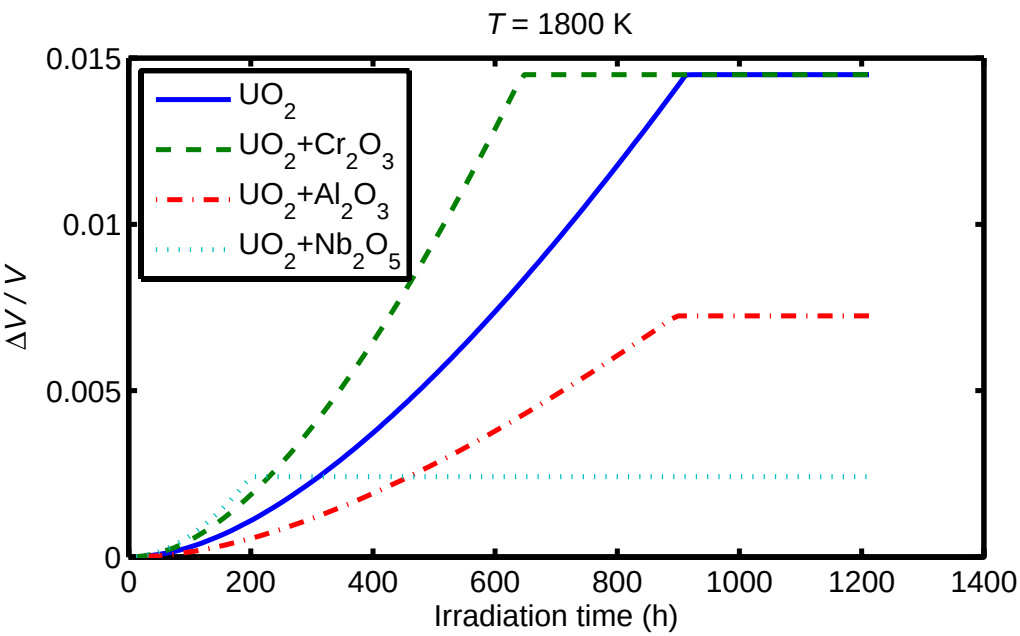

Figure 20: Calculated relative increase in fuel volume versus time for different UO_2-base fuels at a constant temperature of 1800 K, using the gaseous swelling model in [91].

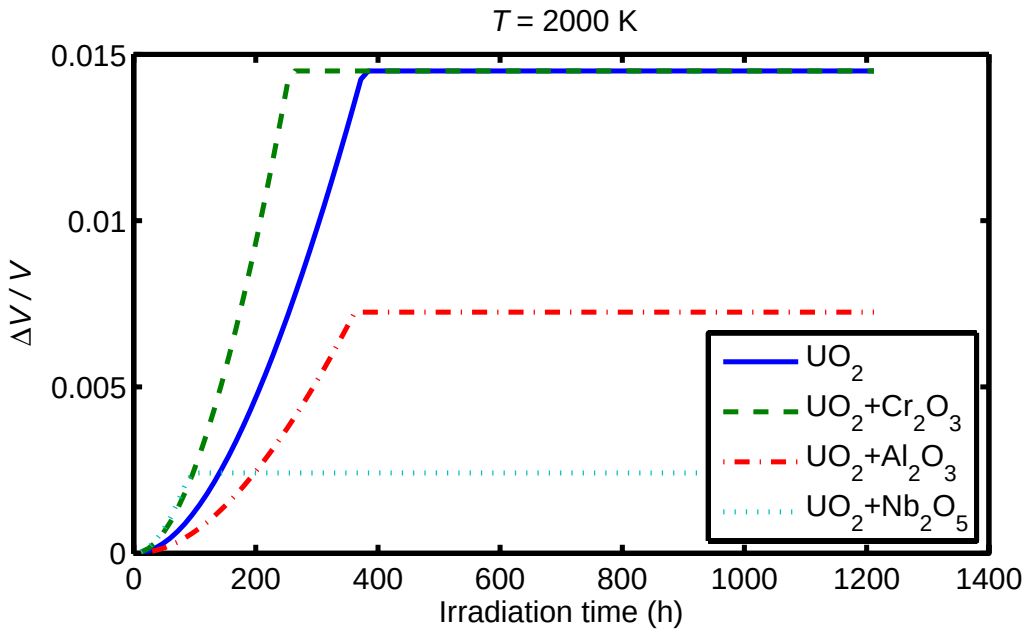

Figure 21: Calculated relative increase in fuel volume versus time for different UO_2-base fuels at a constant temperature of 2000 K, using the gaseous swelling model in [91].

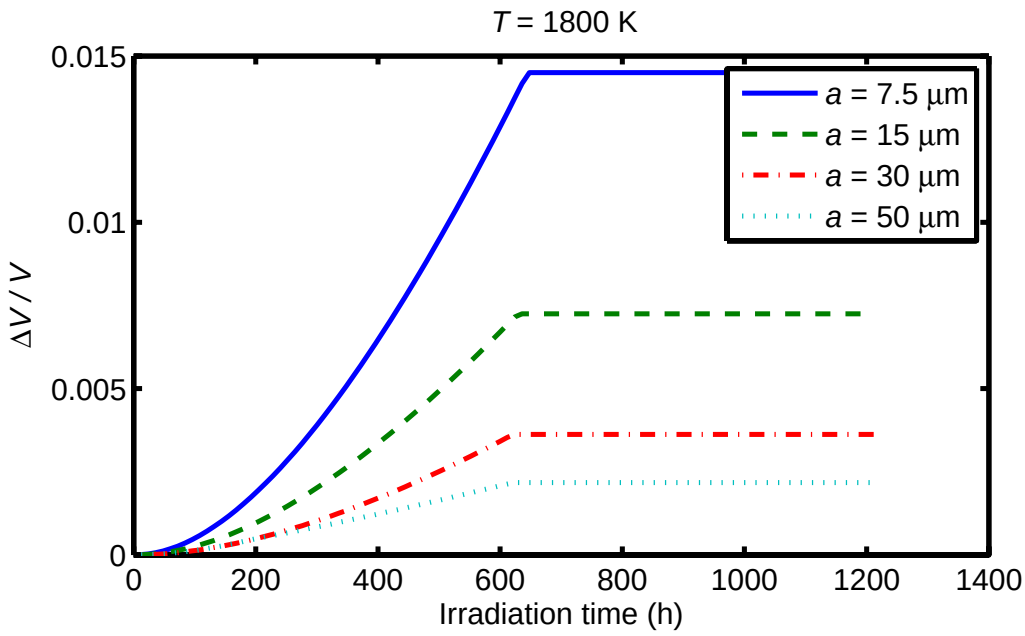

Figure 22: Calculated relative increase in fuel volume versus time for a Cr_2O_3-doped UO_2 sample at a constant temperature of 1800 K for several grain radii, using the gaseous swelling model in [91].

with magnesia and irradiated in the AGR showed that the FGR in the pins containing doped fuel was reduced by a factor of > 2.5 compared with "pure" UO_2 irradiated under identical conditions. (ii) Micro-gamma scanning indicated that there was a much greater retention of ^{137}Cs in MgO-doped fuel than in UO_2 irradiated under identical conditions. (iii) Computer modeling, assuming same fission gas diffusivity for MgO-doped and UO_2 fuel, suggested that the improvement in gas release was largely due to differences in grain size.
Recall that Kashibe-Une's 1998 experiment [11], see table 6, indicated roughly the same ^{133}Xe diffusivity in their MgO-doped and pure UO_2 samples. (iv) No inter-granular gas bubbles were observed in the doped fuel but in the high temperature regions, a high density of large intra-granular bubbles ≈ 0.2 μm in diameter was observed. Sawbridge and company suggest that these large bubbles were stabilized by interaction with the MgO precipitates.
In a related investigation, Killeen in 1994 reported [21] on a series of post-irradiation anneal tests which had been carried out on fuels taken from an experimental stringer from the Hinkley Point B AGR. The stringer was part of an in-reactor study on the effect of large grain size fuel. Three different fuel types were present in separate pins in the stringer. One variant of large grain size fuel had been fabricated by using an MgO dopant in UO_2 with a fuel density of 10.54 g/cm^3, a second variant was fabricated by high temperature sintering of standard fuel, with a density of 10.76 g/cm^3, and the third was a reference UO_2 fuel, with 12 μm grain size and a density of 10.65 g/cm^3. Both large grain size variants had similar grain sizes, i.e. around 35 μm. The experimenters took fuel specimens from highly rated pins from the stringer with local burnups in excess of 25 MWd/kgU and annealed them to temperatures of up to 1810 K under reducing conditions to allow a comparison of fission gas behavior at high release levels. The results showed the favorable effect of large grain size on release rate of ^{85}Kr following gas bubble interlinkage. At low temperatures and release rates, there was no difference between the fuel types, but at temperatures in excess of 1673 K, the release rate was found to be inversely dependent on the fuel grain size. The experiments showed some differences between the doped and undoped large grains size fuel such that in the former the gas bubbles were interlinked at a lower temperature than in the latter fuel, thereby releasing fission gas at an increased rate at that temperature. At higher temperatures, the grain size effect was dominant. The temperature dependence for FGR was determined over a narrow range of temperature and found to be similar for all the three types; for both bubble pre-interlinkage and post-interlinkage releases. The difference between the release rates is then seen to be controlled by grain size. Both Killeen's and Sawbridge et al's results are in qualitative agreement with our analysis.
Finally, it is worth mentioning the 1993 work of Une and coworkers [5], who investigated fission gas behavior of UO_2 fuel pellets with controlled microstructure, irradiated to 23 MWd/kgU in the Halden boiling water test reactor in Norway, by using a post-irradiation annealing experiment. Four types of fuel pellets with or without additives were examined: (i) undoped standard grain size, (ii) undoped large grained, (iii) Nb_2O_5-doped large grained, and (iv) TiO_2-doped large grained (85 μm) fuels. The fuel rods tested by Une et al. had a traditional BWR design. The basic data for the fuel pellets are listed in table 7. The annealing was performed at 1873 or 2073 K for 5 h in reducing or oxidizing atmospheres.
Fission gas release and bubble swelling caused by the high temperature annealing for the two undoped fuels were reduced to about 1/3-1/2 by increasing the grain size from 16 to 43 μm, which roughly corresponded to the ratio of their respective grain size. On the contrary, the performance of the two large grained fuels doped with Nb_2O_5 or TiO_2 was roughly equivalent to, or rather inferior to that of the standard fuel, despite their large grain

sizes of 110 and 85 μm. This may be attributed partly to a much higher diffusivity of fission gases in these doped fuels at high temperatures as noted in section 4.1, see figure 11. The fission gas behavior of undoped fuels was intensified by increasing the chemical potential of oxygen in the annealing atmosphere, while that of additive doped fuels did not depend on it. Une and coworkers found that the diffusivities of undoped large grained and standard fuels were enhanced by about three and one orders of magnitude, respectively, by changing the annealing atmosphere from reducing to oxidizing. They observed that for undoped fuels, intergranular bubble swelling was predominant, while for additive doped fuels, both coarsened inter- and intragranular bubbles contributed to larger swelling. Une et al.'s results on FGR and bubble swelling for microstructure controlled UO_2-base fuels indicate a close relationship between gas diffusion and cation vacancy diffusion [5].

Table 7: Fuel pellet data in Une et al.'s 1993 study [5].

Fuel type	Additive conc.	Grain size	Density	Pelllet Ø
-	wt%	μm	g/cm^3	mm
Undoped standard	...	16	10.6	10.35
Undoped large grain	...	43	10.5	10.35
Nb_2O_5-doped	0.7	110	10.8	10.35
TiO_2-doped	0.2	85	10.8	10.35

Some words of explanation regarding our sample computations on grain boundary bubble swelling (sec. 4.2.2) are in order here. Our computations showed that both swelling rate and the threshold for swelling saturation, which is intimately related to the onset of FGR, are a reciprocal function of the grain size, using the model described in [91]. Regarding the latter quantity, the model gives the swelling saturation by

$$\left(\frac{\Delta V}{V}\right)_{\mathrm{gs}} = B_g f_{\mathrm{b}} \frac{r_{\mathrm{bs}}}{2a}, \tag{16}$$

where B_g is a gas bubble geometry factor, f_{b} is the fractional coverage of grain boundary by the bubbles, r_{bs} is the bubble radius at the onset of interlinkage, and a is the mean grain radius. In the parametric computations in section 4.2.2, we kept all these parameters except the grain radius constant. If, for that matter, r_{bs} is related somehow to the fuel grain size, then that empirical correlation is unknown to us. Computations presented in section 4.2.2 should be regarded as a parametric study to accentuate the influence of grain size on FGR and bubble swelling which, however, seem to conform, in general, with experimental results reported in the literature. Our analysis of gaseous swelling does not include the contribution of intragranular bubbles, which may become important in case of large grain fuel.

The effect of doping UO_2 on its crystal defect structure and its consequent impact on fission gas behavior has been discussed sporadically in the literature [2, 11, 25, 76, 93]. The conventional understanding is that, in general, adding dopants such as Nb_2O_5 should lead to hyperstoichiometric fuel UO_{2+x}, i.e. produce uranium vacancies, while adding trivalent dopants such as Cr_2O_3 or Gd_2O_3 will produce oxygen vacancies and hence hypostoichiometric fuel UO_{2-x}. It has also been known for a long time, based on the work of Miekeley and Felix [73], that xenon diffusivity in UO_{2+x} is much higher than in UO_2 and vice versa in UO_{2-x}. The schematic picture shown in figure 23 illustrates this effect as a log-log plot of fission gas diffusivity versus the fission density (fission/m^3). The reduction in diffusivity

is attributed to the presence of the Frenkel defects (oxygen vacancy-interstitial pairs) and Schottky trivacancies (a cation vacancy and two anion vacancies) [94], which may act as traps to fission product gases [25]. Thus, it is expected that dopant concentration would affect the O/M ratio and that in turn influence the gas diffusivity [75, 95, 96].

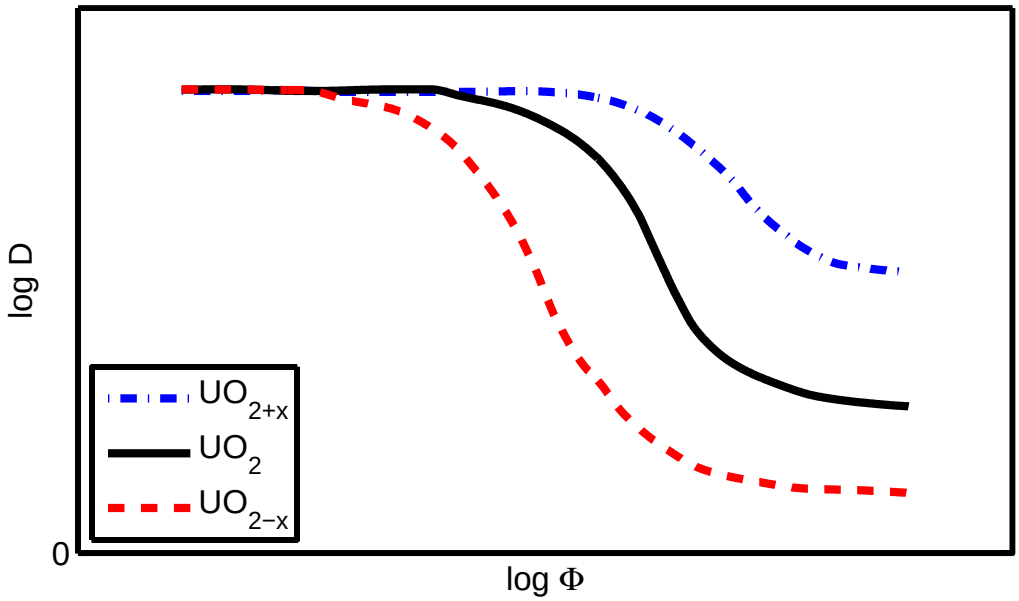

Figure 23: Schematic dependence of gas diffusivity D versus fission density (dose) Φ on the O/U-ratio at constant temperature; after Matzke [25].

The fission gas release rate is roughly proportional to the square root of gas diffusivity $\propto \sqrt{D}$ and inversely to the fuel grain size $\propto 1/d_g$. It has been known that xenon diffusivities in UO_2 and $(Gd,U)O_2$ are markedly lower in hypostoichiometric regime than in hyperstoichiometric regime [73, 93, 97] or in stoichiometric UO_2. So hypostoichiometric $(Gd,U)O_2$ fuel may experience lower fission gas release rate than hyperstoichiometric $(Gd,U)O_2$ or UO_2 even if it posses a smaller grain size than the latter fuels as noted in [97]. In the hypostoichiometric regime, the xenon atoms are considered to get trapped in the Schottky defects [94], thereby reducing the effective gas diffusivity. In hyperstoichiometry, however, the cation vacancies enhance the diffusivity of xenon in UO_{2+x} [95].
Finally, we should mention some results from the work of Hirai et al. [93] regarding fission gas diffusivity in UO_2 and $(U,Gd)O_2$ fuels. These workers, *inter alia*, examined the oxygen-to-metal ratio dependance of diffusion coefficient at 1673 K for these fuels. Figure 24 shows these results for three kinds of specimen, table 8. Below the stoichiometric composition, the diffusion coefficient decreases only slightly, but increases sharply with increasing O/M above and near stoichiometry. The decrease in the diffusivity for G81 specimens are hardly visible from figure 24 due to the log scale of the ordinate. Indeed, the decrease in diffusivity in G81 from about O/M = 2.00 to O/M = 1.99 is 1.78×10^{-19} to 1.45×10^{-19} m^2/s, respectively.

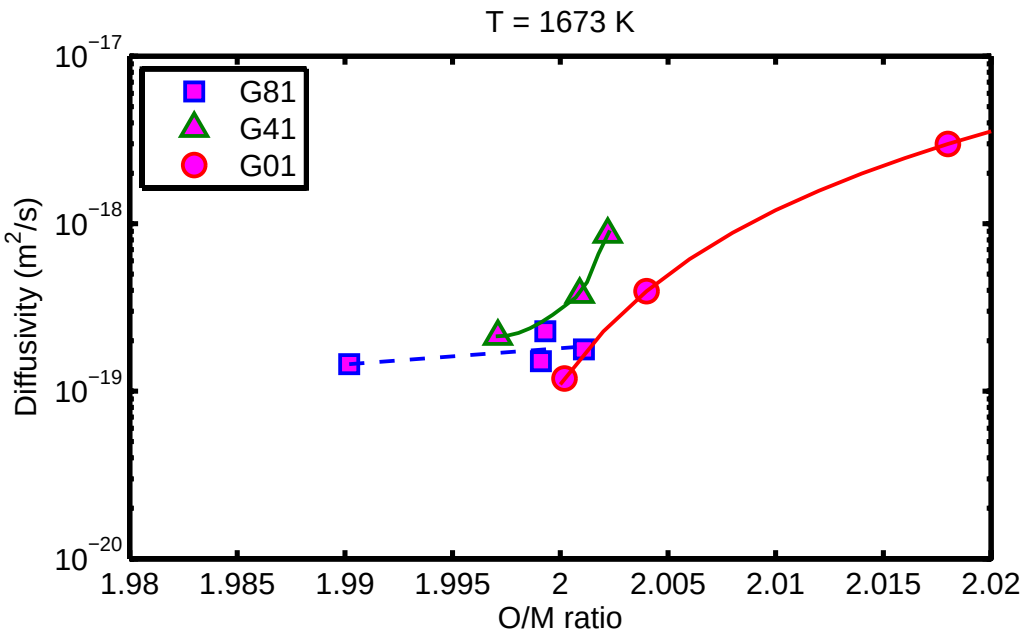

Figure 24: Oxygen-to-metal ratio (O/M) dependence of fission gas diffusivity in (U,Gd)O_2 fuel specimens (table 8), read off from figure 19 of Hirai et al. [93].

Table 8: Fuel data in Hirai et al.'s study [93].

Parameter	Unit	G01	G41	G81
Gd_2O_3 content	wt%	0	4	8
Sintered density	%TD	96.2	96.1	96.1
Grain size	μm	31	29	38
Nominal O/M ratio	-	2.004	1.992	1.996

5 Mechanical properties

Doping of UO_2 fuel to improve its pellet-cladding interaction (PCI) resistance during reactor operation through enhanced fuel plasticity has been discussed in the literature over the years [8, 98]. In this section, we only provide a brief survey of the literature regarding the effect of additives on the thermal creep rate of UO_2 fuel and its yield stress.[7] No modeling effort has been expended to describe this phenomenon. The present SSM version of the fuel performance code FRAPCON-3.3 [99] does not model fuel creep in any form. A very brief survey of both thermal and irradiation-induced creep of UO_2 was made earlier in [100]; a more detailed exposition is given by Olander [86].

A noted work among the early thermal creep studies is the 1981 paper of Sawbridge and coworkers [98] who investigated the creep of UO_2 fuel doped with Nb_2O_5. They investigated the creep of UO_2 containing small additions of Nb_2O_5 in the stress range 0.5-90 MPa at temperatures between 1422 and 1573 K in the Berkeley Nuclear Laboratories, Berkeley, UK. Compression creep tests were carried out under a constant load in atmosphere of flowing purified argon. They report data on the creep rate of seven dopant concentrations from 0.2 mol% to 1.0 mol% Nb_2O_5. The samples examined had different mean (linear intercept) grain sizes, depicted in figure 25.

At high stresses, Sawbridge et al. found a strong dependence of creep rate on stress, typical of dislocation-controlled creep. At lower stresses (< 70 MPa), a roughly linear dependence, typical of diffusion creep was observed. It is the lower stress regions, typified by a linear stress dependence, that are the most significant creep modes under normal reactor operating conditions. Sawbridge et al. established that in all the specimens the secondary creep rate could be represented by the equation of the form

$$\dot{\epsilon} = A\sigma^n \exp(-\frac{Q}{RT}), \tag{17}$$

where $\dot{\epsilon}$ is the steady state creep strain rate (per unit time), σ the uniaxial stress, Q the activation energy, and A and n are constants for each material, and RT has its usual meaning. Sawbridge and colleagues observed that Nb_2O_5 additions can cause a dramatic increase in the steady state creep rate as long as the niobium ion is maintained in the Nb^{5+} valence state. Material containing 0.4 mol% Nb_2O_5 crept three orders of magnitude faster than the "pure" UO_2 material.

Figure 26 shows the variation of creep rate with Nb_2O_5 content, at a temperature of 1523 K and normalized stress of 20 MPa. As can be seen, the variation of creep rate with composition is not smooth. The main reason for this is that the grain size of the different batches of material is not constant, cf. figure 25. To normalize the creep rates, Sawbridge et al. plotted the grain size compensated viscosity η/d_g^2, against Nb_2O_5 concentration. This smoothened the data somewhat, however, we could not reproduce it. The η/d_g^2 term arises, since it was noted that diffusional creep rate varies as the reciprocal square of the grain size d_g, which is in accordance to the Nabarro-Herring creep law [86], namely $\dot{\epsilon} \propto \sigma D_v/d_g^2$, where D_v is the uranium volume diffusion coefficient. The viscosity of a solid is defined as the reciprocal of the shear rate per unit shear stress. In the present case of uniaxial stress, we have $\eta \equiv \sigma/\dot{\epsilon}$.

Instead of depicting the logarithm of fuel viscosity as a function of Nb_2O_5 concentration à la Sawbridge and co., we have scaled the creep data with d_g^2/σ and plotted the results in figure 27. To analyze further, we have considered a model outlined in [98], which utilizes the Nabarro-Herring creep model with the uranium volume diffusivity. In more detail, $D_v = D_{\mathrm{U}}U_v$, where D_{U} is the diffusion coefficient for uranium vacancies and U_v is the uranium

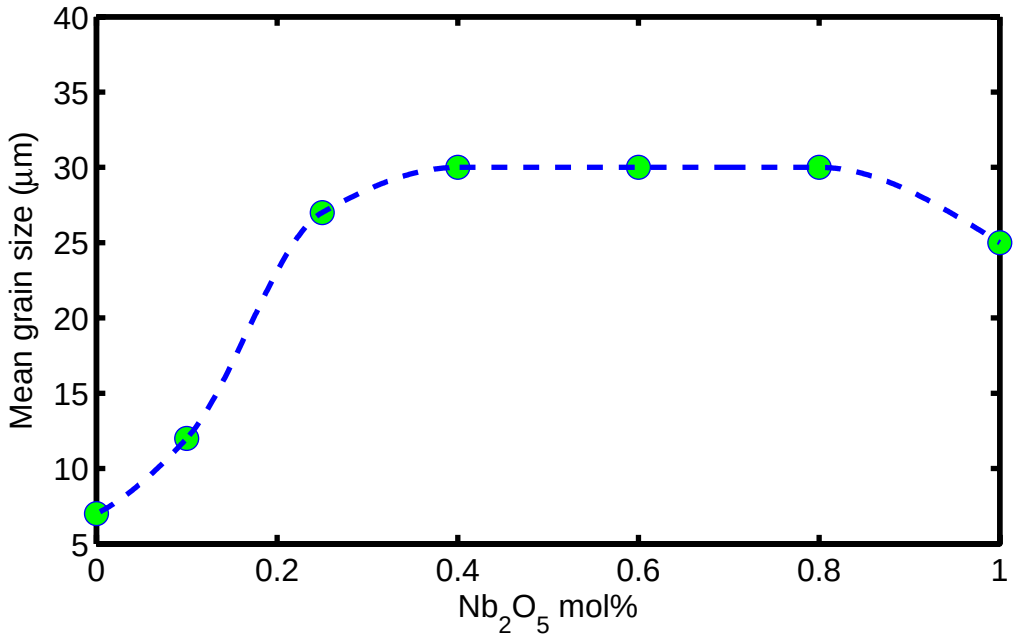

Figure 25: UO_2 fuel grain size versus Nb_2O_5 concentration in samples tested by Sawbridge et al. [98].

vacancy concentration, the latter depending on the concentration (mole fraction) of dopant Nb_2O_5, here denoted by x. Sawbridge et al. derived the following relations for the thermal creep rate of Nb_2O_5-doped UO_2

$$\dot{\epsilon} = A\frac{\sigma}{d_g^2}\exp\Big(-\frac{Q_u+E_2-E_1}{RT}\Big), \quad \text{as} \quad x\to 0, \tag{18}$$

$$\dot{\epsilon} = A\frac{\sigma x^2}{d_g^2}\exp\Big(-\frac{Q_u+E_2-2E_1}{RT}\Big), \text{ for} \quad x>0, \tag{19}$$

where Q_u is the activation energy for the diffusivity of uranium vacancies, and E_1 and E_2 are the formation energies of the Frenkel and Schottky defects, respectively. A more complete derivation is given elsewhere [42].

Unfortunately, the authors of [98] do not provide numerical values for the aforementioned energy parameters; hence, we could not use relation (19) faithfully to evaluate the creep rate data presented in figure 26. Nevertheless, we have attempted to fit the data to a relation in the form $\mathscr{S} \equiv \dot{\epsilon}d_g^2/\sigma$ versus x^2, which may be sensible at $T = 1523$ K and $\sigma = 20$ MPa. The result $\mathscr{S} = 6.65\times 10^{-8}x^2$, where $\mathscr{S}$ has units of [μm^2/MPa·s], is plotted as a dashed line (Nabarro-Herring fit) along the measured data as a function of Nb_2O_5 content in figure 27. *N.B.*, here x is in mole fraction, whereas in the figure $\mathscr{S}$ versus mole% is displayed.

The results in figure 27 clearly show that the Nabarro-Herring fit is quite proper for up to 0.5% mole Nb_2O_5, but it overestimates the measurements for higher concentrations of Nb_2O_5. Likewise, computation made on (logarithm of) fuel viscosity versus x by Sawbridge et al., which is presented in their figure 11 [98], indicates a similar trend.

The main conclusions of Sawbridge et al.'s paper [98] are as follows:

- In the stress range applicable to normal reactor operation, UO_2 doped with Nb_2O_5 deforms by a diffusional creep mechanism (Nabarro-Herring) and the creep rate is

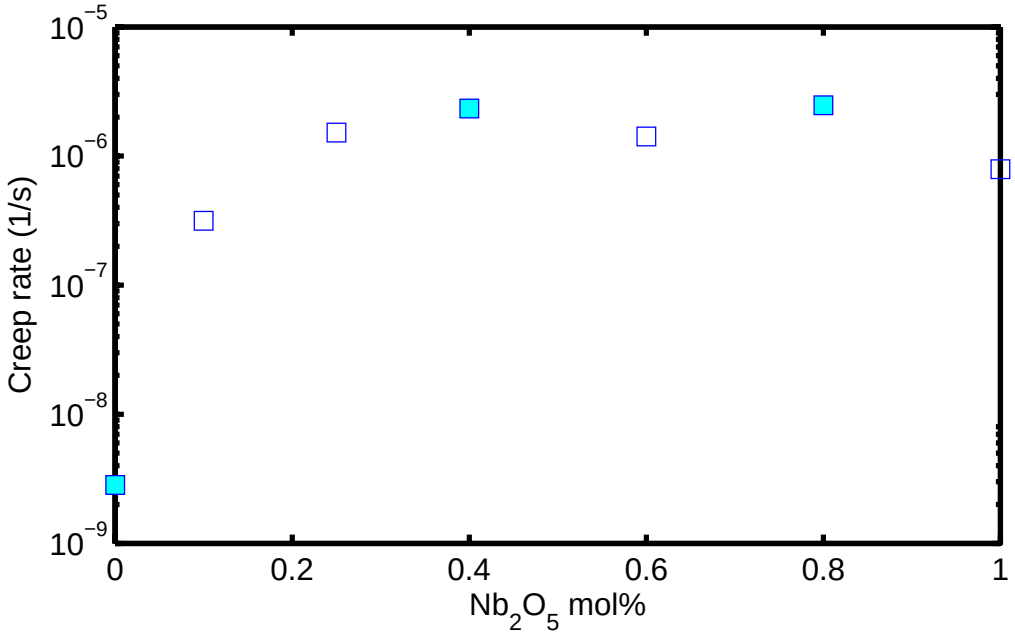

Figure 26: Thermal creep rate of UO_2-base fuel versus Nb_2O_5 concentration at 1523 K and normalized stress of 20 MPa; from Sawbridge et al. [98].

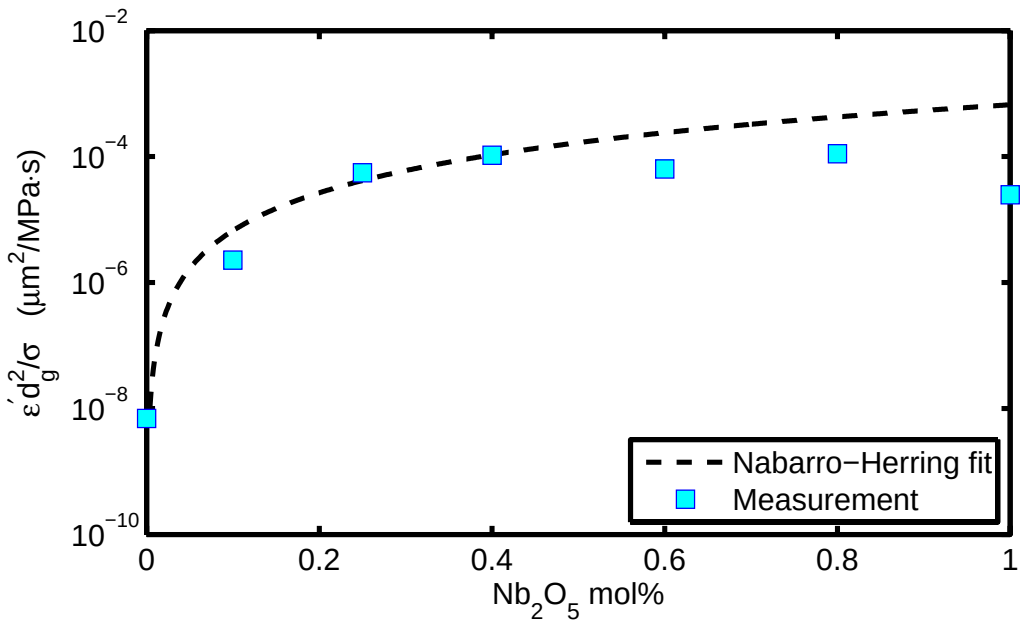

Figure 27: Scaled creep rate of UO_2, with square of grain size divided by stress (20 MPa), versus Nb_2O_5 concentration at 1523 K, based on the data in figs. 25-26 .

linearly proportional to the applied stress.

- The addition of Nb_2O_5 leads to a sharp increase in the creep rate of UO_2. This is credited to the suppression of the U^{5+} ion concentration and the modification of the crystal defect structure by the addition of Nb^{5+} ions.

- The Nb^{5+} ion can be rapidly reduced in atmospheres with a low partial molar free energy of oxygen. When this occurred by switching the test atmosphere from argon to dry hydrogen, the creep rate was reverted to that of undoped uranium dioxide.

Another relevant work on the subject of thermal creep of doped UO_2 detailed here is Dugay et al.'s study [101, 102] on the influence of the dopants Cr_2O_3 and Al_2O_3 on the thermal creep behavior of UO_2 and its yield (flow) stress. Here, their work on Cr_2O_3 dopant is assessed. They tested five batches of PWR-geometry fuel pellets, without dishing. One undoped batch, serving as a reference material, and four doped batches with Cr_2O_3 concentrations ranging from 0.025 to 0.2 wt% in UO_2 were prepared for testing. The mixture of powders was dry blended by ball-milling. The mixture was then sintered under H_2+1.7%H_2O atmosphere at 1700°C, thereby restricting the hyperstoichiometric range of UO_{2+x} to $x = x_{\max} = 5 \times 10^{-4}$ which promoted grain growth. The basic characteristics of the sintered materials are listed in table 9. Grain size was determined by linear intercept measurements.

Table 9: Dugay et al. UO_2-Cr_2O_3 fuel material data [102].

Cr_2O_3 conc. wt%	Fraction of T.D. -	Density[a] g/cm^3	Grain size μm
0.0	0.968	10.62	7
0.025	0.958	10.51	15
0.06	0.970	10.64	27
0.1	0.975	10.70	45
0.2	0.976	10.71	70

[a] UO_2 theoretical density (T.D.) of 10.97 g/cm^3 is used.

Dugay et al. [101, 102] conducted two kinds of tests in a CEA-Grenoble laboratory in France, namely, (i) compression tests under a constant applied strain rate, from which the stress versus strain curves were produced beyond the yield point, and (ii) compression creep tests in which the strain rate as a function of stress level was determined.
The constant strain rate compression tests were done at 1773 K under argon gas with 4% hydrogen to maintain the stoichiometry of the specimens during the experiment. The tests were conducted at a crosshead speed of 20 μm/min. corresponding to a strain rate of 0.09/h. The stress-strain curves presented in [101, 102] show that Cr_2O_3 additions cause a decrease in the yield stress from about 85 MPa (undoped UO_2 specimen) to 70 MPa (0.1 wt% Cr_2O_3) at 1773 K. However, when the doped specimens (with 0.06 wt% Cr_2O_3) were reduced in hydrogen atmosphere at 1773 K for 12 h or 24 h, their stress-strain curves exhibited peaks close to that of the yield stress of undoped UO_2 (≈ 85 MPa), especially the specimen which was reduced for 24 h in hydrogen; see refs. [101, 102] for more details.
All the creep tests were done by compression under argon or reducing (hydrogenated argon) milieu comprising temperatures 1623-1923 K on unirradiated specimens. In particular, measurements of creep rate were made at 1773 K subject to applied stresses varying from

20 to 70 MPa. The Grenoble workers found that Cr_2O_3 additions starkly increase the creep rate relative to that of pure UO_2 in argon atmosphere. All the doped specimens were assumed to follow equation (17) with varying stress exponent n, which varied from 4.9 to 6.3, in contrast to the Sawbridge et al.'s measurements on Nb_2O_5-doped UO_2, which exhibited $n \approx 1$ dependence. In table 10, we have listed the creep parameters given in [102], which the authors apparently have taken from the 1773 K data. Moreover, we have included in this table the values of the creep model parameter A that we deduced from the creep-rate data presented in [102] at 1773 K and 45 MPa. We have also narrowed the stress range of applicability for the doped specimens compared to [102], which is ranged from 30-65 MPa, based on our own evaluation of data. Dugay et al. [102] also state that doping UO_2 with Al_2O_3 would lead to similar observations.

Table 10: UO_2-Cr_2O_3 creep model[a] parameters at 1773 K from [102].

Cr_2O_3 conc. wt%	Stress range MPa	A^b (MPa)$^{-n}$s^{-1}	n -	Q kJ/mol
0.0	20-45	1.176×10^{2}	2.1	410
0.025	40-65	9.129×10^{-3}	6.3	487
0.06	40-65	5.919×10^{-3}	6.1	466
0.1	40-65	3.625×10^{2}	4.9	551
0.2	40-65	1.236×10^{2}	5.2	550

[a] $\dot{\epsilon} = A\sigma^n \exp(-Q/RT)$; [b] Values are determined from measured data at $\sigma = 45$ MPa.

The parameters in table 10 are used to plot creep strain rate as a function of Cr_2O_3 concentration in UO_2 at high temperatures at 45 MPa, figure 28. It is seen that, for example at 1773 K, the creep rate of UO_2-0.1wt%Cr_2O_3 increases roughly by a factor of 5 relative to that of pure UO_2. For pure UO_2, Dugay et al. [102] found that in the stress range 45-60 MPa, $n = 4.8$. Hence, there is a shift in creep mechanism around 45 MPa at 1773 K from $n \approx 2$ to $n \approx 5$. This result is somewhat in agreement with the 1970 work of Langdon on creep mechanisms in pure UO_2 [103], which showed a transition stress of about 40 MPa at 1808 K, at which the stress exponent changed from $n \approx 1$ to $n \approx 4.5$. To compare these results with the thermal creep behavior of niobia-doped UO_2, we should mention the work of Ainscough et al. [7], which showed a transition stress of 20 MPa at 1773 K and an oxygen potential of -423 kJ/mol, where the creep rate stress exponent for UO_2-0.4wt%Nb_2O_5 changed from $n = 1.1$ to $n = 2.4$.

Of course, different creep stress exponents mean different creep mechanisms as classified by Langdon and others. Figure 29, taken from a paper by Langdon [104], illustrates this connection. So one may conclude that Dugay et al.'s data [102] on UO_2 creep behavior, in the stress range 20-45 MPa at 1773, with $n \approx 2$ falls into the superplasticity region, while the UO_2-Cr_2O_3 behavior (40-65 MPa) is in the dislocation climb domain, according to Langdon's classification. The various deformation mechanisms have been clarified by Langdon in [105].

To sum up the work of Dugay et al. [102] on Cr_2O_3-doped UO_2 thermal creep, there is a large scatter in the raw data, and hence difficult to build a usable or an empirical model to describe the thermal creep behavior of this material in the wide range of applicable stress and temperature for various Cr_2O_3 concentrations. Additional and more refined measurements in a carefully controlled laboratory environment are necessary for this endeavor. Moreover, the influence of grain size on creep rate was not examined by Dugay and com-

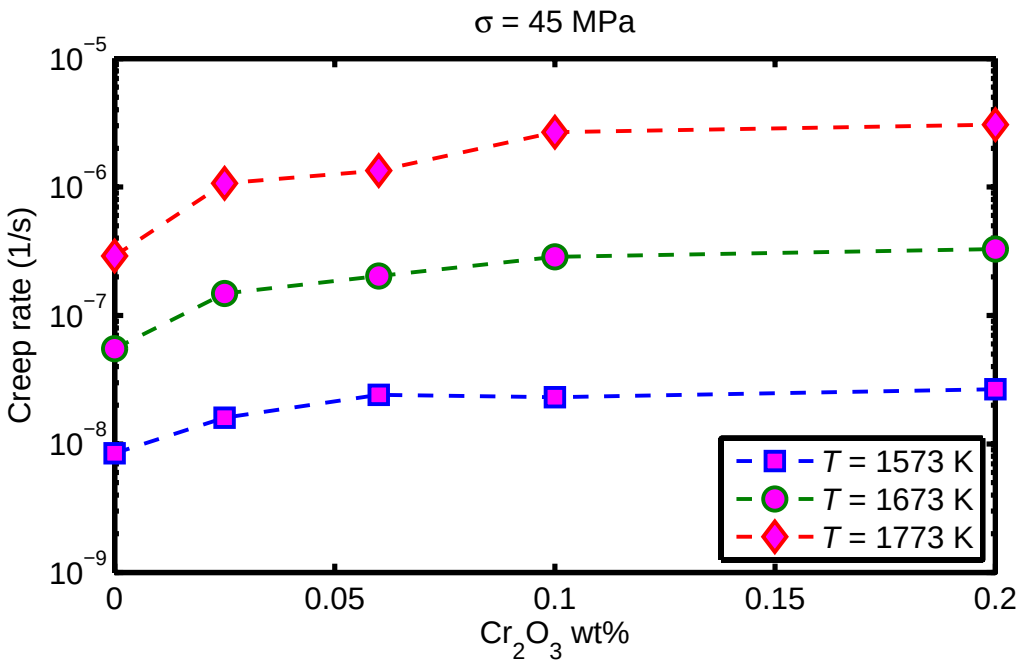

Figure 28: Thermal creep rate of UO_2-base fuel versus Cr_2O_3 concentration at a stress level of 45 MPa using the data in table 10.

pany, which as discussed earlier can be significant.

Thermal creep behavior of Cr_2O_3-doped UO_2 has also been examined experimentally by Nonon et al. [106]. Nonon and company report on creep tests that were performed at 1743 K and 45 MPa, under a controlled atmosphere of argon with 5% hydrogen to prevent oxidation and stoichiometry changes of the samples during the experiment. They compared the creep rate under compression in the same experimental conditions of an undoped UO_2 sample and different Cr_2O_3-doped samples with the dopant concentration varying from 0.075 to 0.225 wt%. They found that addition of Cr_2O_3 increases considerably the creep rate of the material, i.e., by up to a factor of 10. However, this effect saturates at higher additive contents (≈ 0.2 wt%).

Nonon et al. [106] also examined the effect of stress on thermal creep rate. They obtained results at several applied stresses (20 to 60 MPa), under the same experimental conditions ($T = 1743$ K) in order to evaluate a creep law. As in Dugay et al.'s study [102], the steady state creep rate of UO_2 doped with Cr_2O_3 was described by equation of the form (17). Nonon and coworkers only found a single creep regime with a stress exponent value of $n = 4$ and a creep activation energy Q close to the uranium self-diffusion energy in UO_2, which according to Matzke [107] is about 460 kJ/mol. Nonon et al.'s value of $n = 4$ is lower than those found by Dugay and co. for the same material, cf. table 10. Details of the measurements and data are not given in [106].

Other published works on the the creep behavior of doped UO_2 include the study by Rhee et al. [108] on the effect of SiO_2-CaO-Cr_2O_3 or SCC additive and the investigation by Matsunaga et al. [15] on Al-Si-O additive.

Rhee and coworkers conducted compressive creep tests in Ar-5%H_2 atmosphere subject to 20, 35, 50, and 65 MPa uniaxial stress at 1773 K. They observed that the creep rate of the 0.07 wt% SCC-added UO_2 was lower than that of the pure UO_2, whereas, the creep of the

0.22 wt% SCC-added UO_2 was about 3.48 times faster than that of the pure UO_2, depending on the applied stress in the lower stress range (20-35 MPa). In the case of the 0.35 wt% SCC-added UO_2, the creep rate decreased in comparison with that of the 0.22 wt% SCC-added UO_2. They suggested that the increase in the creep rate of the 0.22 wt% material could be due to the enhanced diffusivity through the amorphous intergranular phases and to the low viscosity of the second phase. Whereas, in the case of 0.35 wt% SCC-doped fuel, the creep rate decreased in comparison with the 0.22 wt% SCC-doped material, due to grain size of the 0.35 wt% SCC-added UO_2, which was three times larger than those of the pure UO_2 and the 0.22 wt% SCC-added UO_2 (8 μm).

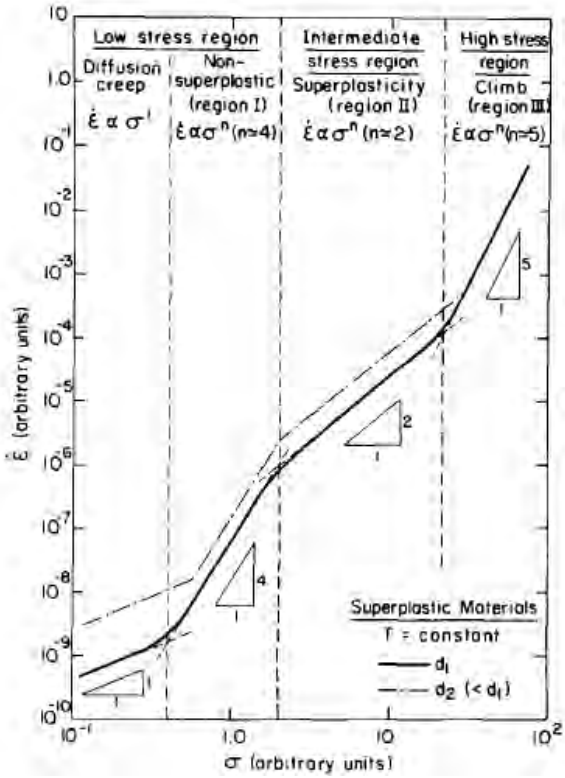

Figure 29: Langdon's schematic diagram of strain rate $\dot{\varepsilon}$ vs. stress σ showing the partition into different regions of creep behavior at constant temperature T. It also shows the effect of grain size from d_1 to $d_2 < d_1$. The relation $\dot{\varepsilon} \propto \sigma^n$ is obtained with $n = 1$ in the diffusion creep region, $n \approx 4$ in the non-superplastic region, $n \approx 2$ in the superplasticity region, and $n \approx 5$ in the climb region; from [104].

Matsunaga et al.'s [15] determined the steady creep rate and the yield stress under uniaxial compression at a constant load in dry 8%H_2+92%N_2 gas flow for (Al-Si-O)-doped UO_2 specimens with a dopant concentration of 0.025 wt%. For the creep test, the applied stresses were about 12 MPa and temperature ranged from 1723 to 1823 K. For the yield stress test, temperature ranged from 1273 to 1673 K, and the strain rate chosen was 0.1/min. Matsunaga et al. showed that the steady state creep rate of (Al-Si-O)-UO_2 fuel is higher than that of standard UO_2; whereas the yield stress of (Al-Si-O)-doped fuel is slightly lower than that of the standard UO_2 fuel and the difference gets larger with increase of temperature, figure 30. At lower temperatures, the Al-Si-O precipitation effect and grain size effect would be balanced, hence the difference in yield stress would be small. At higher

temperatures, the precipitation effect would be reduced due to the softer Al-Si-O phase, according to Matsunaga and coworkers [15].

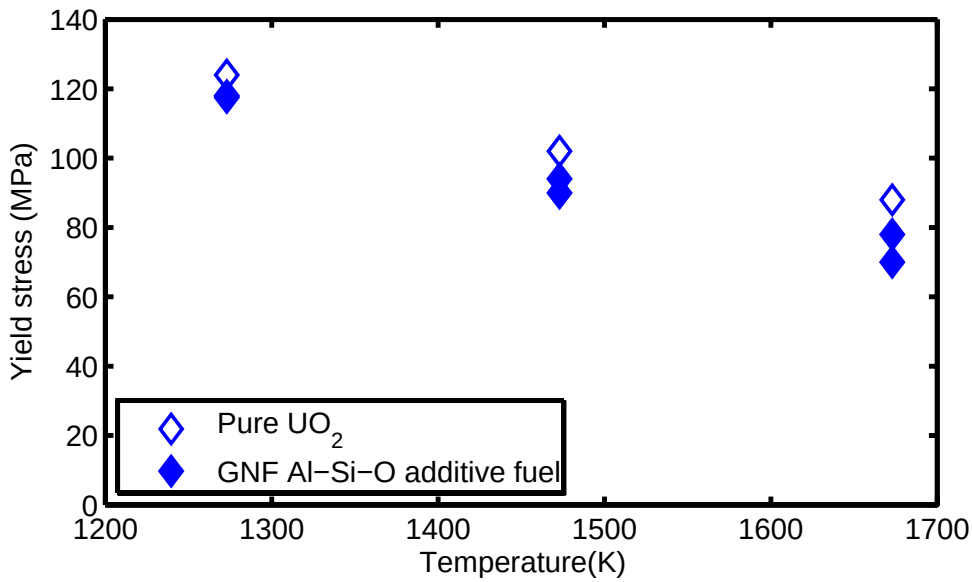

Figure 30: Effect of Al-Si-O additive (0.025 wt%) on yield stress of UO_2; after Matsunaga et al. [15].

6 Irradiation tests and experience

There has been a number of irradiation or "qualification" programs to compare in-reactor fuel performance of UO_2 fuel with additives against that of standard "pure" UO_2. The results of these programs are usually presented in conferences and published in the proceedings and hence, are not subjected to rigorous peer review process commonly exercised for journal publications. As such, the quality of the presentations may vary considerably from one study to another. In this section, we provide a brief survey of some results from these programs as presented in the publications.

Arborelius and colleagues [17] have reported an outcome of a comprehensive demonstration program on doped UO_2 fuel performance. The fuel rods were first irradiated in a boiling water reactor then subjected to power ramps in a test reactor. In this program, two segmented rods containing fuel pellets (table 11) were irradiated at the Barsebäck 2 BWR in Sweden. Each of the two rods consisted of five segments with five different pellet types, Std, Std Opt2 and three variants of doped fuel denoted by D1, D2 and D3 in table 11. The fuel pellets of the rods had a diameter of 8.36 mm with length of 10 mm. The two rods were irradiated in a fuel assembly to a burnup of about 30 MWd/kgU under normal BWR conditions. The rod power history of base irradiation is shown in [17]. The three middle segments of each rod were examined after irradiation at the Studsvik Nuclear laboratories, Nyköping, Sweden. Examination after base irradiation using both the cladding profilometry and pellet-cladding gap measurement at Studsvik Nuclear revealed that the volume change of the pellets was -0.2% for the Std Opt2 pellets and between +0.8 to +1.4% (positive sign $\equiv$ swelling) for the doped pellets D1, D2 and D3. Ceramographic examination performed at mid pellet position on D2 pellets indicated fuel grain growth in the central part of the pellet [17].

Table 11: Fuel types used in a Swedish BWR irradiation program [17].

Specimen	UO_2 fuel composition	Density g/cm^3	Grain size μm	$^{235}U^*$ wt%
Std	UO_2	10.52	10-12	1.7, 2.8
Std Opt2	UO_2	10.60	10-12	4.2
D1	+ 0.1wt%Cr_2O_3	10.66	44	4.2
D2	+ 0.1wt%Cr_2O_3+0.01wt%MgO	10.68	42	4.2
D3	+ 0.1wt%Cr_2O_3+0.02wt%Al_2O_3	10.68	52	4.2

* Uranium-235 enrichment.

Subsequent to the post irradiation examination (PIE), two rod segments, Std Opt2 and D1, were refabricated into rodlets of roughly 600 mm in length and ramp tested under BWR simulated coolant conditions (9 MPa, 285°C) in the R2 test reactor at Studsvik Nuclear. The details of power ramping are described in [17]. The peak linear power densities reached for Std Opt2 and D1 rodlets were 56.7 and 57.7 kW/m, respectively; with hold times 7-12 h. Both of the rodlets survived the ramp test. In a similar experiment, referred to as “bump test”, two rodlets with Std Opt2 and D3 pellets were post-irradiated in R2 to moderate power levels. The bump test irradiation was initiated from a linear power density of 22 kW/m, then ramped to 46.4 and 45.1 kW/m for the Std Opt2 and the D3, respectively; both with a hold time of 17.5 days. Following the test, the rodlets were punctured to examine fission gas release of the two pellet types.

PIE after the ramp tests showed that the fractional fission gas release (FGR) of D1 and Std

Opt2 were 17.2 and 30.2%, respectively. Furthermore, the ceramography of peak power region of the rodlets revealed that the D1 pellets had formed a central hole, in contrast to the Std Opt2 pellets. This was attributed to D1's slightly higher linear power density (57.7 versus 56.7 kW/m). Post-irradiation measurements after the bump tests showed that FGR was 29.7 and 20.5% for Std Opt2 and D3 segment, respectively. Hence, D3 pellets had roughly 30% lower FGR than the Std Opt2 pellets. The lower FGR measured in these doped fuels is primarily due to the much larger grain size of the fuel (table 11) as our computations on the influence of grain size on FGR in section 4.2 indicate.

Besides the PIEs and measurements, Arborelius and company [17] also report results from BWR pool-side measurements made on doped UO_2 fuels, with similar characteristics as the ones presented in table 11. The pool-side rod axial length measurements show a higher fuel rod irradiation-induced growth for rods containing doped UO_2 than those holding Std fuel pellets. Subsequent data presented in [109, 110] confirm this effect. That is, the rod growth with doped UO_2 is appreciably faster than that with pure UO_2 fuel pellets. This may be attributed to a higher fuel swelling rate and/or lower fuel in-reactor densification of doped fuel, which closes the fuel-cladding gap earlier during irradiation, thereby leading to a larger rod length increase. Note that the nominal as-fabricated densities of doped fuels are larger than Std fuel (table 11), hence less in-rector densification of doped fuel.

In a parallel paper to that of Arborelius et al., the same group led by Zhou [111] provided further data and computational results on the Westinghouse doped UO_2 versus undoped UO_2 subjected to the aforementioned ramp/bump tests. Here, we only refer to their profilometry measurements of cladding outer diameter along the rodlets containing D1 and Std Opt2 pellets after the ramps, figure 31. It is seen that the D1 fuel cladding experienced appreciably larger strains than Std Opt2.

In a 2009 presentation by Backman et al. [110], additional data on FGR of Westinghouse doped UO_2 fuels obtained by reactor pool-side gamma scanning (i.e. non-destructive examination) of rods (in two fuel assemblies) which were irradiated under normal BWR operation to burnups of up to 55 MWd/kgU, and also on rods that were subjected to heavy-duty power histories in the Halden test reactor are cursorily mentioned.

The pool-side gamma scanning of Cr_2O_3-Al_2O_3 doped UO_2 fuel exhibited lower fractional FGR (2 rods with 1.3%) than undoped UO_2 fuel rods (3 rods with 1.5-2.1%) at burnups in the range 50-55 MWd/kgU. However, since the individual power histories for these rods are not specified, it is hard to draw confident conclusions about the outcome. Also more data in this burnup range are needed to confirm the trend.

The fuels tested in the Halden IFA-677 test rig comprised two Cr_2O_3-Al_2O_3 doped UO_2 rods and one pure UO_2 rod irradiated to about 24 MWd/kgU in BWR conditions. The doped fuels had 0.09wt%Cr_2O_3-0.02wt%Al_2O_3 (rod 1) and 0.05wt%Cr_2O_3-0.02wt%Al_2O_3 (rod 5). The mean fuel grain sizes were 56 μm (rod 1), 46 μm (rod 5) and ≈ 12 μm for pure UO_2 (rod 6) [112]. The fractional FGR of the tested rods were similar, that is, 22% (rod 1), 17% (rod 5) and 19% (rod 6) [112]. One may conclude that rods that are subjected to high power densities (> 35 kW/m) for sufficiently long periods would have similar FGR whether they are doped with Cr_2O_3-Al_2O_3 or not.

Industrial groups in France led by AREVA NP (formerly Framatome ANP) have utilized and advanced doped UO_2 fuels for LWRs over the years [18, 19, 32, 33]. Chromium oxide with concentration of 0.16 wt% is used as an additive with grain size varying in the range 50 to 60 μm. This type of fuels have densities in a range of 96 to 97 %TD and are reported to have less densification. Both separate effect irradiation experiments in test reactor [32, 106] and irradiation campaigns in LWRs [18, 19, 33] have been conducted to assess the

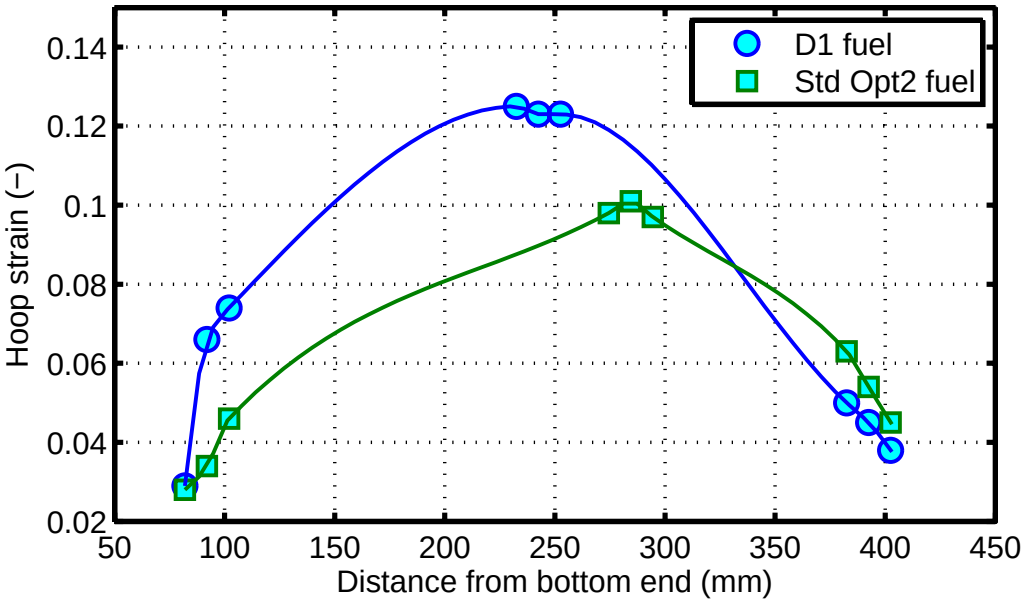

Figure 31: Engineering plastic hoop strain of fuel cladding after power ramp along the axial position of the rodlet. The cladding outer diameters are measured, whereas the strains are calculated from the nominal as-fabricated outer diameter of 9.63 mm; from table 2 of Zhou et al. [111]. The lines are piecewise cubic interpolations through the points; see table 11 for sample identification.

performance of doped UO_2 versus standard pure UO_2 fuel.
Valin and company [32] have tested fission gas retention and release of a variety of experimental doped and undoped UO_2 fuels irradiated in a facility at the periphery of the Siloé test reactor in Grenoble to burnup of about 10 MWd/kgU. They kept the central temperature of the annular pellets below 973 K to avoid triggering of thermal fission gas release. After irradiation, the rodlets were punctured and their gas contents were analyzed, which showed very low release during the base irradiation. Then, the fission gas retention capacities of the fuel pellets were examined by post-irradiation annealing tests made in a dedicated facility. The annealing was done in a high frequency furnace at 1973 K for either 30 minutes or 5 hours, whereupon ^{85}Kr released from the fuel was measured by gamma spectrometry. In figure 32, we reproduce Valin et al.'s informative diagram, showing ^{85}Kr release after 5 h at 1973 K versus grain size for the tested samples. Note that every data point belongs to a different kind of fuel. The samples included several variants (concentrations) of Cr_2O_3-doped UO_2 plus MgO-, SiO_2-, Al_2O_3-, ZrO_2-doped, and several alternates of non-standard UO_2.
As Valin et al. noted, the highest gas retention samples were fuels having the larger grain sizes (over 50 μm). This characteristic, however, was not sufficient, since the large-grained UO_2 fuel release reached 30%. They point out that the other important feature for an improved fission gas retention is the presence of intragranular sites, which are favorable to bubble nucleation and pinning. These sites are structural defects due to the hyperstoichiometry in UO_{2+x} and second phase precipitates in fuels doped with 0.2% Cr_2O_3. The intragranular bubbles formed on these sites were observed on the micrographs, which suggest that the annealing in reduced milieu made on some fuel batches eliminated some of these precipitates, thereby resulting in higher release and fewer gas bubbles. According to Valin and coworkers, the fuels containing only Cr_2O_3 as a dopant showed an improved gas re-

tention, especially those with 0.2% Cr_2O_3. This improvement in gas retention was not only attributed to a larger grain size, but also to the presence of dopant in the fuel.

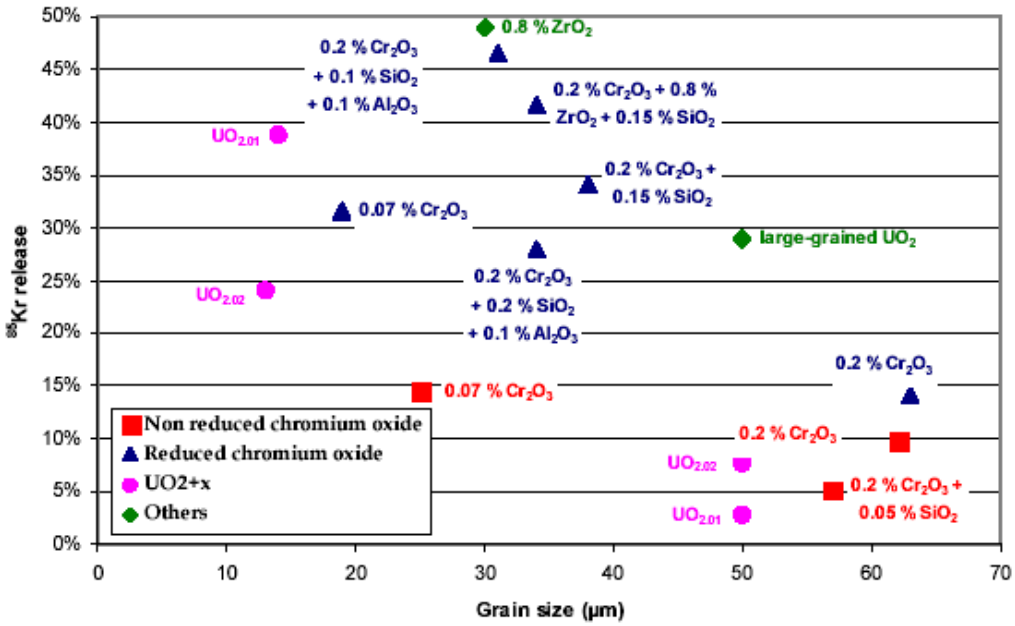

Figure 32: Valin et al. results on ^{85}Kr release after annealing tests of 5 hours at 1973 K [32].

Nonon and colleagues [106] report on the performance of Cr_2O_3-doped UO_2 fuels submitted to power ramps after pre-irradiation up to 30 MWd/kgU in a PWR. The power ramps were conducted in the test reactor OSIRIS at CEA Saclay, France. The ramp terminal power densities, after preconditioning at 20 kW/m for 12 h, were 47 and 53.5 kW/m for the doped fuel rodlets, whereas they were 44 and 40 for the standard UO_2 rodlets. The ramp rate from the preconditioning level to peak power was around 10 kW/m·min and the ramp peak power hold time was 12 h. No fuel failures were detected after the ramps. The rodlets embracing Cr_2O_3-doped UO_2 fuel experienced a much larger cladding diameter deformation (about factor of 2) during the ramps than the undoped rodlet as we could interpret from figure 7 in [106]. The relative fission gas release from the two doped rods were 8 and 10%, which seem fairly low relative to what one has experience from standard UO_2 fuel rodlets subjected to such ramps. Very little quantitative results regarding fuel characteristics and post-irradiation measurements are provided in [106].

Delafoy and coworkers in [19, 33] note that the AREVA NP chromia-doped UO_2 fuel has an optimum Cr_2O_3 concentration of 0.16 wt%, which leads to grain sizes in the range of 50 to 60 μm and fuel densities typically in the range of 96 to 97%TD. They report on the PWR irradiation program CONCERTO in which extensive PIEs have been carried out with respect to this type of Cr_2O_3-doped UO_2 fuel. They point out that in comparison with standard Zircaloy-4 clad UO_2 rods, non-destructive examinations have revealed a slightly higher fuel rod growth and diametral rod deformation in Cr_2O_3-doped UO_2 fuel rodlets. This behavior is attributed to an earlier in life pellet-cladding contact, considering that the Cr_2O_3-doped fuels exhibit a lower densification. The density measurements have confirmed the higher dimensional stability of Cr_2O_3-doped fuel up to 62 MWd/kgU with a very low early in-life fuel densification relative to un-doped UO_2. Rod punctures of the CONCERTO rods after 5 cycles of reactor operation showed fractional FGR values below 2% for Cr_2O_3-

doped fuel. Moreover, the microstructural examinations showed that precipitation of fission gases occurred in the intragranular bubbles rather than the intergranular bubbles, in contrast to what observed in the undoped UO_2 fuel. The microstructural examinations also revealed a great stability of the Cr_2O_3-doped fuel, in particular no grain growth had occurred during irradiation up to about 60 MWd/kgU. This behavior is in line with the observations made by Westinghouse in Sweden, as we alluded earlier in this section. For additional data and PCI test results performed on this type of doped fuel, briefed by Delafoy et al., the reader may consult their presentations [19, 33].

The effects of high burnup at low fuel temperatures on Mg-doped UO_2 fuel's swelling and fission gas retention capacity have been investigated by Fujino et al. [13, 67]. Fuel pellets of undoped and doped UO_2, with different ^{235}U enrichments, were irradiated in a special capsule in the JRR-3M test reactor of Japan Atomic Energy Research Institute (JAERI) to burnups ranging from 19 to 94 MWd/kgU at temperatures 820-1100 K. The doped pellets included Mg concentrations: 2.5, 5, 10, and 15 mol%. To vary burnup, the samples were prepared with ^{235}U enrichments: 6, 10 and 20 wt%. The sintering for these pellets was done at 1983 K, 5 h, in a stream of 4%H_2-He. The addition of magnesium caused large grain size fuel on sintering. Table 12 lists the grain sizes and densities for the 10 wt% ^{235}U samples.

The aim of Fujino et al.'s study was to simulate and give information on irradiation behavior near pellet periphery of the LWR fuel at high burnups. Thermal conductivity of unirradiated Mg-UO_2 was higher than that of undoped UO_2 (see section 3.3), which apparently seemed to also hold for irradiated specimens. Limited measurements indicated that the swelling of Mg-doped and undoped UO_2 as a function of burnup was similar. By the same token, fission product gas xenon retention capacity of the doped versus undoped fuels was similar. Fujino et al. study [67] indicates that the effect of addition of metal oxides on fission gas release seems to be small or subsidiary at high burnups. The large doping effects were not observed even for 5%Mg-5%Nb-UO_2 and 3.5%Ti-UO_2 specimens. This could be due to the heavily-damaged fuel matrix structure resulted in at high burnups.

Table 12: Fuel (10% ^{235}U) data used in Fujino et al.'s study [67].

Specimen	Mg content mol%	Grain size μm	Density g/cm^3
UO_2	-	30	10.51
UO_2-2.5Mg	2.5	47	10.52
UO_2-5Mg	5.0	50	10.49
UO_2-10Mg	10.0	NA	10.49[a]
UO_2-15Mg	15.0	71	10.19

[a] Calculated from fuel swelling data.

Yanagisawa has investigated the behavior of Nb_2O_5 doped UO_2 fuel under reactivity initiated accident (RIA) conditions [113, 114]. In a 1991 paper [113], Yanagisawa reported the behavior of UO_2 fuel containing 0.29 wt% Nb_2O_5 additive using 14×14 PWR fuel rods pre-pressurized with pure helium gas to 3.4 MPa. He found that the failure threshold, in terms of peak fuel enthalpy, of the pressurized doped fuel was equal or greater than that of the earlier experimental data obtained from the Nuclear Safety Research Reactor (NSRR) in JAERI. Failure mechanism was ballooning of cladding followed by rupture, which was attributed mainly to the pre-pressurization. No significant differences in the failure mechanism existed between the doped and undoped pre-pressurized fuels, the latter were used in the earlier NSRR experiments.

In a subsequent 1995 paper [114], Yanagisawa reported the results of RIA experiments using un-pressurized UO_2 fuel pellets containing Nb_2O_5 additive. Two kinds of fuel rods were tested; one rod contained a fuel doped with 0.30 wt% Nb_2O_5 and the other contained undoped fuel pellets. The average grain size determined by two-dimensional linear intercept method was 29 μm for the doped fuel and 9 μm for the undoped one. All the tested fuel rods, except for the two doped fuel rods, which had 100% He without pre-pressurization, had a gas composition of 95%He+l%Kr+4%Xe.
From the result of post-pulse irradiation examination, such as visual inspection, dimensional measurement and metallography, fuel failure threshold and failure mechanism were examined. The following conclusions were reached from Yanagisawa's study:

- The failure threshold of the un-pressurized Nb_2O_5 doped fuel under RIA was almost equal to that of the previous NSRR experimental data on undoped UO_2 fuel. That is, no significant differences in the threshold for mechanical energy release existed between the un-pressurized Nb_2O_5 doped fuel and the previous NSRR experimental data. For a recent review of RIA, see [115].

- Failure mechanism in both the doped and undoped fuels was cladding melting followed by embrittlement of thinned cladding wall. Bonding between fuel and cladding occurred at a lower fuel enthalpy level (1155 J/g·fuel) in the doped fuel than that (1427 J/g·fuel) in the undoped fuels. The bonding was usually accompanied by fuel microstructural change at fuel periphery.

- Magnitude of axial strain, due to pellet-cladding mechanical interaction, in the doped fuel increased with increasing energy deposition or fuel enthalpy. It ranged from 8 to 16%, figure 33. This was larger than that observed in pre-pressurized doped fuel. Major structural changes in the form of small radial cracks at bonded area and large lenticular cracks at fuel periphery occurred in doped fuels.

Finally, we should mention a study by Une and coworkers [16] on the fuel rim structure formation and high burnup fuel behavior of large-grained (Al-Si-O)-UO_2 and pure UO_2 fuels, with a grain-size range of 37-63 μm, versus that of standard grain-sized pure UO_2, with a grain-size range of 9-12 μm. The fuels were irradiated in the Halden heavy water reactor up to a cross-sectional pellet average burnup of 86 MWd/kg. Une and colleagues examined the effect of grain size on the rim structure formation quantitatively, in terms of the average xenon depletion (or depression) in the pellet outer region, measured by electron probe microanalysis. The Xe depression in the high burnup pellets above 60 MWd/kg was proportional to: $\propto d_g^{-1/2}$ to $\propto d_g^{-1.0}$ (d_g: grain size), and the two kinds of large-grained pellets exhibited noted resistance to the rim structure formation. Une et al. observed that a high density of dislocations preferentially decorated the as-fabricated grain boundaries, and the sub-divided grain structure was localized in that region. Although the swelling rate of the two large-grained pellets up to the middle burnup of about 30 MWd/kg was larger than that for the standard pellet, it became smaller at higher burnups beyond 30 MWd/kg [16].

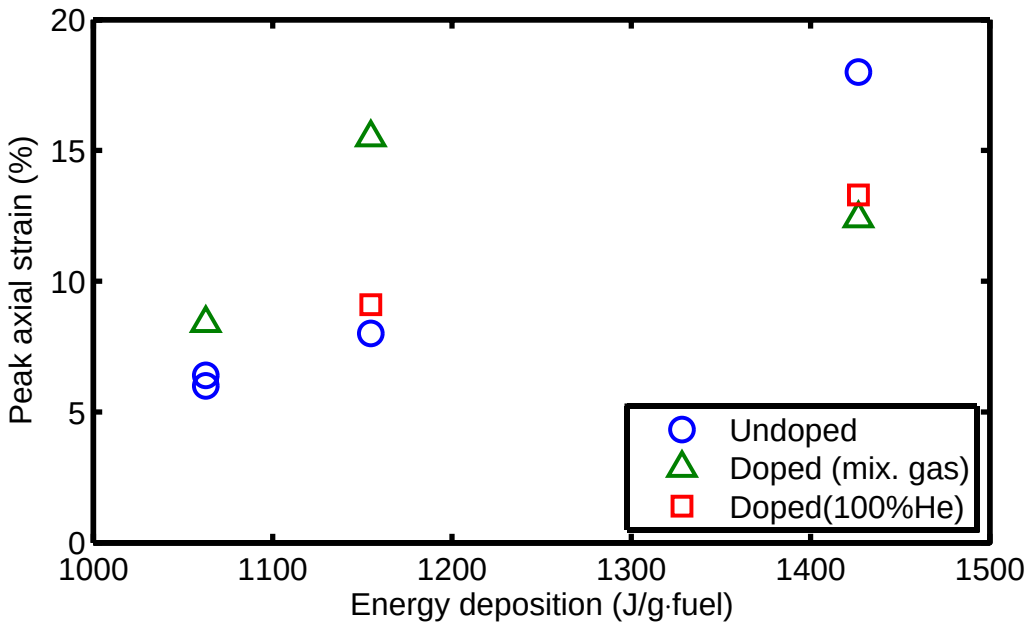

Figure 33: Yanagisawa's data on cladding axial strain versus energy deposition [114]. Here, mix. gas ≡ 95%He+l%Kr+4%Xe gas composition of fuel rods.

7 Summary and conclusions

In this report, we have reviewed the effects of various additives on UO_2 fuel behavior. Additives are introduced in UO_2 during fabrication of fuel pellet to enlarge fuel grain size, reduce fuel porosity and enhance fuel plasticity. These changes emanate from redistribution of point defects and generation of new ones in the UO_2 polycrystalline lattice. Doping of UO_2 with an additive would modify thermophysical properties, fission gas diffusion and release in and from fuel, high temperature creep of UO_2 and fuel densification during irradiation.

Among the thermophysical properties, the heat capacity and thermal conductivity are most influenced by additives, however, for small concentrations (≤ 0.2 wt%) of dopants, for example Cr_2O_3 and Al_2O_3, the effects would be negligible. For certain dopants such as MgO and the burnable absorber Gd_2O_3, where high concentrations are used in UO_2, the effects are non-negligible. Also, for UO_2 doped with these additives, measured data and appropriate correlations as a function of dopant concentration are available, which are summarized in this report (section 3 and Appendix A). However, for important dopants Cr_2O_3 and Al_2O_3 such data and correlations, which would depend on the dopant concentration, have not been reported in the literature. For these trivalent oxides, generically designated as M_2O_3, one may utilize the thermophysical quantities of Gd_2O_3, with consideration given to the mass difference between the trivalent ions, as a first approximation.

Fission product gas retention and release in and from fuel, and also gaseous fuel swelling get affected by additives, namely (i) the larger grain size, which extends the diffusion path to fuel grain boundaries, and (ii) by the change in fission gas diffusivity caused by restructuring of point defects in the fuel. In general, oxides that simulate hypostoichiometry UO_{2-x}, e.g. by doping with Gd_2O_3 or Y_2O_3, reduce the cation (U) diffusion coefficient through increased trapping. In contrast, those that simulate hyperstoichiometry UO_{2+x}, e.g. by doping with Nb_2O_5, enhance the cation diffusion coefficient and show less pronounced trapping, thereby resulting in higher xenon release.

There is dearth of data on gas diffusivity in doped UO_2 fuels in the literature. But there are some data available regarding the effect of additives Al_2O_3, Cr_2O_3, SiO_2, TiO_2, MgO, and Nb_2O_5 on thermal diffusivity of ^{133}Xe in UO_2, obtained by means of a post-irradiation annealing technique [11, 41]. We have compared xenon diffusivities in these materials with each other and with that of undoped UO_2 as a function of temperature. The literature data indicate that xenon diffusivity in (slightly hyperstoichiometric Al_2O_3 and slightly hypostoichiometric MgO)-doped UO_2 is close to that in undoped UO_2; whereas the diffusivities in (Cr_2O_3, SiO_2 or TiO_2)-doped are different that in undoped UO_2. In particular, based on the limited available data, the xenon diffusivity (temperature range $\approx$ 1200 to 1900 K) in the Nb_2O_5-doped UO_2 is consistently higher than in undoped UO_2; whereas in a slightly hyperstoichiometric Cr_2O_3-doped UO_2, the Xe diffusivity is close or slightly higher than UO_2 above 1500 K and somewhat lower than in UO_2 below 1500 K (figure 12). Hence, appropriate Arrhenius-type relations for fission gas diffusivity (cf. table 6) should be considered, when such fuels are analyzed with a fuel rod modeling code.

We have made sample computations on fission gas release and intergranular gaseous swelling, using the aforementioned diffusivities with varying grain sizes as input to a standard model (section 4.2), to illustrate the effect of these parameters on gas release and swelling as a function of irradiation time under isothermal conditions. The results of our computations of thermal fission gas release versus irradiation time at temperatures 1600-2000 K, for Cr_2O_3-, Al_2O_3-, and Nb_2O_5-doped and "pure" UO_2 fuels indicated that among these, the Nb_2O_5-

doped UO_2 has the largest FGR while the Al_2O_3-doped the lowest. The relative gas release from the Cr_2O_3-doped sample depends on the temperature, e.g., at 1600 K its release is in the order of that from "pure" UO_2, while at 2000 K it is close to that from Nb_2O_5-doped sample. The gas release rate, as expected, was predicted to be inversely dependent on the fuel grain size while is roughly proportional to the square root of gas diffusivity in the fuel. Regarding fuel gaseous swelling, our computations showed that among the aforementioned four fuel types, the Cr_2O_3-doped sample has the highest swelling rate, while the Nb_2O_5-doped sample has the lowest. It is the combination of gas diffusion, grain boundary saturation and grain size, which yields this behavior. It was observed that the larger is the grain size, the smaller is the swelling rate and the saturation value.
Thermal creep rate of doped UO_2 was assessed in section 5. Fuel additives usually enhance the thermal creep rate of UO_2. The creep rate depends on the applied stress, temperature, grain size, and the O/U ratio [86]. The main feature of the creep rate versus stress curves is the separation between a region in which the strain rate is linearly dependent on the applied stress, and one manifested by a power law creep, i.e. $\dot{\epsilon} \propto \sigma^n$, for which the stress exponent varies from $n \approx 4$ to $n \approx 6$. The former region is described by a diffusional creep with a grain size dependence d_g^{-2}, whereas the latter one is consistent with the dislocation climb creep, and is regarded to be independent of grain size. The transition stress from one region to another is considered to be temperature independent and may vary with grain size [86].
The limited published data show that there exist considerable variations in creep rate among the additives. Measurements made on Nb_2O_5-doped UO_2 at a uniaxial stress around 20 MPa indicates that creep occurs by Nabarro-Herring diffusion with a d_g^{-2} dependence creep rate. It is observed that Nb_2O_5 addition causes a dramatic increase in the steady-state creep as long as the niobium ion is kept in the Nb^{5+} valence state [98]. Similarly, Cr_2O_3 and Al_2O_3 dopants (up to 0.1 wt%) both enhance the thermal creep rate of UO_2 [102]. The creep tests made on these materials at temperatures 1620-1920 K and stress levels 50-65 MPa show that the creep rate may follow a dislocation climb mechanism.
In-reactor irradiation of Cr_2O_3-doped UO_2 fuel under normal BWR operation to exposures 30.5-33.5 MWd/kgU shows that the chromia-doped UO_2 fuel in-reactor volume increase is appreciably larger than that of undoped UO_2 (section 6). After the pre-irradiated rods were subjected to power ramps in a test reactor, the chromia-doped fuel exhibited less fission gas release than the undoped UO_2. However, the cladding diameter increase caused by pellet-cladding mechanical interaction was larger in the former than the latter. Also, rod axial length measurements, after long BWR exposures, indicate appreciably larger growth of chromia bearing rods than pure UO_2 rods [17, 109, 110]. The difference in the fuel volume change, rod growth, and the cladding diametral increase under power ramps, partly can be due to the lower in-reactor densification of Cr_2O_3-doped UO_2 relative to pure UO_2 fuel. Suchlike fuel behavior has also been observed in a PWR [19].
The data and models appraised in this report should offer an experimental/theoretical basis for modeling doped UO_2 fuel behavior through their applications in a fuel rod computer code. The code then needs to be validated with pertinent irradiation data, such as those being produced through the Halden reactor IFA-677 and IFA-716 experiments.

Acknowledgements. I wish to thank L.O. Jernkvist and T. Manngård for discussions, and also L.O.J. for critical reading of the manuscript and comments thereof. The work was sponsored by the Swedish Safety Authority (SSM) through grant DNR SSM2012-2653/2030040-05.

Notes

[1]*Frenkel defects* are vacancies and interstitials of the same species in equilibrium. For example in UO_2, one finds oxygen vacancies and oxygen interstitials in pairs. *Schottky defects* are only vacancies, e.g. when two oppositely charged ions leave their normal lattice positions forming two vacancies in the lattice structure [49].

[2]Critical temperature, critical phenomena and phase transitions are central and active subjects in condensed matter physics; among introductory textbooks and reviews, we mention [116–118].

[3]In more detail, $\sigma = (a^3\omega_D/k_B v^3)^{1/2}$, where a^3 is the atomic volume, ω_D the Debye frequency, and v the phonon velocity.

[4]More accurately, Booth's short time approximation for post-irradiation annealing condition would result in $F(t) \approx \frac{6}{a_e}\sqrt{Dt/\pi} - 3Dt/a_e^2$, which is valid for $F \leq 0.9$ [71].

[5]BET device is used in surface area measurements of powder or batch samples and pore size and pore size distribution. The device determines needed gas quantity to cover the sample surface with a molecular layer and calculates surface area using Brunauer, Emmett and Teller (BET) theory [119].

[6] In the gaseous swelling model, for the grain boundary gas saturation, the Van der Waals equation of state is used rather than the ideal gas equation of state, as it is assumed in fission gas release computations for convenience. Moreover, an external pressure of 1 MPa is used in the VdW equation of state, rather than $P_{ext} = 0$, see [91].

[7]Yield stress or yield strength, even called flow stress, is a stress level related to the onset of irreversible plastic deformation of solid materials [120].

References

[1] J. A. Turnbull. The effect of grain size on the swelling and gas release properties of UO_2 during irradiation. *J. Nucl. Mater.*, 50:62–68, 1974.

[2] H. Matzke. On the effect of TiO_2 additions on sintering of UO_2. *J. Nucl. Mater.*, 20:328–331, 1966.

[3] I. Amato, R. L. Columbo, and A. P. Balzari. Grain growth in pure and titania-doped uranium dioxide. *J. Nucl. Mater.*, 18:252–260, 1966.

[4] J. B. Ainscough, F. Rigby, and S. C. Osborn. The effect of titania on grain growth and densification of sintered UO_2. *J. Nucl. Mater.*, 52:191–203, 1974.

[5] K. Une, S. Kashibe, and K. Ito. Fission gas behavior during postirradiation annealing of large grained UO_2 fuels irradiated to 23 GWd/t. *J. Nucl. Sci. Techn.*, 30:221–231, 1993.

[6] J. C. Killeen. The effect of additives on the irradiation behaviour of UO_2. *J. Nucl. Mater.*, 58:39–46, 1975.

[7] J. B. Ainscough, F. Rigby, and S. A. Morrow. Effect of oxygen potential on the thermal creep of niobia-doped UO_2. *J. Amer. Ceram. Soc.*, 64:315–318, 1981.

[8] H. Assmann, W. Dörr, G. Gradel, G. Maier, and M. Peehs. Doping UO_2 with niobia - beneficial or not? *J. Nucl. Mater.*, 98:216–220, 1981.

[9] K. W. Song, S. H. Kim, and S. H. Na et al. Effects of Nb_2O_5 addition on grain growth and densification in UO_2 pellets under reducing and/or oxidizing atmospheres. *J. Nucl. Mater.*, 209:280–285, 1994.

[10] J. C. Killeen. The measurement of the electron-to-hole mobility in UO_2 and its effect on thermal conductivity. *J. Nucl. Mater.*, 92:136–140, 1980.

[11] S. Kashibe and K. Une. Effect of additives (Cr_2O_3, Al_2O_3, SiO_2, MgO) on diffusion release of Xe-133 from UO_2 fuel. *J. Nucl. Mater.*, 254:234–242, 1998.

[12] T. Fujino, N. Sato, and K. Fukuda. Changes of thermodynamic properties of UO_2 fuel doped with magnesium and other alloys. In *1997 Internat. Topical Meeting on Light Water Reactor Fuel Performance*, pages 565–575, Portland, Oregon, 2-6 March 1997. American Nuclear Society.

[13] T. Fujino, N. Sato, and K. Yamada et al. Post-irradiation examinations of high burnup Mg-doped UO_2. In *Internat. Topical Meeting on Light Water Fuel Performance*, pages 641–651, Park City, Utah, 2000. American Nuclear Society.

[14] T. Matsuda, Y. Yuasa, S. Kobayashi, and M. Toba. Characteristics of fuel pellets with additive of Al and Si. In *Advances in Fuel Pellet Technology for Improved Performance*, IAEA-TECDOC-1036, International Atomic Energy Agency, Vienna, Austria, 1998.

[15] J. Matsunaga, Y. Takagawa, and K. Kusagaya et al. Fundamentals of GNF Al-Si-O additive fuel. In *Proc. of Top Fuel 2009*, pages 767–772, Paris, France, 6-10 September 2009.

[16] K. Une, M. Hirai, and K. Nogita et al. Rim structure formation and high burnup fuel behavior of large-grained UO_2 fuels. *J. Nucl. Mater.*, 278:54–63, 2000.

[17] J. Arborelius, K. Backman, and L. Hallstadius et al. Advanced doped UO_2 pellets in LWR applications. *J. Nucl. Sci. Techn.*, 43:967–976, 2006. Also in Proceedings of Water Reactor Fuel Performance Meeting, 2-6 October, 2006, Kyoto, Japan.

[18] C. Delafoy, P. Blanpain, and C. Maury. Advanced UO_2 fuel with improved PCI resistance and fission gas retention capability. In *Proceedings of the ANS/ENS Top Fuel 2003 Meeting*. European Nuclear Society, 16-19 March 2003.

[19] C. Delafoy and P. Dewes. AREVA NP new UO_2 fuel development and qualification for LWRs applications. In *Top Fuel 2006*, pages 1–7, Salmanca, Spain, October 2006. European Nuclear Society.

[20] B. E. Ingleby and K. Hand. Fabrication and performance of large-grained UO_2-MgO fuel. In I. J. Hastings, editor, *Fission Product Behavior in Ceramic Nuclear Fuel*, volume 17 of *Advances in Ceramics*, pages 57–72. The American Ceramic Society, Columbus, Ohio, 1986.

[21] J. C. Killeen. Fission gas release during post irradiation annealing of large grain size fuels from Hinkley Point B. In *Water Reactor Fuel Element Modelling at High burnup and Experimental Support*, IAEA-TECDOC-957, pages 467–479, International Atomic Energy Agency, Vienna, Austria, 1994.

[22] IAEA. Characteristics and use of urania-gadolinia fuels. Technical Report IAEA-TECDOC-844, IAEA, Vienna, Austria, 1995.

[23] L. V. Corsetti, S. C. Hatfield, and A. Jansson. Recent advances in PWR fuel design at ABB-CE. In *International Topical Meeting on LWR Fuel Performance*, pages 113–121, Avignon, France, April 21-24 1991. European Nuclear Society.

[24] H. S. Kim, Y. K. Yoon, and M. S. Yang. Thermodynamic study on the $(U_{1-y},Er_y)O_{2\pm x}$ solid solutions. *J. Nucl. Mater.*, 209:286–293, 1994.

[25] H. Matzke. Gas release mechanism in UO_2 - a critical review. *Radiation Effects*, 53:219–242, 1980.

[26] J. A. Lange. *Handbook of Chemistry*. McGraw-Hill, New York, 1979.

[27] V. Peres, L. Bourgeois, and P. Dehaudt. Grain growth and Ostwald ripening in chromia-doped uranium dioxide. *J. de Physique IV*, 3:1477–1480, 1993.

[28] T. Cardinaels, J. Hertog, and B. Vos et al. Dopant solubility and lattice contraction in gadolinia and gadolinia-chromia doped UO_2 fuels. *J. Nucl. Mater.*, 424:289–306, 2012.

[29] S. C. Middleburgh, R. W. Grimes, K. H. Desai, and et al. Swelling due to fission products and additives dissolved within the uranium. *J. Nucl. Mater.*, 427:359–363, 2012.

[30] J. D. B. Lambert and R. Strain. Oxide fuels. In R. W. Cahn, P. Haasen, and E. J. Kramer, editors, *Nuclear Materials*, volume 10A of *Material Science and Technology*, chapter 7. VCH, Weinheim, Germany, 1994. Volume editor B.R.T. Frost.

[31] K. C. Radford and J. M. Pope. UO_2 fuel pellet microstructure modification through impurity additions. *J. Nucl. Mater.*, 116:305–313, 1983.

[32] S. Valin, L. Cailot, and Ph. Dehaudt et al. Synthesis of the results obtained on the advanced UO_2 microstructures irradiated in the TANOX device. In *Advanced Fuel Pellet Materials and Fuel Rod Design for Water Cooled Reactors*, IAEA-TECDOC-1416, International Atomic Energy Agency, Vienna, Austria, 2003.

[33] C. Delafoy, P. Dewes, and T. Miles. AREVA Cr_2O_3-doped fuel development for BWRs. In *Proceedings of the 2007 International LWR Fuel Performance Meeting*, pages 1–7, San Francisco, California, October 2007. American Nuclear Society.

[34] L. Bourgeois, Ph. Dehaudt, C. Lemaignan, and A. Hammou. Factors governing microstructure development of Cr_2O_3-doped UO_2 during sintering. *J. Nucl. Mater.*, 297:313–326, 2001.

[35] A. Leenaers, L. de Tollenaere, C. Delafoy, and S. Van den Berghe. On the solubility of chromium sesquioxide in uranium dioxide fuel. *J. Nucl. Mater.*, 317:62–68, 2003.

[36] T. Cardinaels, K. Govers, and B. Vos et al. Chromia doped UO_2 fuel: Investigation of the lattice parameter. *J. Nucl. Mater.*, 424:252–260, 2012.

[37] O. Brémond. IFA-716.1 fission gas release mechanisms. Technical Report HWR-1008, Institutt for Energiteknik, Halden, Norway, 2011.

[38] R. J. M. Konings, T. Wiss, and C. Guéneau. Nuclear fuels. In L. R. Morss, N. M. Edelstein, and J. Fuger, editors, *The Chemistry of the Actinide and Transactinide Elements*, volume 6, chapter 34. Springer, Dordrecht, The Netherlands, 2011.

[39] X. Y. Liu, D. A. Andersson, and B. P. Uberuaga. First-principle DFT modeling of nuclear fuel materials. *J. Mater. Sci.*, 47:7367–7384, 2012.

[40] T. Matsui and K. Naito. Electrical conductivity measurement and thermogravimetric study of pure and niobium-doped uranium dioxide. *J. Nucl. Mater.*, 136:59–68, 1985.

[41] K. Une, I. Tanabe, and M. Oguma. Effects of additives and the oxygen potential on the fission gas diffusion in UO_2 fuel. *J. Nucl. Mater.*, 150:93–99, 1987.

[42] A. R. Massih. Effect of additives on self-diffusion and creep of UO_2. Preprint, 2013.

[43] K. W. Song, K. S. Kim, K. W. Kang, and Y. H. Jung. Effects of Nb_2O_5 and oxygen potential on sintering behavior of UO_2 fuel pellets. *J. Korean Nucl. Soc.*, 31:335–343, 1999.

[44] E. Muller, T. Lambert, and N. L'Hullier et al. Thermal behavior of advanced UO_2 fuel at high burnup. In *Proceedings of the 2007 International LWR Fuel Performance Meeting*, pages 40–46, San Francisco, California, October 2007. American Nuclear Society.

[45] G. J. Hyland and R. W. Ohse. The heat capacity and enthalpy of condensed UO_2: A critical review and assessment. *J. Nucl. Mater.*, 140:149–170, 1986.

[46] C. Ronchi and G. J. Hyland. Analysis of recent measurements of the heat capacity of uranium dioxide. *J. Alloys & Compounds*, 213/214:159–168, 1994.

[47] C. Kittel. *Solid State Physics*. John Wiley & Sons, New York, seventh edition, 1996. Chapter 5.

[48] N. H. March, D. D. Richardson, and M. P. Tosi. Correlations of the superionic transition temperature and the Frenkel energy of fluorite crystals. *Solid State Commun.*, 35:903–905, 1980.

[49] W. Hayes and A. M. Stoneham. *Defects and Defect Processes in Nonmetallic Solids*. John Wiley & Sons, New York, 1985. Chapter 3; Dover reprint 2004.

[50] K. Clausen, W. Hayes, J. E. Macdonald, and R. Osborn. Observations of oxygen Frenkel disorder in uranium dioxide above 2000 K by use of neutron-scattering techniques. *Phys. Rev. Lett.*, 52:1238–1241, 1984.

[51] K. Clausen, M. A. Hackett, and W. Hayes et al. Coherent diffuse neutron-scattering from UO_2 and ThO_2 at temperatures above 2000 K. *Physica B*, 156/157:103–106, 1989.

[52] R. Szwarc. The defect contribution to the excess enthalpy of uranium dioxide calculation of the Frenkel energy. *J. Phys. Chem. Solids*, 30:705–711, 1969.

[53] T. Matsui, Y. Arita, and K. Naito. High temperature heat capacities and electrical conductivities of UO_2 doped with yttrium and simulated fission products. *J. Nucl. Mater.*, 188:205–209, 1992.

[54] K. Naito. High temperature heat capacities of UO_2 and doped UO_2. *J. Nucl. Mater.*, 189:30–35, 1989.

[55] H. Inaba, K. Naito, and M. Oguma. Heat capacity measurements of $U_{1-y}Gd_yO_2$ ($0.00 \leq y \leq 0.142$) from 310 to 1577 K. *J. Nucl. Mater.*, 149:341–348, 1987.

[56] IAEA. Thermophysical properties database of materials for light water reactors and heavy water reactors. Technical Report IAEA-TECDOC-1496, IAEA, Vienna, Austria, 2006.

[57] K. Une. Thermal expansion of UO_2-Gd_2O_3 fuel pellets. *J. Nucl. Sci. Techn.*, 23:84–86, 1986.

[58] N. W. Ashcroft and N. D. Mermin. *Solid State Physics*. Harcourt College Publishers, New York, 1976. Chapter 25.

[59] T. Yamashita, N. Nitani, T. Tsuji, and T. Kato. Thermal expansion of neptunium-uranium mixed oxides. *J. Nucl. Mater.*, 247:90–93, 1997.

[60] T. Ivanova, K. Gesheva, A. Cziraki, A. Szekeres, and E. Vlaikova. Structural transformations and their relation to the optoelectronic properties of chromium oxide thin films. *Journal of Physics: Conference Series*, 113:012030, 2008.

[61] P. G. Klemens. Thermal resistance due to point defects at high temperatures. *Phys. Rev.*, 119:507–509, 1960.

[62] B. Abeles. Lattice thermal conductivity of disordered semiconductor alloys at high temperatures. *Phys. Rev.*, 131:1906–1911, 1963.

[63] J. M. Casado, J. H. Harding, and G. J. Hyland. Small-polaron hopping in Mott-insulating UO_2. *J. Phys.: Condens. Matter*, 6:4685–4698, 1994.

[64] Q. Yin and S. Y. Savrasov. Origin of low thermal conductivity in nuclear fuels. *Phys. Rev. Lett.*, 100:225504, 2008.

[65] C. Ronchi and G. J. Hyland. Thermal conductivity of uranium dioxide up to 2900 K from simultaneous measurement of the heat capacity and thermal diffusiviy. *J. Appl. Phys.*, 85:776–789, 1999.

[66] R. A. Young. Model for electronic contribution to the thermal and transport properties of ThO_2, UO_2 and PuO_2 in solid and liquid phases. *J. Nucl. Mater.*, 87:283–296, 1979.

[67] T. Fujino, T. Shiratori, N. Sato, and K. Fukuda et al. Post-irradiation examination of high burnup Mg doped UO_2 in comparison with undoped UO_2, Mg-Nb doped UO_2 and Ti doped UO_2. *J. Nucl. Mater.*, 297:176–205, 2001.

[68] L. O. Jernkvist and A. R. Massih. Models for fuel rod behaviour at high burn-up. Technical Report 2005:41, Swedish Nuclear Power Inspectorate (SKI), Stockholm, Sweden, 2005. Available at: www.ssm.se.

[69] R. W. Grimes and C. R. A. Caltlow. The stability of fission products in uranium oxide. *Phil. Trans. R. Soc. Lon.*, 335:609–634, 1990.

[70] M. O. Tucker. Grain boundary porosity and gas release in irradiated UO_2. *Radaition Effects*, 53:251–256, 1980.

[71] K. Lassmann and H. Benk. Numerical algorithms for intragranular fission gas release. *J. Nucl. Mater.*, 280:127–135, 2000.

[72] INSAG. Defence in depth in nuclear safety. Technical Report INSAG-10, IAEA, Vienna, Austria, 1996. A report by the International Safety Advisory Group.

[73] W. Miekeley and F. W. Felix. Effect of stoichiometry on diffusion of xenon in UO_2. *J. Nucl. Mater.*, 42:297–306, 1972.

[74] K. Shiba. Fission iodine and xenon release from the UO_2-U_3O_8 system with emphasis on radiation damage. *J. Nucl. Mater.*, 57:271–279, 1975.

[75] C.R.A. Catlow. Theory of fission gas migration in UO_2. *Radiation Effects*, 53:127–132, 1980.

[76] H. Matzke. Diffusion in doped UO_2. *Nucl. Appl.*, 2:131–137, 1966.

[77] G. Long, W. P. Stanaway, and D. Davies. Experiments relating to the mechanism of the diffusion of xenon-133 in uranium dioxide. Technical Report AERE-M-1251, AERE Harwell, Didcot, U.K., 1964.

[78] R. D. MacDonald. The effect of TiO_2 and Nb_2O_5 additions on the irradiation behaviour of sintered UO_2. Technical Report AECL-1810, Atomic Energy of Canada Ltd., Chalk River, Ontario, Canada, 1963.

[79] J. C. Killeen. Fission gas release and swelling in UO_2 doped with Cr_2O_3. *J. Nucl. Mater.*, 88:177–184, 1980.

[80] D. Davies and G. Long. The emission of xenon-133 from lightly irradiated uranium dioxide spheroids and powders. Technical Report AERE-R-4347, AERE Harwell, Didcot, U.K., 1963.

[81] A. H. Booth. A method of calculating gas diffusion from UO_2 fuel and its application to the X-2-f test. Technical Report AECL 496 CRDC-721, Atomic Energy of Canada Limited, 1957.

[82] J. A. Turnbull, C. A. Friskney, J. R. Findlay, F. A. Johnson, and A. J. Walter. The diffusion coefficient of gaseous and voltile species during irradiation of uranium dioxide. *J. Nucl. Mater.*, 107:168–184, 1982.

[83] K. Forsberg and A. R. Massih. Diffusion theory of fission gas migration in irradiated nuclear fuel. *J. Nucl. Mater.*, 135:140–148, 1985.

[84] M. V. Speight. A calculation on the migration of fission gas in material exhibiting precipitation and re-solution of gas atoms under irradiation. *Nuclear Science and Engineering*, 37:180–185, 1969.

[85] K. Forsberg, A. R. Massih, and K. Andersson. A calculation of fission gas migration in nuclear fuel with re-solution effect. In *Transactions of the Enlarged Halden Programme Group Meeting on Fuel Performance Experiments and Analysis, Sanderstolen, Norway, 2-7 March, 1986*. OECD Halden Reactor Project, 1986. Halden Project Report HPR-330.

[86] D. R. Olander. *Fundamental Aspects of Nuclear Reactor Fuel Elements*. National Technology Information Services, Springfield, Virginia, 1976.

[87] J. Spino, J. Rest, W. Goll, and C. T. Walker. Matrix swelling rate and cavity volume balance of UO_2 fuels at high burnup. *J. Nucl. Mater.*, 346:131–144, 2005.

[88] G. L. Reynolds and G. H. Bannister. Examination of neutron-irradiated UO_2 using the scanning electron microscope. *J. Mater. Sci.*, 5:84–85, 1970.

[89] W. Beeré and G. I. Reynolds. The morphology and growth rate of interlinked porosity in irradiated UO_2. *J. Nucl. Mater.*, 47:51–57, 1973.

[90] J. A. Turnbull and M. O. Tucker. Swelling in UO_2 under conditions of gas release. *Phil. Mag.*, 30:47–63, 1974.

[91] A. R. Massih and K. Forsberg. Calculation of grain boundary gaseous swelling in UO_2. *J. Nucl. Mater.*, 377:406–408, 2008.

[92] P. T. Sawbridge, C. Baker, R. M. Cornell, K. W. Jones, D. Reed, and J.B. Ainscough. The irradiation performance of magnesia-doped UO_2 fuel. *J. Nucl. Mater.*, 95:119–128, 1980.

[93] M. Hirai, J. H. Davies, and R. Williamson. Diffusivities of fission gas species in UO_2 and $(U,Gd)O_2$ nuclear fuels during irradiation. *J. Nucl. Mater.*, 226:238–251, 1995.

[94] R. J. Ball and R. W. Grimes. Diffusion of Xe in UO_2. *J. Chem. Soc. Faraday Trans.*, 86:1257–1261, 1990.

[95] A. B. Lidiard. Self-diffusion of uranium in UO_2. *J. Nucl. Mater.*, 19:106–108, 1966.

[96] M. J. Norgett and A. B. Lidiard. The migration of inert gases in ionic crystals. *Phil. Mag.*, 18:1193–1210, 1968.

[97] K. Une and M. Oguma. Oxygen potential of $U_{0.96}Gd_{0.04}O_2$ (UO_2-3wt% Gd_2O_3) solid solution. *J. Nucl. Mater.*, 131:88–91, 1985.

[98] P. T. Sawbridge, G. L. Reynolds, and B. Burton. The creep of UO_2 fuel doped with Nb_2O_5. *J. Nucl. Mater.*, 97:300–308, 1981.

[99] L. O. Jernkvist. The SKI version of the FRAPCON-3.3 computer code: FRAPCON-3.3.1-SKI. Technical Report TR08-001, Quantum Technologies AB, Uppsala, Sweden, 2008.

[100] A. R. Massih. Models for MOX fuel behaviour. Technical Report 2006:10, Swedish Nuclear Power Inspectorate (SKI), Stockholm, Sweden, 2006. Available at: www.ssm.se.

[101] C. Duguay, A. Mocellin, P. Dehaudt, and G. Fantozzi. High temperature compression tests performed on doped fuels. *Key Engineering Materials*, 132-136:579–582, 1997.

[102] C. Dugay, A. Mocellin, P. Dehaudt, and M. Sladkoff. High temperature mechanical tests performed on doped fuels. In *Advances in Fuel Pellet Technology for Improved Performance*, IAEA-TECDOC-1036, International Atomic Energy Agency, Vienna, Austria, 1998.

[103] T. G. Langdon. Creep mechanisms in stoichiometric uranium dioxide. *J. Nucl. Mater.*, 38:88–92, 1971.

[104] T. G. Langdon. Deformation of polycrystalline materials at high temperatures. In N. Hansen, A. Horsewell, T. Leffers, and H. Lilholt, editors, *Deformation of polycrystals: Mechanisms and microstructures*, pages 45–54, Risø National laboratory, Roskilde, Denmark, 14-18 September 1981.

[105] T. G. Langdon. The physics of superplastic deformation. *Mater. Sci. Eng. A*, 137:1–11, 1991.

[106] C. Nonon, J. C. Menard, and S. Lansiart et al. PCI behaviour of chromium oxide doped fuel. In *International Seminar on Pellet-Clad Interaction in Water Reactor Fuels*, Aix en Provence, France, 9-11 March 2004.

[107] H. Matzke. On uranium self-diffusion in UO_2 and UO_{2+x}. *J. Nucl. Mater.*, 30:26–35, 1969.

[108] Y. W. Rhee, K. W. Kang, and K. S. Kim et al. Effect of SiO_2-CaO-Cr_2O_3 on the creep property of uranium dioxide. *Nucl. Eng. & Techn.*, 37:287–292, 2005.

[109] G. Zhou, A. R. Massih, and L. Hallstadius et al. Fuel performance experience, analysis and modeling: Deformations, fission gas release and pellet-clad interaction. In *Proceedings of the 2007 International LWR Fuel Performance Meeting*, pages 143–152, San Francisco, California, October 2007. American Nuclear Society.

[110] K. Backman, L. Hallstadius, and G. Rönnberg. Westinghouse advanced doped pellet characteristics and irradiation behaviour. In *Advanced Fuel Pellet Materials and Fuel Rod Design for Water Cooled Reactors*, IAEA-TECDOC-1654, International Atomic Energy Agency, Vienna, Austria, 2009.

[111] G. Zhou, J. Arborelius, and L. Hallstadius et al. Westinghouse advanced UO_2 fuel behaviors during power transients. In *2005 Water Reactor Fuel Performance Meeting, Kyoto, Japan, 2-6 October 2005*. Atomic Energy Society of Japan, 2005.

[112] R. Josek. The high initial rating test IFA-677.1: Final report on in-pile results. Technical Report HWR-872, Institutt for Energiteknik, Halden, Norway, 2008.

[113] K. Yanagisawa. Behavior of Nb_2O_5 doped UO_2 fuel in reactivity initiated accident conditions. *J. Nucl. Sci. Techn.*, 28:459–471, 1991.

[114] K. Yanagisawa. Behavior of Nb_2O_5 doped unpressurized UO_2 fuel under transient. *J. Nucl. Sci. Techn.*, 32:111–117, 1995.

[115] OECD-NEA. Nuclear fuel behaviour under reactivity-initiated accident (RIA) conditions. Technical Report 6847, Nuclear Energy Agency, Paris, France, 2010.

[116] H. E. Stanley. *Introduction to Phase Transitions and Critical Phenommena*. Oxford University Press, Oxford, U.K., 1971.

[117] H. E. Stanley. Scaling, univarsility, and renormalizations: three pillars of modern critical phenomena. *Rev. Mod. Phys.*, 71:S358–S666, 1999.

[118] H. Nishimori and G. Ortiz. *Elements of Phase Transitions and Critical Phenommena*. Oxford University Press, Oxford, U.K., 2011.

[119] S. Brunauer, P. H. Emmett, and E. Teller. Adsorption of gases in multimolecular layers. *J. Am. Chem. Soc.*, 60:309–319, 1938.

[120] J. Lemaitre and J. L. Chaboche. *Mechanics of Solid Materials*. Cambridge University Press, Cambridge, U.K., 1990.

[121] S. Ishimoto, M. Hirai, K. Ito, and Y. Korei. Effects of soluble fission products on thermal conductivities of nuclear fuel pellets. *J. Nucl. Sci. Techn.*, 31:796–802, 1994.

Appendix A Thermophysical correlations

The correlations for thermophysical properties listed here are the enthalpy, the heat capacity (specific heat), the coefficient of thermal expansion, and the thermal conductivity. No such correlations or data have been published in the literature for the utilized doped UO_2 fuels, such as dopants Cr_2O_3 or Al_2O_3, as a function of temperature and dopant concentration, except for dopant Gd_2O_3, which is used as burnable-absorber. All the listed correlations pertain to unirradiated fuels.

Enthalpy The $(U_{1-y},M_y)O_2$ enthalpy (J/mol) relative to the enthalpy at room temperature is given by [56]

$$\Delta H = H(T) - H(298.15), \tag{A.1}$$

where

$$H(T) = aT + \frac{b}{2}T^2 + \frac{c}{T} + \sqrt{2}\Delta H_f \exp\Big(\frac{\Delta S_f T - \Delta H_f}{2RT}\Big), \tag{A.2}$$

$$a = 79.8 \tag{A.3}$$

$$b = 0.1263y^2 - 0.0073y + 0.0061 \tag{A.4}$$

$$c = (1.68 - 1.48y) \times 10^6 \tag{A.5}$$

and

$$\Delta H_f = (-73880y^3 + 10190y^2 - 612.13y + 310) \times 10^3 \tag{A.6}$$

$$\Delta S_f = 61.969 - 45.56y \tag{A.7}$$

where ΔS_f, ΔH_f are the entropy and enthalpy of formation per Frenkel pair, T is temperature in kelvin and $R = 8.3145$ J/molK.

Heat capacity The corresponding expression for the heat capacity at constant pressure, $C_p = (\partial H/\partial T)_P$, is

$$C_p(T) = a + bT - \frac{c}{T^2} + \Delta C_p, \tag{A.8}$$

where

$$\Delta C_p = \frac{(\Delta H_f)^2}{\sqrt{2}RT^2} \exp\Big(\frac{\Delta S_f T - \Delta H_f}{2RT}\Big). \tag{A.9}$$

Thermal expansion The linear thermal expansion for $(U,Gd)O_2$ fuel is [56]

$$\begin{aligned} L(T)/L(273) &= 0.99866 + 7.2512 \times 10^{-6}T + (2.0463 \times 10^{-13}g^2 \\ &\quad +3.4846 \times 10^{-11}g + 2.0653 \times 10^{-9})T^2, \end{aligned} \tag{A.10}$$

where $L(T)$ and $L(273)$ are the lengths at temperature T and 273 K, respectively, and g is wt% Gd_2O_3 in UO_2. The plots of thermal expansion versus temperature are shown in figure A1 for up to 0.5 wt% dopant concentration.

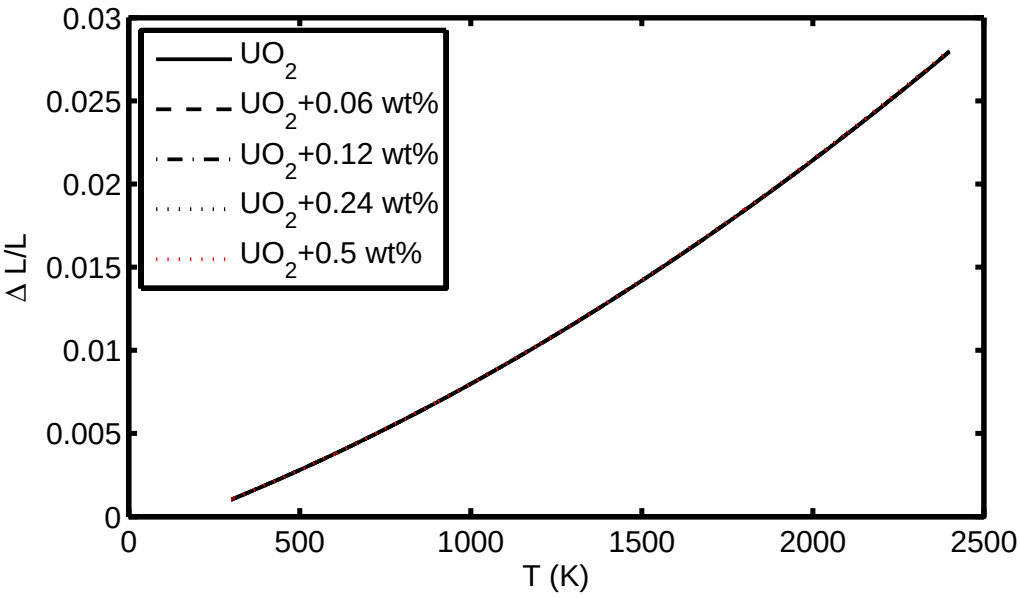

Figure A1: Calculated relative thermal expansion, $\Delta L/L \equiv [L(T) - L(273)]/L(273)$ according to eq. (A.10).

Thermal conductivity The thermal conductivity of (95% TD) fuel, from [65, 121], in the temperature range 300-2800 K is

$$\lambda = \frac{\lambda_0}{w}\arctan(w) + \frac{6600}{\bar{T}^{3/2}}\exp(-16.35/\bar{T}), \quad \text{(A.11)}$$

$$\lambda_0 = \frac{1}{2.45\times10^{-2} + 2.56\times10^{-4}T}, \quad \text{(A.12)}$$

$$w = 3.31\exp(-7.61\times10^{-4}T)\sqrt{x\lambda_0}, \quad \text{(A.13)}$$

$$\bar{T} \equiv T/1000; \quad \text{(A.14)}$$

where λ is in W/mK, the temperature T in K, λ_0 is the thermal conductivity for point defect free UO_2, w is the phonon scattering parameter by the impurities, and x is the Gd_2O_3 content (mole fraction). The first term in (A.11) represents the contribution from phonons (λ_p) and the second term that of electrons (λ_e). To adjust for fuel porosity, one may use the Maxwell-Eucken correction factor given by $\lambda = \lambda_{100}(1-P)/(1+\beta P)$, where λ_{100} is the thermal conductivity of fully (100%) dense material, P the fractional porosity, and $\beta = 0.5$ a constant.

The phonon thermal conductivity of Mg-UO_2 ($Mg_yU_{1-y}O_{2-y}$) fuel based on the work of Fujino et al. [67] has the form

$$\lambda_p = \frac{1}{A+BT}, \quad \text{(A.15)}$$

$$A = 2.268\times10^{-2} + 0.46047y - 2.6933y^2, \quad \text{(A.16)}$$

$$B = 2.32\times10^{-4} - 2.2\times10^{-4}y. \quad \text{(A.17)}$$

where λ_p is in W/mK, the temperature T in K and y is the Mg atom fraction in UO_2. The undoped UO_2 thermal conductivity pertains to that of 96%TD unirradiated fuel. The measurements were made from 473 to 1673 K [67].

Appendix B Fission gas release equations

The mole of gas in the intergranular gas bubbles per unit area of grain boundary at time t, $N_{gb}(t)$, which considers the influence of irradiation-induced re-solution of gas atoms has been derived in a number of publications in the past [83, 85, 91]. Here, the resulting equations used in the computations of section 4.2 are outlined as follows: For $\tau/a^2 \leq 1/\pi^2$:

$$\begin{aligned} N_{gb}(\tau) &= \frac{2\beta_e}{h_1}\Big(\tau + \frac{1}{h_2 h_3} - \\ &\quad - \frac{h_2 \exp(h_3^2\tau)\mathrm{erfc}(h_3\tau^{1/2}) + h_3 \exp(h_2^2\tau)\mathrm{erfc}(-h_2\tau^{1/2})}{h_2 h_3 (h_2 + h_3)}\Big) + O(\tau^{\infty}), \end{aligned} \tag{B.1}$$

where

$$h_1 = \frac{\lambda\nu(t)}{D(t)}, \tag{B.2}$$

$$\beta_e = \frac{\beta(t)}{D(t)}, \tag{B.3}$$

$$h_2 = -\frac{h_1}{2} + \sqrt{\frac{h_1^2}{4} + \frac{h_1}{a}}, \tag{B.4}$$

$$h_3 = \frac{h_1}{2} + \sqrt{\frac{h_1^2}{4} + \frac{h_1}{a}}, \tag{B.5}$$

$$\tau(t) = \int_0^t D(s)ds. \tag{B.6}$$

Here, the ratios h_1 and β_e are assumed to be time-independent, a is the grain radius, ν is the gas atom re-solution rate (frequency) off the intergranular gas bubbles, λ is the corresponding re-solution distance back into the grain, D is the effective fission gas diffusion coefficient in the fuel matrix, and β is the fission gas production rate per unit volume.
For late times, $\tau/a^2 > 1/\pi^2$:

$$\begin{aligned} N_{gb}(\tau) &= \frac{2\beta_e a}{3 + h_1 a}\Big(\tau - \frac{a^2}{5(3 + h_1 a)}\Big) + \\ &\quad + \sum_{m=1}^{\infty} \frac{4\beta_e a^3 e^{-(u_m/a)^2\tau}}{u_m^2[u_m^2 + a h_1(3 + a h_1)]} \end{aligned} \tag{B.7}$$

where

$$u_m = \arctan\Big(\frac{a h_1 u_m}{u_m^2 + a h_1}\Big) + m\pi. \tag{B.8}$$

The model assumes that thermal fission gas release occurs when $N_{gb} = N_{gs}$, where N_{gs} is the grain boundary fission gas concentration upon saturation, which is calculated from an ideal gas equation of state

$$N_{gs} = \frac{8.72 \times 10^{-9}}{T}\Big(\frac{2\gamma}{r_f} + P_{ext}\Big), \tag{B.9}$$

where N_{gs} is in mole/m^2, T is the absolute temperature, γ is the surface tension of gas bubble, r_f is the projected radius of grain boundary bubble at saturation, P_{ext} is the external

Table B1: Input values to the model parameters used for fission gas release and gaseous swelling computations.

Parameter	Unit	Definition
$\beta = 0.3\dot{F}_m$	mol m^{-3}s^{-1}	Fission gas production rate
$\dot{F}_m = 5.189 \times 10^{-14} q_v$	mol m^{-3}s^{-1}	Fission rate density (molar)
$\dot{F} = N_A \dot{F}_m$	m^{-3}s^{-1}	Fission rate density
$N_A = 6.022 \times 10^{23}$	mol^{-1}	Avogadro constant
$q_v = q_l / 4\pi r_{\mathrm{p}}^2$	W m^{-3}	Power density
$q_l = 30000$	W m^{-1}	Linear power density
$r_{\mathrm{p}} = 4.24$	mm	Fuel pellet radius
$\rho_{\mathrm{T}} = 10.96$	g cm^{-3}	Fuel theoretical density
$P_{\mathrm{ext}} = 0$ or 1^*	MPa	External pressure
$2\gamma / r_f = 2.4$	MPa	Gas bubble surface tension to radius ratio
$\nu\lambda = 5.7 \times 10^{-8}\beta$	ms^{-1}	Re-solution rate

*See end-note 6.

pressure, see e.g. [68, 85] for more details. The fractional fission gas release from fuel is calculated according to

$$F_{gr}(t) = \frac{3}{2a}\Big(\frac{\max(N_{gb}(t) - N_{gs}, 0)}{\int_0^t \beta(s)s}\Big). \tag{B.10}$$

2014:21

The Swedish Radiation Safety Authority has a comprehensive responsibility to ensure that society is safe from the effects of radiation. The Authority works to achieve radiation safety in a number of areas: nuclear power, medical care as well as commercial products and services. The Authority also works to achieve protection from natural radiation and to increase the level of radiation safety internationally.

The Swedish Radiation Safety Authority works proactively and preventively to protect people and the environment from the harmful effects of radiation, now and in the future. The Authority issues regulations and supervises compliance, while also supporting research, providing training and information, and issuing advice. Often, activities involving radiation require licences issued by the Authority. The Swedish Radiation Safety Authority maintains emergency preparedness around the clock with the aim of limiting the aftermath of radiation accidents and the unintentional spreading of radioactive substances. The Authority participates in international co-operation in order to promote radiation safety and finances projects aiming to raise the level of radiation safety in certain Eastern European countries.

The Authority reports to the Ministry of the Environment and has around 300 employees with competencies in the fields of engineering, natural and behavioural sciences, law, economics and communications. We have received quality, environmental and working environment certification.

Strålsäkerhetsmyndigheten
Swedish Radiation Safety Authority

SE-171 16 Stockholm
Solna strandväg 96

Tel: +46 8 799 40 00
Fax: +46 8 799 40 10

E-mail: registrator@ssm.se
Web: stralsakerhetsmyndigheten.se